

# THE STOCHASTIC DYNAMICS OF EPIDEMIC MODELS

A THESIS SUBMITTED TO THE UNIVERSITY OF MANCHESTER  
FOR THE DEGREE OF DOCTOR OF PHILOSOPHY  
IN THE FACULTY OF ENGINEERING AND PHYSICAL SCIENCES

2010

By  
Andrew James Black  
School of Physics and Astronomy

# Contents

---

<b>Abstract</b>	<b>6</b>
<b>Declaration</b>	<b>7</b>
<b>Copyright</b>	<b>8</b>
<b>Acknowledgements</b>	<b>9</b>
<b>Publications</b>	<b>10</b>
<b>1 Introduction</b>	<b>11</b>
1.1 Recurrent epidemics . . . . .	13
1.2 The SIR model of epidemics . . . . .	16
1.2.1 Seasonal forcing . . . . .	20
1.2.2 Stochasticity . . . . .	22
1.3 Individual based models . . . . .	23
1.4 Outlook . . . . .	25
<b>2 Technical background</b>	<b>27</b>
2.1 Stochastic processes and master equations . . . . .	27
2.2 A stochastic SIR model . . . . .	29
2.3 Monte-Carlo simulation . . . . .	31
2.4 Expansion of the master equation . . . . .	34
2.4.1 General expansion . . . . .	36
2.4.2 Langevin formalism . . . . .	37
2.5 Deterministic dynamics . . . . .	39
2.6 Stochastic fluctuations . . . . .	40
2.6.1 General power spectra . . . . .	44
2.6.2 Stochastic amplification . . . . .	45
2.7 Summary . . . . .	46

<b>3 Immigration in the SIR model</b>	<b>47</b>
3.1 Deterministic analysis . . . . .	48
3.2 Stochastic fluctuations . . . . .	50
3.3 Small- $N$ deviations . . . . .	51
3.3.1 Higher-order corrections . . . . .	53
3.4 Summary . . . . .	55
<b>4 Staged epidemic models</b>	<b>56</b>
4.1 Infectious period distributions . . . . .	57
4.2 Staged SIR model . . . . .	58
4.3 Power spectrum . . . . .	62
4.4 Discussion . . . . .	65
<b>5 Whooping cough model</b>	<b>67</b>
5.1 Staged SEIR model . . . . .	68
5.2 Power spectrum . . . . .	72
5.3 Whooping cough analysis . . . . .	73
5.3.1 Results . . . . .	75
5.4 Discussion . . . . .	78
<b>6 Seasonal forcing</b>	<b>80</b>
6.1 Deterministic dynamics . . . . .	81
6.2 Annual limit cycle . . . . .	83
6.3 Period doubling and measles transitions . . . . .	86
6.3.1 Review of Earn's original analysis . . . . .	86
6.3.2 Analytic predictions . . . . .	88
6.3.3 Near the bifurcation point . . . . .	91
6.3.4 Smaller populations . . . . .	91
6.3.5 Switching between attractors . . . . .	94
6.4 Discussion . . . . .	95
<b>7 Conclusions and further work</b>	<b>98</b>
<b>A Staged model matrices</b>	<b>108</b>
<b>B Floquet theory</b>	<b>111</b>
<b>Bibliography</b>	<b>114</b>

# List of Figures

---

1.1	Measles case reports in Copenhagen. . . . .	14
1.2	Measles case reports in Baltimore. . . . .	14
1.3	Measles in London before and after vaccination . . . . .	15
1.4	Solutions of the deterministic SIR equations . . . . .	18
1.5	Solutions of the forced SIR model . . . . .	21
1.6	Stochastic amplification . . . . .	22
2.1	Stochastic oscillations in the SIR model . . . . .	40
2.2	Power spectra for the stochastic SIR model . . . . .	42
2.3	Theoretical power spectrum and the normalised fluctuations . . . . .	43
3.1	Fixed points of the SIR model, with and without immigration . .	50
3.2	The trace of the Jacobian as a function of $\beta$ . . . . .	51
3.3	Power spectra with and without immigration . . . . .	52
3.4	Amplification, $A_0$ , mapped into parameter space . . . . .	53
3.5	Power spectra at decreasing population sizes . . . . .	54
4.1	Distributions of infectious periods . . . . .	59
4.2	Analytical power spectra with distributed infectious periods . . .	63
4.3	Amplification with increasing $L$ . . . . .	64
4.4	Comparison of analytic and numerical power spectra . . . . .	64
5.1	Probability of infection in the staged-SEIR model . . . . .	70
5.2	The amplitude and peak frequency of the analytic power spectrum as a function of $M$ . . . . .	74
5.3	The amplitude and peak frequency of the analytic power spectrum as a function of $L$ . . . . .	74
5.4	Whooping cough model power spectra . . . . .	76
5.5	Theoretical and numerical power spectra for the whooping cough model . . . . .	77

6.1	A limit cycle solution of the forced SIR model . . . . .	82
6.2	Stochastic phase portrait of the forced SIR model . . . . .	84
6.3	Power spectrum with an annual limit cycle . . . . .	85
6.4	Earn’s original bifurcation diagram . . . . .	87
6.5	Bifurcation diagram and Floquet multipliers . . . . .	88
6.6	Floquet multipliers near the bifurcation point . . . . .	89
6.7	Analytic and numerical spectra for a range of $R_0$ . . . . .	90
6.8	Power spectra through the bifurcation point . . . . .	92
6.9	Power spectra for smaller populations . . . . .	93
6.10	Anomalous enhancement of the power spectrum . . . . .	94
6.11	Time series with switching between triennial and annual patterns	95
7.1	Bursts of coherent oscillations in the SIR model . . . . .	106

# Abstract

---

THE UNIVERSITY OF MANCHESTER

Doctor of Philosophy

**The stochastic dynamics of epidemic models**, by Andrew James Black.

September, 2010.

This thesis is concerned with quantifying the dynamical role of stochasticity in models of recurrent epidemics. Although the simulation of stochastic models can accurately capture the qualitative epidemic patterns of childhood diseases, there is still considerable discussion concerning the basic mechanisms generating these patterns. The novel aspect of this thesis is the use of analytic methods to quantify the results from simulations. All the models are formulated as continuous time Markov processes, the temporal evolutions of which is described by a master equation. This is expanded in the inverse system size, which decomposes the full stochastic dynamics into a macroscopic part, described by deterministic equations, plus a stochastic fluctuating part.

The first part examines the inclusion of non-exponential latent and infectious periods into the standard susceptible-infectious-recovered model. The method of stages is used to formulate the problem as a Markov process and thus derive a power spectrum for the stochastic oscillations. This model is used to understand the dynamics of whooping cough, which we show to be the mixture of an annual limit cycle plus resonant stochastic oscillations. This limit cycle is generated by the time-dependent external forcing, but we show that the spectrum is close to that predicted by the unforced model. It is demonstrated that adding distributed infectious periods only changes the frequency and amplitude of the stochastic oscillations—the basic mechanisms remain the same.

In the final part of this thesis, the effect of seasonal forcing is studied with an analysis of the full time-dependent master equation. The comprehensive nature of this approach allows us to give a coherent picture of the dynamics which unifies past work, but which also provides a systematic method for predicting the periods of oscillations seen in measles epidemics. In the pre-vaccination regime the dynamics are dominated by a period doubling bifurcation, which leads to large biennial oscillations in the deterministic dynamics. Vaccination is shown to move the system away from the biennial limit cycle and into a region where there is an annual limit cycle and stochastic oscillations, similar to whooping cough. Finite size effects are investigated and found to be of considerable importance for measles dynamics, especially in the biennial regime.

# **Declaration**

---

No portion of the work referred to in this thesis has been submitted in support of an application for another degree or qualification of this or any other university or other institute of learning.

# Copyright

---

- (i) The author of this thesis (including any appendices and/or schedules to this thesis) owns certain copyright or related rights in it (the “Copyright”) and he has given The University of Manchester certain rights to use such Copyright, including for administrative purposes.
- (ii) Copies of this thesis, either in full or in extracts and whether in hard or electronic copy, may be made **only** in accordance with the Copyright, Designs and Patents Act 1988 (as amended) and regulations issued under it or, where appropriate, in accordance with licensing agreements which the University has from time to time. This page must form part of any such copies made.
- (iii) The ownership of certain Copyright, patents, designs, trade marks and other intellectual property (the “Intellectual Property”) and any reproductions of copyright works in the thesis, for example graphs and tables (“Reproductions”), which may be described in this thesis, may not be owned by the author and may be owned by third parties. Such Intellectual Property and Reproductions cannot and must not be made available for use without the prior written permission of the owner(s) of the relevant Intellectual Property and/or Reproductions.
- (iv) Further information on the conditions under which disclosure, publication and commercialisation of this thesis, the Copyright and any Intellectual Property and/or Reproductions described in it may take place is available in the University IP Policy (see <http://www.campus.manchester.ac.uk/medialibrary/policies/intellectual-property.pdf>), in any relevant Thesis restriction declarations deposited in the University Library, The University Library’s regulations (see <http://www.manchester.ac.uk/library/aboutus/regulations>) and in The University’s policy on presentation of Theses.

# Acknowledgements

---

I would like to start by thanking my supervisor, Alan McKane, for his wisdom and help in completing this thesis. Thanks also to Tobias Galla for his support and various German adventures.

Thanks to the guys in the office for a good laugh and putting up with my horticultural experiments: Carlos, Ian, Richard S., Boland, Chris, Duncan, Alex, Richard M., Mohammad and Joe. I should also mention Brian, for providing much entertainment over the years.

I would like to acknowledge my favourite drinking establishments for their part in helping me finish this thesis: Trof, OP, SandBar, The Ducie and Temple.

Finally thanks to everyone else, friends and family, who have supported me for the last four years.

# Publications

---

The work described in Chapter 4 of this thesis was done in collaboration with Alan McKane, Ana Nunes and Andrea Parisi, and has previously been published as:

- A. J. Black, A. J. McKane, A. Nunes and A. Parisi, 2009. Stochastic fluctuations in the susceptible-infectious-recovered model with distributed infectious periods. *Phys. Rev. E.*, **80**, 021922, (doi:10.1103/PhysRevE.80.021922).

The work described in Chapter 5 and Chapter 6 was done in collaboration with Alan McKane. This has been published as:

- A. J. Black and A. J. McKane, 2010. Stochasticity in staged models of epidemics: quantifying the dynamics of whooping cough. *J. R. Soc. Interface*, **7**, 1219-1227, (doi:10.1098/rsif.2009.0514).
- A. J. Black and A. J. McKane, 2010. Stochastic amplification in an epidemic model with seasonal forcing. *J. Theor. Biol.*, **267**, 85-94, (doi:10.1016/j.jtbi.2010.08.014).

# Chapter 1

## Introduction

---

Perhaps no events of human experience interest us so continuously, from generation to generation, as those which are, or seem to be, periodic. – H. E. Soper, J. R. Stat. Soc. 92, (1929).

The dynamics of childhood diseases have long proved fascinating for modellers for two reasons: firstly, they are notifiable diseases and thus long, detailed, incidence time-series exist on the level of individual cities [1]. Secondly, the basic epidemiology is relatively straightforward, thus simple models are applicable [2]. Traditionally deterministic models have formed the bedrock of mathematical epidemiology. The standard approaches such as the susceptible-infected-recovered (SIR) and the susceptible-exposed-infected-recovered (SEIR) models [2, 3] have shaped much of our present day understanding of recurrent epidemics. Stochasticity has long been recognised as an important factor within epidemic modelling, but there is still much debate as to its precise dynamical role and how it can be understood from a theoretical point of view [4, 5].

To see where this element of stochasticity comes from, we need to consider how we could predict the spread of infection through a population. Clearly this is a very complicated process; to capture every aspect we would have to know how the disease interacts with different immune systems, how it is spread, the movement patterns of all individuals, etc. It should be obvious that we can never practically know even a small amount of the details; the process is so complex it essentially appears random. Our ignorance of so many aspects means the only way forward is a stochastic model. With this type of model, we can only predict

the probabilities of the system being in a certain state at a future time. This is contrasted with a deterministic model where, given an initial condition, we can calculate the entire future trajectory exactly. To form a model we must make many approximations. So, for example, we cannot predict when an individual will recover, but we can accurately define an average recovery time and infectious period distribution function. So in this way we have coarse-grained out all the complexities of how the disease develops within an individual, and replaced it with a random aspect.

The level of approximation we use leads to a number of different models. The most complicated would be the so called agent-based approach. This is where each individual is a distinct agent with many internal states. The population is made up of these agents, which then spread the disease. The only way that such a model can be investigated is via computer simulations, but almost limitless amounts of detail can in principle be included. The downside of this is that the number of parameters required is high and general results are hard to obtain. Taking the other extreme we can consider just fractions of the overall population, in which case we reduce the model down to a small number of independent variables. One assumes that the population is large enough that we can approximate the process described by discrete variables by continuous variables; we essentially average out the stochastic element. The process is then modelled by a system of ordinary differential equations, which are deterministic. By making these further simplifications we have arrived at a model which is much easier to analyse at the expense of realism. These are still very useful though, as they can provide insight not available from simulations.

The idea of demographic stochasticity arises from this last approximation. This is the stochastic element introduced into a model by the fact that a population is actually made up of individuals and evolves via random processes [6]. The only way to capture the effect of this is to use an individual based model, which is again inherently stochastic. This can be viewed as an intermediate approximation between a deterministic and an agent-based model. The population is made up of identical individuals with a state classified according to their epidemiological status. Such a model can only be solved ‘exactly’ by simulation, but is simple enough that analytic tools can also be brought to bear on the problem.

Traditionally there are two ways in which a stochastic model is different from a deterministic one. Most trivially, because the process is random, different realisations will show variation. Secondly (and traditionally why stochastic epidemic models were first investigated), because there is the chance of extinction, which cannot happen in a deterministic model. In recent years there has been a growing body of research advocating the importance of stochasticity to population level dynamics [7]. This thesis is devoted to understanding this phenomena in epidemic models of childhood diseases. In the rest of this chapter I introduce recurrent epidemics, concentrating on two diseases, measles and whooping cough, which although similar in many respects show contrasting dynamics. Next I look in detail at the different modelling approaches, open questions we seek to answer, as well as our general modelling approach. Finally I give an outlook for the rest of the thesis.

## 1.1 Recurrent epidemics

Measles, whooping cough and chicken pox are all known as childhood diseases. This is due to the fact that they are strongly immunising (so an individual cannot catch it once recovered) and highly infectious, so almost all the population will have had it before the age of 18. Although vaccination programs have almost eradicated most of these, there is continued interest because the quality of the time series makes these a good testing ground for ecological theory. The ubiquitous feature of all these diseases is the large oscillations in their incidence (number of cases per unit time). These outbreaks are known as recurrent epidemics, as opposed to other endemic infections which show a more constant incidence [2]. We can imagine a pool of susceptibles which is constantly filled by new births. At some point the number of susceptibles will be large enough to support an outbreak, which will rapidly deplete the pool as the infectious period is orders of magnitude shorter than the average life time. This account of an outbreak is simple to give, but this is only a *description* not an explanation and it is not clear a priori, without modelling, why we should see large oscillations and not for example a constant number of cases [8].

There is a wide variety of patterns of recurrence, not just between different diseases, but between different locations and periods, which can range from highly periodic to irregular. Measles is the canonical example of a disease which

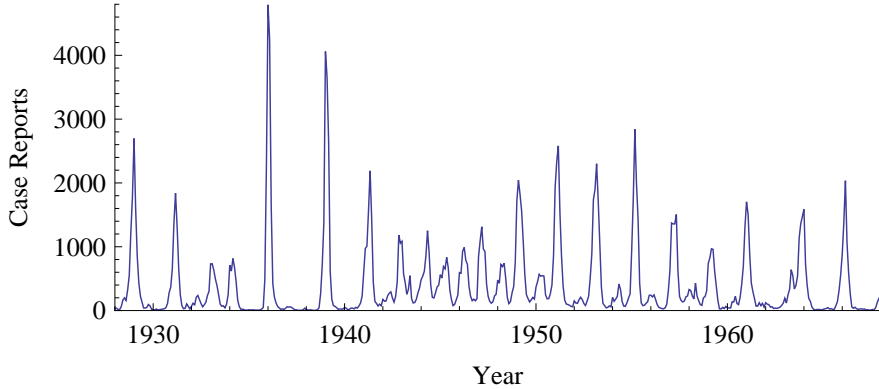


Figure 1.1: Measles case reports in Copenhagen, Denmark. Data originally from [9].

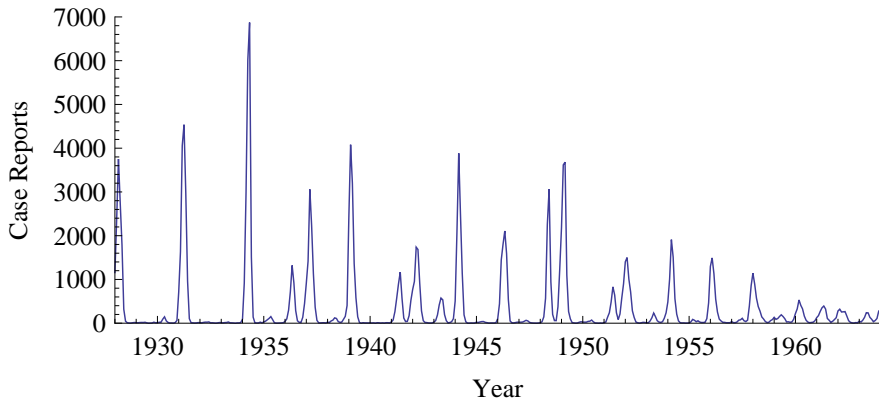


Figure 1.2: Measles case report in Baltimore, US. Data originally from [10].

shows recurrent behaviour and one of the most widely studied. Figure 1.1 shows measles case reports from Copenhagen and illustrates a number of trends which are observed in other time series. We observe large recurrent outbreaks, but the patterns change through time. Between 1943 and 1949 we observe annual outbreaks which then smoothly change into a biennial pattern around 1950. We can contrast this with the period before 1940 and in Baltimore, shown in Figure 1.2, where the patterns are much more irregular through time.

The best data set for measles is derived from the Registrar General's Weekly Return for England and Wales (E&W) [1, 11, 12]. This represents the most detailed spatio-temporal data set in all of ecology [13]. One of the most important features of this is that it captures the dynamic effect of mass vaccination which starts in 1968. This can be considered a kind of natural experiment [13], in which the parameters controlling the spread of measles are changed. This is very

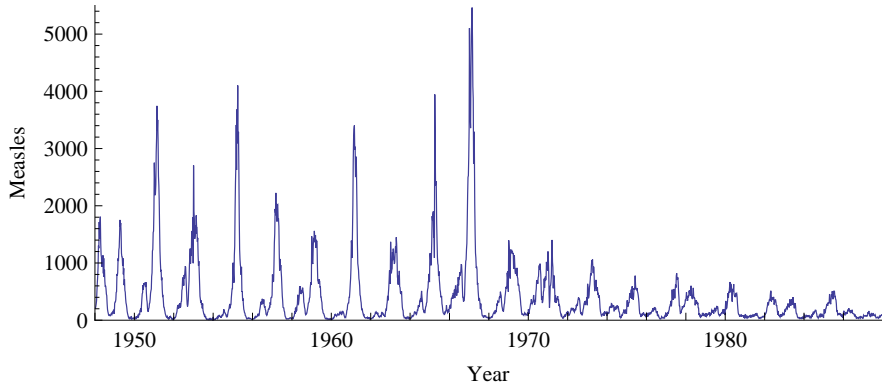


Figure 1.3: Measles case reports from London. Mass vaccination starts in 1968.

valuable as it gives much more insight into the transmission process; any good model should be able to recreate both the pre- and post-vaccination dynamics. Figure 1.3 shows the case reports from the largest city in this set: London. Before vaccination we observe large biennial (two yearly) outbreaks. Although there is variation in the amplitude of these outbreaks, the timing is very regular. After vaccination the biennial pattern is destroyed and epidemics become much more irregular and un-synchronised between cities [14–16]. More detailed studies have uncovered other patterns in this data such as travelling waves emitted from large population centres [17, 18].

Whooping cough is another childhood disease which is in many ways similar to measles but shows starkly contrasting dynamics [16, 19]. The same data set exists for whooping cough as measles, but is not yet publicly available. Before vaccination, time series of case reports are strongly multiennial (variety of periodicities), but after vaccination in the 1950s quite regular 3.5–4 year epidemics cycles occur, which are correlated between large cities [16, 20]. This is essentially the opposite of measles [15].

Power spectra have proved very useful tools in distinguishing the different periodicities in these time-series [21]. These show how power is distributed between different spectral frequencies [22]. In general we can distinguish two types of peaks. The first arising from seasonal forces show up as large peaks at integer multiples of a year. All childhood diseases have a strong seasonal component [23], but for measles this is especially pronounced. The second type of peak is non-seasonal, and tends to be at lower frequencies [14, 21]. So pre-vaccination, the multiennial oscillations of whooping cough show up as a mixture of a small annual peak and a wider non-seasonal peak centred on 2–3 years [21, 24].

## 1.2 The SIR model of epidemics

The foundations of mathematical epidemiology were laid over one hundred years ago. The regular periodicity of measles suggested that the spread of disease might follow a law that could be modelled mathematically [25]. In this endeavour, Hamer [26] represents a turning point in actually defining an *a priori* mathematical model. Up until that point most work had been of an empirical nature [25, 27] and many hypotheses existed to try and explain the course of epidemics. The subject was formalised by Kermack and McKendrick, who wrote down the first rigorous mathematical models for disease transmission in a form that is still used today [28, 29]. The SIR model describes the spread of an infectious disease from which recovered individuals gain immunity from re-infection. It is highly simplified, omitting many finer details, but we can make a surprising amount of progress by considering the simplest model.

The fundamental idea is that the population can be split into three different classes or compartments: susceptibles, infected and recovered.  $S(t)$  is the number of people susceptible to the disease at time  $t$ , and who have not yet been infected.  $I(t)$  is the number of infectious individuals, who can spread the disease via contact with a susceptible. Finally,  $R(t)$  is the number of recovered individuals, who are no longer susceptible to the disease, or able to spread the infection. The population is taken to be homogeneously mixed, thus everyone has contact with everyone else.

The model is then formulated in terms of differential equations for the transfer of individuals between the three classes. There are two important time scales which must be considered. The demographic time scale, measuring the average turn over of individuals due to births and deaths and the time scale of the disease, i.e. the average infectious period. If the epidemic time scale is short compared to the demographic time scale then demographic effects can be ignored as the population does not change appreciably during the epidemic. A disease for which this is true is influenza [30]. If an infected individual is introduced into a susceptible population the disease quickly develops but then dies out rapidly after a certain time, leaving a proportion of the community untouched [30]. The opposite is true of diseases such as measles, whooping cough and rubella, which show endemic behaviour. This is where the number of infectives tends to, and usually oscillates about, a mean value over time. Such behaviour can only be possible if there is a supply of new susceptibles into the population, thus births and deaths must be

included in the model. The assumptions can be summed up as follows:

- Birth: Assume a per capita birthrate,  $b$  and that the birthrate is proportional to the total population. Thus the total number of new susceptibles born per unit time is  $b(I + S + R)$
- Death: Death occurs at the same rate  $\mu$  for all classes. With this we are implicitly assuming that the infectious disease is non-lethal and that the average lifespan of an individual is exponentially distributed, implying that the mean lifespan is  $1/\mu$  [30]. Throughout this thesis we take  $1/\mu = 50$  years.
- Internal infection: An average infective will make sufficient contact to transmit the disease with  $\beta$  other individuals per unit time. The fraction of those individuals who are susceptible is  $S/N$ , where  $N = I + S + R$ , is the total population. Thus the total number of new infectives per unit time is the product of the number of infectious contacts and the proportion of susceptibles (simple mass action), i.e.  $\beta SI/N$  [26]. Here we are implicitly assuming frequency-dependent mixing [31], which means that the transmission rate is independent of the population size (so transmission only depends on the frequency of contacts). This has been shown to be a good approximation [1].
- Recovery: Infected individuals recover at a constant rate  $\gamma$ . This implies that the average length of the infectious period is distributed exponentially, with mean  $1/\gamma$ .

The three differential equations describing the rates of change of the numbers in each class are then:

$$\begin{aligned}\dot{S} &= -\frac{\beta S}{N}I - \mu S + b(I + S + R), \\ \dot{I} &= \frac{\beta S}{N}I - \mu I - \gamma I, \\ \dot{R} &= -\mu R + \gamma I.\end{aligned}\tag{1.1}$$

These collectively define the open-SIR model: open because the population can grow or shrink depending on the ratio of  $b$  to  $\mu$ . This can be seen by adding all

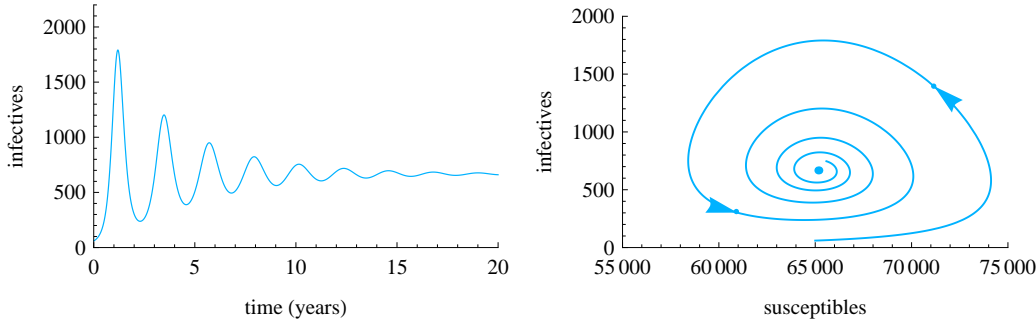


Figure 1.4: Solutions of the deterministic equations (1.2). The phase portrait show a stable spiral fixed point.  $N = 10^6$ .

three equations (1.1) above to give,

$$\frac{d}{dt}(I + R + S) = (b - \mu)(I + R + S).$$

If  $b > \mu$  then the population will grow exponentially and if  $b < \mu$  then it will die out. By taking  $b = \mu$  the total population will remain constant and we can make some simplifications. The equation  $N = S + R + I$  becomes a constraint on the system and can be used to eliminate the equation for  $R$ , resulting in the two equations,

$$\begin{aligned}\dot{S} &= \mu(N - S) - \frac{\beta SI}{N}, \\ \dot{I} &= \frac{\beta SI}{N} - (\gamma + \mu)I,\end{aligned}\tag{1.2}$$

which we refer to as the SIR model. Equations (1.2) cannot be solved in closed form and must be integrated numerically [32]. A solution is shown in Figure 1.4, which shows typical behaviour for parameters typical of childhood diseases: damped oscillations tending to a fixed point. One of Kermack and McKendrick's most important results concerns the existence of an epidemic threshold [29]. This is defined in terms of the parameter  $R_0 = \beta/(\gamma + \mu)$ , which is the average number of secondary infections caused by an infected individual in a completely susceptible population. For a disease to be endemic within a population,  $R_0 > 1$ , otherwise it will fade-out.  $R_0$  can be shown to be related to the average age of infection and is one of the more easily measurable parameters [2].

One of the most common modifications to the basic SIR model is the addition of a new exposed class,  $E$ , to create the SEIR model. Thus when first infected, an individual is exposed before becoming infectious at a constant rate  $\sigma$ . This

is biologically realistic for all childhood diseases which have long latent periods, but has limited consequences for the model [2]. One can show that the dynamics rapidly converge to a centre manifold and are well approximated by rescaled SIR equations [33] with,

$$\frac{1}{\gamma_{\text{SIR}}} = \frac{1}{\gamma} + \frac{1}{\sigma}. \quad (1.3)$$

Table 1.1 gives some typical parameters for four childhood disease.

As discussed in the previous section, vaccination is an important process which can be incorporated easily into this model. If we assume that a fraction,  $p$ , of the population is vaccinated at birth (which then directly enter the  $R$  class) then the open-SIR equations become,

$$\begin{aligned} \dot{S} &= -\frac{\beta S}{N}I - \mu S + b(1-p)(I + S + R), \\ \dot{I} &= \frac{\beta S}{N}I - \mu I - \gamma I, \\ \dot{R} &= -\mu R + \gamma I + bp(S + R + I). \end{aligned} \quad (1.4)$$

If we now make a change of variables:  $S \rightarrow S'(1-p)$ ,  $I \rightarrow I'(1-p)$  and  $R \rightarrow R'(1-p) + (b/\mu)pN$ , then one finds that the equations for the primed variables are the same as the original open-SIR equations (1.1), but with  $\beta \rightarrow \beta(1-p)$  [34, 35]. Thus vaccination is equivalent to scaling  $\beta$ , effectively lowering the transmission rate. This applies exactly the same to the SIR equations (1.2) with linked births and deaths, but is less straightforward to prove.

The basic problem with the SIR model is that, much like the original Lokta-Volterra equations which model predator-prey oscillations [36], they only produce damped oscillations tending to a stable fixed point, not recurrent behaviour. Many modifications have been proposed to the basic deterministic model with a view to obtaining robust oscillations as well as more biological realism. Some examples are age structure in the population [37, 38], delays [39], and nonlinearities in the infection term [40]. The problem is that although these modifications can produce sustained oscillations, they do not predict the regular patterns of most epidemics. Within the literature there is a broad consensus that there are two main elements needed to correctly model these oscillations: firstly stochasticity, due to the individual nature of the population [41, 42]; and secondly, seasonal forcing, arising from the term-time aggregation of children in schools, which is deterministic [10, 37, 43, 44]. Independently these two factors are well understood,

Disease	$R_0$	$1/\sigma$ (days)	$1/\gamma$ (days)
Measles	16-18	8	5
Whooping Cough	16-18	8	14
Rubella	6-7	10	7
Chicken Pox	10-12	10	5

Table 1.1: Parameters for four childhood diseases [2].

but how they interact when both included in the same model is still an open question [5, 45, 46].

### 1.2.1 Seasonal forcing

Seasonal variation in transmission was one of the first factors to be recognised as important in the spread of childhood diseases. Soper [47] was the first to postulate that some sort of seasonal variation in transmission would sustain oscillations in his deterministic proto-SIR model. It was not till much later on that London & York [10] demonstrated that there was seasonal variation in the contact rate  $\beta$ , which could be attributed to the aggregation of children in schools. So during school terms, children are in close proximity and transmission is higher than during holidays. Later, Fine & Clarkson [11, 48] showed the same variation using data for England and Wales and a discrete time model. The further development of discrete time models [49, 50] and more recently Markov chain and Bayesian inference techniques [51] have revealed the same effect.

The most popular approaches to modelling this are to make  $\beta$  a function of time, for instance,

$$\beta(t) = \beta_0(1 + \beta_1 \cos(2\pi/365 t)), \quad (1.5)$$

where  $\beta_0$  is the base line contact rate and  $\beta_1$  the magnitude of forcing [33, 52]. More realistically, we can replace the cosine term with a step function which alternates between high and low values in pattern with school term dates [37, 45]. These deterministic forced models can display a wide range of dynamic behaviour. The most common solutions are limit cycles or attractors at periods that are integer multiples of a year. As  $\beta_1$  is increased, the limit cycle grows (although typically not linearly with  $\beta_1$ ) and at critical values bifurcations are induced to longer period solutions [53, 54]. Figure 1.5 illustrates some of the periodic solutions which can be found with increasing magnitudes of seasonal forcing. These longer period solutions are known as sub-harmonic resonances [52].

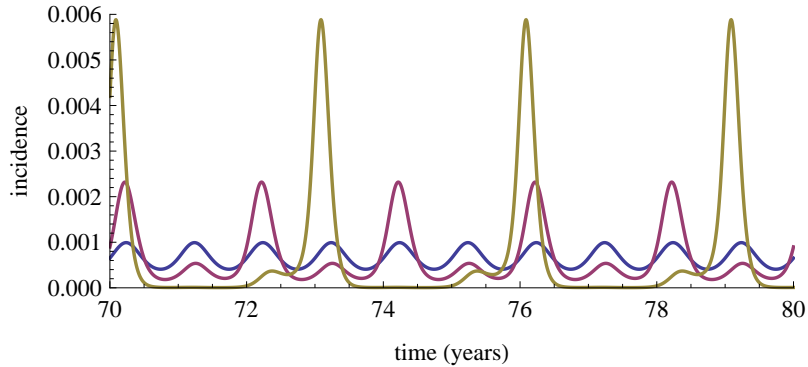


Figure 1.5: Solutions of the SIR model with seasonal forcing as specified by Eq. (1.5). As the magnitude of forcing is increased we see longer period solutions: annual (blue), biennial (red) and triennial (yellow).  $\beta_1 = 0.08, 0.15$  and  $0.2$ .

There also exists parameter regimes in which multiple co-existing attractors exist [53]. So different initial conditions will lead to different long-time solutions. The basins of attractions (the set of initial conditions which lead to a given long time solution) can either be large or densely intertwined [19, 35]. Regions of chaotic behaviour have also been found, which has spawned a large body of research [55, 56]. Chaos has been proposed as the mechanism behind the dynamics of some diseases, especially measles [9, 57], but most evidence refutes these ideas. Firstly, chaos is only found for magnitudes of forcing which are unrealistic [58], and typically generates very small incidence levels ( $I \sim 10^{-18}$ ). Secondly, the addition of simple heterogeneities, such as age-structure or spatial structure remove the propensity for chaos [59–61].

Aside for the question of chaos, simple deterministic models with seasonal forcing do capture many aspects of measles epidemics: annual, biennial and higher period oscillations are all observed in the time series, see Figure 1.1. But clearly this cannot be the whole story, because they are deterministic, a trajectory will stay on a given attractor. Some sort of stochasticity must be included to produce the natural variation seen in these epidemics. Regular oscillations are only observed in large populations [11]; smaller populations tend to show more irregular dynamics [1]. Another factor that is unexplained by the current theory is the transitions between different periods of regular oscillations: there is no indication whether these arise naturally from the dynamics or are due to external forces. The most serious deficiency of these simple forced models is that they cannot capture the dynamics of whooping cough. For all sensible parameters, deterministic

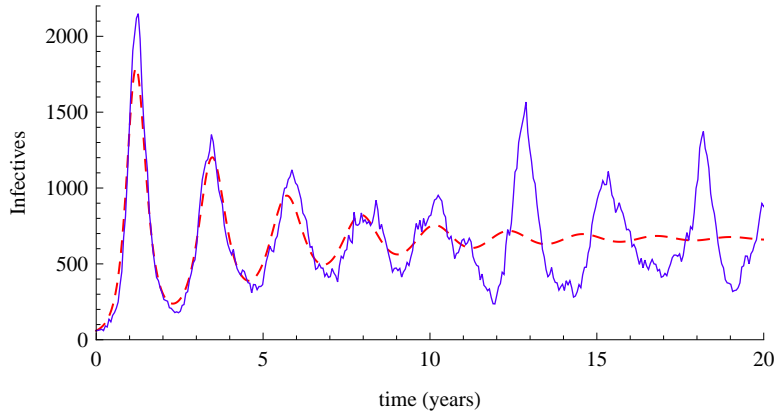


Figure 1.6: Deterministic (red dashed) and stochastic (solid blue) solutions of the SIR equations.

models only predict annual epidemics [16, 24, 38]. To capture and investigate all these aspects requires some sort of stochastic model.

### 1.2.2 Stochasticity

This thesis is devoted to stochastic models, but so far everything we have discussed has been deterministic. Stochastic models *without* seasonal forcing are easier to understand. The construction and simulation of these models is discussed in Section 1.3 and Chapter 2. The first stochastic simulations of an epidemiological model were carried out by Bartlett [62] on the then new Manchester electronic computer. He was primarily interested in extinction dynamics [27, 63–65], but also recognised that the simple deterministic models of Hamer and Soper would give recurrent dynamics with the addition of stochasticity; in other words, that noise could maintain oscillations by constantly perturbing the system away from its steady state [66]; this is illustrated in Figure 1.6. Since then the same phenomena has been found in a number of systems, such as predatory-prey and chemical systems [6, 66–68]. Essentially, whenever a deterministic model shows damped oscillatory behaviour, the stochastic analog tends to show sustained noisy oscillations [69]. This has been quantified as stochastic amplification [68], or sometimes coherence resonance [70] (the theory behind this is discussed in the next chapter).

Clearly any model which hopes to capture these epidemic dynamics needs to include both seasonal forcing and stochasticity. Formulating a stochastic model with forcing is straightforward and depending on assumptions can qualitatively capture the correct dynamics of both whooping cough and measles [16, 44]. But,

it is less clear how the stochasticity interacts with the cyclic solutions that are produced [5, 45, 46]. This forms one of the main questions which this thesis attempts to answer: how do these two forces interact to produce the observed patterns and what are the mechanisms at work? The common interpretations for the role of stochasticity can be roughly be divided into two categories: active and passive [5].

Active noise is where there is some sort of interaction between the non-linear dynamics and noise, which produces novel patterns which the deterministic model alone cannot capture. The dynamics of whooping cough are given as the paradigmatic example of this type of behaviour [5, 45, 46]. The second, passive, interpretation of noise is more conservative, where typically understanding the ‘deterministic skeleton’ is most important [5], from which stochastic effects are added on [71]. One of the most prevalent theories for measles dynamics is to do with switching between attractors [72]. In the previous section we discussed how the forced model has different solutions for different initial conditions. Noise then acts to kick the system between these states, and the pattern will somewhat depend on the basins of attraction. Large basins would produce long periods of regular behaviour, many tightly intertwined basins, irregular patterns.

Undoubtedly this passive noise interpretation has gained weight because it seems to explain the behaviour of time-series and simulations. This basic idea was later elaborated by Earn et al in explaining the dynamical transitions in measles epidemics [35]. They showed that changes in birth rates and vaccination put the model into different regions, with different co-existing attractors. More recently, Nguyen & Rohani [19] have proposed that an SEIR model with realistically distributed latent and infectious periods can capture the dynamics of whooping cough using the same mechanism. This moves away from the active interpretation, in favour of a passive one.

### 1.3 Individual based models

The challenge in epidemic modelling is to form a model which captures the observed dynamics but also elucidates the mechanisms behind them [6, 71]. There are many different approaches which can capture the dynamics, but they offer little understanding of the mechanisms. A major factor in the debate over the role of stochasticity in recurrent epidemics is the dominant modelling paradigm which

exists in the field, and to a large extent in theoretical ecology in general.

The most popular approach tends to have two steps: first to create a suitable population level model (PLM), usually in terms of ordinary differential equations which are deterministic. Next the corresponding individual based model (IBM) is formed, and then simulated, to investigate any stochastic properties [6, 42, 73, 74]. As discussed at the beginning of this chapter, logically the procedure should be reversed: real populations are finite and the PLM is always an approximation to the underlying IBM [74]. Usually it is assumed that the PLM will be accurate in the limit of large populations, but what is meant by large must first be defined [75]. The work described in the previous section has been an amalgam of analytical work on the PLM and simulations of the IBM [45, 46]. While this has yielded valuable insights, fundamentally one is left with the problem of interpreting stochastic simulations in terms of deterministic results.

Clearly the IBM, rather than the PLM, should be adopted as the starting point of an investigation. Once an IBM has been defined, it is usually studied using computer simulations. However simulations are still inferior in at least one respect to the analysis that can be carried out on PLMs: general results valid over a wide range of models and parameters cannot in general be established. In addition, many insights and a deeper understanding can frequently be obtained from analytical studies than can be found from computer simulation. Knowledge of the mathematics required to analyse stochastic models has lagged behind that used to study non-linear differential equations. Recently, more effort has been put into this area [7, 70, 75–77], although the lack of analytical studies of IBMs has held back the study of stochastic, and other effects, in models of epidemics.

We take the IBM approach in this thesis, but as well as simulating the models we also use an analytic approach to derive the emergent population level dynamics. The novel aspect of this work is that we calculate the power spectrum of the oscillations analytically and compare the results with stochastic simulations. We do this by formulating the model as a master equation which can then be studied using van Kampen’s [78] expansion in the inverse system size. The macroscopic dynamics can then be viewed as a sum of a deterministic and a stochastic part. The value of the analytic approach is that we can more easily deduce the mechanisms behind the dynamics and better understand the interplay between the deterministic and stochastic forces.

## 1.4 Outlook

This thesis aims to give a much more quantitative account of the role of stochasticity in recurrent epidemics than has been given to date. This is mainly through the use of analytic techniques to complement the traditional simulation results. This allows us to formulate a picture of epidemic dynamics which unifies previous work, especially with regards to the interaction of seasonal forcing and demographic stochasticity, and give a coherent explanation for the contrasting dynamics of measles and whooping cough.

The starting point for this thesis is the stochastic SIR model developed by Alonso *et al.* [7]. This was the first study to take a more rigorous approach to quantifying the stochastic dynamics by starting with an IBM and using analytic techniques to derive the fluctuation spectrum. Chapter 2 presents the theoretical and technical background to this thesis. It covers the derivation of the stochastic SIR model and its analysis via the master equation and the van Kampen expansion. Chapter 3 gives an in depth analysis of the dynamics of this model. In particular, we discuss the validity of the analytic techniques and the effect of including some form of spatial coupling in the form of immigration. This turns out to be an important aspect for all of the models studied in this thesis.

One of the obvious deficiencies of the basic SIR model is that the infectious period is exponentially distributed. In Chapter 4 we explore the inclusion of distributed infectious periods into the basic SIR model. This is carried out by adding a time dependence to the recovery process, and we show how this can be handled in the van Kampen scheme via the method of stages. Adding distributed periods has been shown to destabilise these models [79–81]. We quantify this effect and show how changing the distribution alters the spectrum of the fluctuations.

Chapter 5 is motivated primarily by the recent work by Nyguyen & Rohani [19], which suggests that the dynamics of whooping cough are sensitive to the distribution of the latent and infectious periods and that a deterministic model which incorporates this can then account for the interesting dynamics. To investigate this we use the staged SEIR model. With the use of a suitable approximation for the seasonal forcing we apply this model to understand the fully forced simulation results.

Chapter 6 examines the explicit inclusion of seasonal forcing in the SIR model and the master equation. We apply our method to elucidate the dynamics investigated by Earn *et al.* [35], which can account for the transitions in measles

epidemics. This is an interesting parameter regime, as the deterministic theory predicts a period doubling bifurcation. Finally, Chapter 7 gives a broad discussion of our results and areas for further research. In particular I discuss the addition of spatial aspects and the possibility of extending the analytic techniques used throughout this thesis.

# Chapter 2

## Technical background

---

This chapter outlines the theoretical and technical background to this thesis. We illustrate these general concepts with the example of the SIR model introduced by Alonso *et al.* [7], which forms the starting point for this thesis. More specific details of this model are developed in the next chapter.

### 2.1 Stochastic processes and master equations

A stochastic process is one in which a state vector,  $\mathbf{n}(t)$ , which describes a given system, evolves randomly with time [82]. If we assume a discrete state space, then  $\mathbf{n}(t)$  is an  $S$  dimensional vector of integers. This is then a jump process, where the system makes instantaneous discrete jumps between states. We can then define a state density function,  $P(\mathbf{n}, t | \mathbf{n}_0, t_0)$ , which is the probability that the system is in state  $\mathbf{n}$  at time  $t$ , given it was in state  $\mathbf{n}_0$  at time  $t_0$ . The stochastic models considered in this thesis all belong to a special class called Markov process. For these the future state of the system only depends on its current state, and not on its past history, so in terms of conditional probabilities,

$$P(\mathbf{n}_2, t_2 | \mathbf{n}_1, t_1; \mathbf{n}_0, t_0) = P(\mathbf{n}_2, t_2 | \mathbf{n}_1, t_1), \quad (2.1)$$

where  $t_2 > t_1 > t_0$ . We are interested in processes that involve random discrete events but which occur continuously in time, the canonical example of which would be a birth / death process. Ultimately we wish to derive an equation which describes the dynamics of such a system. To do this we need to assume the

form of the time dependence for the probability that the system will jump away from its current state. For a Markov process the probability of a jump from  $\mathbf{n}'$  to  $\mathbf{n}$  in the time interval  $(t, t + dt)$ , must be of the form [83],

$$T(\mathbf{n}|\mathbf{n}')dt, \quad (2.2)$$

In writing this we are assuming that the transitions follow a Poisson processes [87]. Intuitively this makes sense because the Poisson process is memory-less, i.e. the waiting time to the next transition is independent of the time waited so far, given that no transition has yet taken place [87]. We can now write,

$$P(\mathbf{n}, t + dt|\mathbf{n}', t) = T(\mathbf{n}|\mathbf{n}')dt + \left[1 - \sum T(\mathbf{n}'|\mathbf{n})dt\right] \delta_{\mathbf{n}', \mathbf{n}} \quad (2.3)$$

where the first term represents the probability of transitioning out of the state and the second term, of staying in the current state. Thus to define our system we only need to know the transition rates between different states. We are now in a position to derive an equation describing the complete dynamics of the system.

Starting with the trivial identity,

$$\begin{aligned} P(\mathbf{n}_2, t_2) &= \sum_{\mathbf{n}_1} P(\mathbf{n}_2, t_2; \mathbf{n}_1, t_1), \\ &= \sum_{\mathbf{n}_1} P(\mathbf{n}_2, t_2|\mathbf{n}_1, t_1)P(\mathbf{n}_1, t_1), \end{aligned} \quad (2.4)$$

if we now add a third conditional, and use the Markov property (2.1), we find,

$$\begin{aligned} P(\mathbf{n}_2, t_2|\mathbf{n}_0, t_0) &= \sum_{\mathbf{n}_1} P(\mathbf{n}_2, t_2|\mathbf{n}_1, t_1; \mathbf{n}_0, t_0)P(\mathbf{n}_1, t_1|\mathbf{n}_0, t_0), \\ &= \sum_{\mathbf{n}_1} P(\mathbf{n}_2, t_2|\mathbf{n}_1, t_1)P(\mathbf{n}_1, t_1|\mathbf{n}_0, t_0). \end{aligned} \quad (2.5)$$

This is known as the *Chapman-Kolmogorov equation*, and gives the probability of going from  $\mathbf{n}_0$  to  $\mathbf{n}_2$ , via all possible intermediate states,  $\mathbf{n}_1$ . In its present form, equation (2.5) is not very useful. Firstly we make a change of variables to obtain,

$$P(\mathbf{n}, t + dt|\mathbf{n}_0, t_0) = \sum_{\mathbf{n}'} P(\mathbf{n}, t + dt|\mathbf{n}', t)P(\mathbf{n}', t|\mathbf{n}_0, t_0). \quad (2.6)$$

Next we substitute in Eq. (2.3) and sum over the delta function giving,

$$\begin{aligned} P(\mathbf{n}, t + dt | \mathbf{n}_0, t_0) &= \sum_{n'} T(\mathbf{n} | \mathbf{n}') P(\mathbf{n}', t | \mathbf{n}_0, t_0) dt \\ &\quad + \left[ 1 - \sum_{n'} T(\mathbf{n}' | \mathbf{n}) dt \right] P(\mathbf{n}, t | \mathbf{n}_0, t_0). \end{aligned} \quad (2.7)$$

Subtracting a factor of  $P(\mathbf{n}, t | \mathbf{n}_0, t_0)$  from both sides of (2.7) and dividing through by  $dt$ ,

$$\begin{aligned} \frac{P(\mathbf{n}, t + dt | \mathbf{n}_0, t_0) - P(\mathbf{n}, t | \mathbf{n}_0, t_0)}{dt} &= - \sum_{n'} T(\mathbf{n}' | \mathbf{n}) P(\mathbf{n}, t | \mathbf{n}_0, t_0) \\ &\quad + \sum_{n'} T(\mathbf{n} | \mathbf{n}') P(\mathbf{n}', t | \mathbf{n}_0, t_0). \end{aligned} \quad (2.8)$$

Now taking the limit  $dt \rightarrow 0$ , we obtain the master equation,

$$\frac{dP(\mathbf{n}, t)}{dt} = \sum_{n' \neq n} T(\mathbf{n} | \mathbf{n}') P(\mathbf{n}', t) - \sum_{n' \neq n} T(\mathbf{n}' | \mathbf{n}) P(\mathbf{n}, t). \quad (2.9)$$

This describes the time evolution of the probability distribution of finding the system in state  $\mathbf{n}$  at time  $t$ . Simply, the change in  $P(\mathbf{n}, t)$  is equal to the sum of the transitions into the state  $\mathbf{n}$ , minus the transitions out of the state. Note that we have dropped the dependence of Eq. (2.9) on  $(\mathbf{n}_0, t_0)$ , which is fixed by an initial condition,  $P(\mathbf{n}, 0) = \delta_{\mathbf{n}, \mathbf{n}_0}$ . If we could solve the master equation for  $P(\mathbf{n}, t)$ , we would obtain a complete description of the stochastic system from which physical quantities, such as moments, can in principle be calculated. In practice, for all but the simplest systems, this is impossible. Sections 2.3 and 2.4 detail two different methods we can use to solve the master equation. The next section illustrates this general background with the example of an individual-based stochastic SIR model [7].

## 2.2 A stochastic SIR model

We consider a closed population of individuals who belong to one of three classes, susceptible, infected or recovered ( $S, I, R$ ). We want to define this in such a way that in the limit  $N \rightarrow \infty$  this becomes the deterministic model defined in Section 1.2. Birth and death rates are set equal to  $\mu$ , and these events are linked, so that the total population  $N = S + I + R$  remains constant. This allows for

the elimination of the variable relating to recovered individuals, reducing the state space down to 2 dimensions. Frequently birth and death processes are assumed to happen at the same rate, but remain as distinct events; this results in fluctuations in the total population size for finite systems. By linking these events at the stochastic level, the population size remains constant at any system size, so that we can still eliminate the variable relating to recovered individuals. This only has an effect on the dynamics for very small populations.

The population is assumed to be homogeneously mixed, with a constant contact rate,  $\beta$  between individuals. Again as  $\beta$  is independent of  $N$ , we are assuming frequency-dependent mixing [31]. Recovery happens at a rate  $\gamma$ , thus the infectious period is exponentially distributed with mean  $1/\gamma$ . We also mimic some sort of spatial coupling to an external reservoir of the disease. We use a commuter formulation, where susceptibles are in contact with a pool of infectives outside the main population [7, 84]. This happens at a small constant rate  $\eta$ . The full consequences of this addition and the importance of the immigration process are studied in the next chapter.

The probability of any event is then independent and only depends on the probabilities of choosing the various individuals from the population as a whole and the rates at which they occur. The state of the system is defined by two integers  $\mathbf{n} \equiv \{S, I\}$  and the transition rates which define the model are:

- (i) Infection:  $S + I \xrightarrow{\beta} I + I$  and  $S \xrightarrow{\eta} I$ .

$$T(S - 1, I + 1 | S, I) = \left( \beta \frac{S}{N} I + \eta S \right). \quad (2.10)$$

- (ii) Recovery:  $I \xrightarrow{\gamma} R$ .

$$T(S, I - 1 | S, I) = \gamma I. \quad (2.11)$$

- (iii) Death of an infected individual:  $I \xrightarrow{\mu} S$ .

$$T(S + 1, I - 1 | S, I) = \mu I. \quad (2.12)$$

- (iv) Death of a recovered individual:  $R \xrightarrow{\mu} S$ .

$$T(S + 1, I | S, I) = \mu(N - S - I), \quad (2.13)$$

We can now write down a master equation for this model. Preempting the analysis of the master equation in Section 2.4, we introduce step operators which allow us to express the master equation in a more compact form. These are defined by their action on the general function  $f(S, I, t)$  as,

$$\begin{aligned}\mathbb{E}_I^{\pm 1} f(S, I, t) &= f(S, I \pm 1, t), \\ \mathbb{E}_S^{\pm 1} f(S, I, t) &= f(S \pm 1, I, t).\end{aligned}\tag{2.14}$$

The full master equation can then be written as,

$$\begin{aligned}\frac{d}{dt} P(S, I, t) = &\left\{ (\mathbb{E}_S \mathbb{E}_I^{-1} - 1) \left( \beta \frac{S}{N} I + \eta S \right) \right. \\ &+ (\mathbb{E}_S^{-1} - 1) \mu (N - S - I) \\ &\left. + (\mathbb{E}_I \mathbb{E}_S^{-1} - 1) \mu I + (\mathbb{E}_I - 1) \gamma I \right\} P(S, I, t).\end{aligned}\tag{2.15}$$

The master equation itself is a large,  $O(N^3)$ , set of coupled ordinary differential equations and so cannot be solved easily. For smaller systems it is possible to numerically integrate this set of equations, but as  $N$  increases this becomes impractical very quickly [85]. There are two approaches we use: conventional Monte-Carlo simulation [86], and an approximate solution scheme developed by van Kampen, valid in the limit of large system sizes [78]. We now describe these in turn.

## 2.3 Monte-Carlo simulation

We can consider the master equation as simultaneously solving for all possible trajectories of the system. In general this will be impossible, but it is easy to solve for a single trajectory,  $\mathbf{n}(t)$  for which  $P(\mathbf{n}, t)$  is the underlying probability distribution. One can then compute statistical quantities such as correlations and means by averaging over many realisations of a given trajectory. In this section we discuss some of the methods for doing this and some of the extensions which are useful for efficient computation.

Just as the master equation is a direct consequence of the assumption (2.2), we can also derive from the same assumption the *next reaction density function*,  $P(\tau, j|\mathbf{n}, t)$ , where  $P(\tau, j|\mathbf{n}, t)d\tau$  is the probability that the next reaction will

occur in the interval  $(t + \tau, t + \tau + d\tau)$  and will be of type  $j$  [86]. Firstly we define the propensity function for each reaction as,

$$a_k(\mathbf{n}) = T(\mathbf{n} + \mathbf{v}_k | \mathbf{n}) \quad (2.16)$$

where  $\mathbf{v}_k$  is a vector representing the change in state caused by the  $k$ 'th reaction. So for example, for reaction (iii) in the SIR model,  $a_3(S, I) = \mu I$  and  $\mathbf{v}_3 = (+1, -1)$ . Assuming there are a total of  $q$  reactions, the probability that no reaction will have happened by time  $\tau$  is  $\exp(-\sum_k a_k(\mathbf{n})\tau)$  [86], then

$$P(\tau, j | \mathbf{n}, t) = a_j(\mathbf{n}) \exp\left(-\sum_{k=1}^q a_k(\mathbf{n})\tau\right). \quad (2.17)$$

From this one can then use Monte-Carlo methods to generate a random pair  $(\tau, j)$  according to the distribution  $P(\tau, j | \mathbf{n}, t)$ , which gives the time to the next reaction and the type. The simplest scheme for this is called Gillespie's direct method or the stochastic simulation algorithm [86]. One step of the algorithm involves drawing a pair of uniform  $(0, 1]$  random numbers,  $(r_1, r_2)$ . The time to the next reaction is then given by  $\tau = 1/a_0 \ln(1/r_1)$ , where  $a_0 = \sum_k a_k(\mathbf{n})$ . Next we find  $j \in [1, \dots, q]$  from,

$$\sum_{k=1}^{j-1} a_k < r_2 a_0 \leqslant \sum_{k=1}^j a_k \quad (2.18)$$

Finally,  $t = t + \tau$ , and the state,  $\mathbf{n}$ , and propensities are updated to reflect the chosen event. This method is sufficient for simulating the SIR model defined in the previous section.

The direct method is easy to implement and efficient, but there are two areas where it does not perform well: when the propensities are time-dependent, as in Chapter 6, or if the waiting times for a given reaction are not exponentially distributed, as we have been implicitly assuming up to this point. In Chapter 4 I show how processes with arbitrary waiting time distributions can be recast as chains of reactions with exponential waiting times [87]; this is one way to circumvent this problem, although these are very inefficient to simulate. In order to accommodate these complications in an efficient manner it is necessary to use a different Monte-Carlo scheme based on Gillespie's first reaction method [86]. The original algorithm can be summed up as:

- (i) Calculate putative waiting times,  $\Delta t_k = \ln(1/r_k)/a_k$ , for each reaction, where  $r_k$  is a uniform  $(0, 1]$  random number. This is essentially drawing times from an exponential distribution.
- (ii) Let  $j$  be the reaction whose putative time is least and set  $\tau = \min\{\Delta t_k\}$ .
- (iii) Update  $t \rightarrow t + \Delta t_j$ , update  $\mathbf{n}$ , recalculate  $a_k(\mathbf{n})$ .
- (iv) Repeat from step 1.

Essentially we compute the putative times for all reactions then implement the one with the smallest time. This can be shown to be equivalent to the Direct method [86], but is clearly much less efficient as it requires the generation of  $q$  random numbers for each time step, instead of two for the direct method. The next reaction method of Gibson & Bruick [88] and the modified next reaction method of Anderson [89] deal with how one can reuse the random numbers and circumvent this inefficiency.

Both time-dependent propensities and non-exponential waiting times can easily be incorporated into this method. Different distributions are incorporated by changing Step 1 to draw random numbers from those distributions, for example a gamma distribution [88]. If there is a time-dependent propensity,  $a_k(\mathbf{n}, t)$ , then we change the second step to calculate the putative time for that reaction. This is found from solving

$$\int_t^{t+\Delta t_k} a_k(\mathbf{n}, s) ds = \ln(1/r_k), \quad (2.19)$$

for  $\Delta t_k$ . For the simulations in Chapter 6, where this is used, there is only one time-dependent propensity and this varies like a step function. Thus (2.19) can be solved exactly with a two step Newton-Raphson method [32].

The most computationally expensive parts of any algorithm are searching for the smallest putative time and updating the propensities  $a_k(\mathbf{n})$  after each reaction. The latter is easily made more efficient with the use of a dependency graph, which lists the minimum number of propensities that need to be updated, given that a certain reaction has occurred [88]. The search algorithm can be sped up with the use of an efficient data structure to store the reaction times, such as an indexed priority queue or a binary tree [88, 90, 91]. For a system with a small number of reactions these additions to the basic algorithm give little benefit, but for larger systems and ones with spatial structure these become necessary.

## 2.4 Expansion of the master equation

The van Kampen expansion is a method for deriving an approximate solution of a master equation [78, 92], valid in the limit of large system sizes. I first discuss this using the example of the SIR model and give the general case in Section 2.4.1.

The master equation (2.15) describes the complete behaviour of the stochastic SIR system, so it describes the macroscopic behaviour plus fluctuations about this. It just so happens that for the SIR model these fluctuations are large (see Figure 2.1), but both parts of the dynamics arise directly from the master equation which is formulated in terms of individual jumps between discrete states. The van Kampen expansion is essentially a perturbative expansion in powers of the inverse system size,  $N$ , which allows one to formally extract these two parts.

It is based on the assumption that when  $N$  is large, the values of the variables ( $S, I$ ) are large, but the size of internal the jumps between states are small ( $\pm 1$  individual). A corollary to this is that the transition rates must scale in the correct way if an expansion is to be possible. They have to be able to be written in terms of the macroscopic variables and the total jump size [82], i.e.

$$T(\mathbf{n}'|\mathbf{n}) = N\Psi\left(\frac{\mathbf{n}}{N}; \Delta\mathbf{n}\right) \quad (2.20)$$

where  $\Delta\mathbf{n} = \mathbf{n}' - \mathbf{n}$ . One can easily see that for the transition rates given in Section 2.2, and indeed all other rates used in this thesis, that this is true; the jump size is fixed and all rates can be written in terms of macroscopic variables.

The fundamental step in carrying out the expansion is in positing an ansatz for the form of the approximate solution. We know that as  $N \rightarrow \infty$  then the solutions will become deterministic, so we can write:  $S = N\phi$  and  $I = N\psi$ , where  $\phi$  and  $\psi$  are macroscopic variables (the densities of  $S$  and  $I$  respectively). For large, but finite  $N$ , we expect that  $P(S, I, t)$  will have a sharp peak with position of order  $N$  and a width of order  $N^{1/2}$ , by the central limit theorem. This suggests the form for our ansatz,

$$\begin{aligned} S &= N\phi + N^{\frac{1}{2}}x, \\ I &= N\psi + N^{\frac{1}{2}}y, \end{aligned} \quad (2.21)$$

where  $x$  and  $y$  are stochastic variables which describe the fluctuations. The

solutions we derive from the expansion will justify the ansatz.

The most straightforward way to expand the master equation (2.15) is to consider the form of the step operator as functions of  $x$  and  $y$ . So for example,  $\mathbb{E}_I$  takes  $I$  to  $I + 1$  and therefore  $\mathbb{E}_I f(y) \rightarrow f(y + N^{-1/2})$ . Taylor expanding the function  $f(y + N^{-1/2})$  gives us the form of the operator in powers of  $N^{-1/2}$ , so in general we get,

$$\begin{aligned}\mathbb{E}_S^{\pm 1} &= 1 \pm N^{-\frac{1}{2}} \frac{\partial}{\partial x} + \frac{1}{2} N^{-1} \frac{\partial^2}{\partial x^2} \pm \dots \\ \mathbb{E}_I^{\pm 1} &= 1 \pm N^{-\frac{1}{2}} \frac{\partial}{\partial y} + \frac{1}{2} N^{-1} \frac{\partial^2}{\partial y^2} \pm \dots\end{aligned}\quad (2.22)$$

Finally we have to write the distribution  $P$  in terms of the new variables  $x$  and  $y$ , thus,  $P(S, I, t) = \Pi(x, y, t)$ . Differentiating this with respect to time, we obtain the relation,

$$\frac{\partial P}{\partial t} = \frac{\partial \Pi}{\partial t} + \frac{dx}{dt} \frac{\partial \Pi}{\partial x} + \frac{dy}{dt} \frac{\partial \Pi}{\partial y}. \quad (2.23)$$

To calculate the factors  $dx/dt$ , we need to remember that when we take the time derivative in Eq. (2.15) we hold  $S$  and  $I$  constant. Taking the derivative of Eq. (2.21) we find,  $dx/dt = -N^{1/2}d\phi/dt$ . This give the expression,

$$\frac{\partial P}{\partial t} = \frac{\partial \Pi}{\partial t} - N^{\frac{1}{2}} \frac{d\phi}{dt} \frac{\partial \Pi}{\partial x} - N^{\frac{1}{2}} \frac{d\psi}{dt} \frac{\partial \Pi}{\partial y}. \quad (2.24)$$

The expansion is carried out by substituting Eqs. (2.21), (2.22) and (2.24) into Eq. (2.15) and equating powers of  $N$ . Equating powers of  $N^{\frac{1}{2}}$ , we find a pair of deterministic mean-field equations,

$$\begin{aligned}\dot{\phi} &= -\beta\phi\psi - \eta\phi + \mu(1 - \phi), \\ \dot{\psi} &= \beta\phi\psi + \eta\phi - (\mu + \gamma)\psi.\end{aligned}\quad (2.25)$$

These correspond to the usual phenomenological SIR equations (1.2), but rescaled and with the additional terms  $\eta\phi$  accounting for immigration. After removing the  $N^{1/2}$  terms from the expansion we are left with a hierarchy of equations in terms of powers of  $N^{-1/2}$  for  $\Pi(x, y, t)$ . To first order,  $N^0$ , this is a linear Fokker-Planck

equation which describes the time evolution of  $\Pi(x, y, t)$ ,

$$\begin{aligned} \frac{\partial \Pi}{\partial t} = & [\beta\psi + \eta + \mu] \frac{\partial}{\partial x}(x\Pi) + [\beta\phi] \frac{\partial}{\partial x}(y\Pi) \\ & + [-\beta\psi - \eta] \frac{\partial}{\partial y}(x\Pi) + [-\beta\phi + \mu + \gamma] \frac{\partial}{\partial y}(y\Pi) \\ & + \frac{1}{2} [\beta\phi\psi + \eta\phi + \mu(1 - \phi)] \frac{\partial^2 \Pi}{\partial x^2} + \frac{1}{2} [\beta\phi\psi + \eta\phi + (\mu + \gamma)\psi] \frac{\partial^2 \Pi}{\partial y^2} \\ & - [\beta\phi\psi + \eta\phi + \mu\psi] \frac{\partial^2 \Pi}{\partial x \partial y}. \end{aligned} \quad (2.26)$$

The solution of this is a simple multi-variate Gaussian [78], with zero mean ( $\langle x \rangle = \langle y \rangle = 0$ ).

At this point it is easier to see what the expansion does. We have approximated  $P(S, I, t)$  by a Gaussian with a mean that follows the deterministic equations (2.25) and whose width is determined from Eq. (2.26). The form of (2.26) justifies the ansatz as it does not depend on  $N$  so the fluctuations are of the order  $N^{1/2}$  as postulated in the ansatz; this is known as the linear noise approximation [78]. Higher-order corrections can be included in the expression for  $\Pi$ , but these only give deviations from the Gaussian form; this is discussed further for the SIR model in Section 3.3.

### 2.4.1 General expansion

The system-size expansion detailed in the previous section is easily generalised to higher-dimensional systems, such as are considered in Chapters 4 and 5. We assume we have a master equation (2.9) for a set of  $n_i$  stochastic variables, which can be written in terms of step operators,  $\mathbb{E}_{n_i}^{\pm 1}$ . Assuming the transition rates scale with  $N$  in the correct way [78, 82], we introduce a set of ansaetze,  $n_i = N\theta_i(t) + N^{1/2}x_i$ , where  $\theta_i$  are macroscopic variables and  $x_i$  are stochastic corrections.

To expand the master equation we first introduce the fluctuation probability distribution,  $\Pi(\mathbf{x}, t)$ , for which one can derive the relation,

$$\frac{dP}{dt} = \frac{\partial \Pi(\mathbf{x}, t)}{\partial t} - N^{1/2} \sum_i \dot{\theta}_i \frac{\partial \Pi}{\partial x_i}, \quad (2.27)$$

where we have used the fact that  $dx_i/dt = -N^{1/2}d\theta_i/dt$ . Next we expand the

step operators in terms of  $x_i$ ,

$$\mathbb{E}_{n_i}^{\pm 1} = 1 \pm N^{-\frac{1}{2}} \frac{\partial}{\partial x_i} + \frac{1}{2} N^{-1} \frac{\partial^2}{\partial x_i^2} \pm \dots \quad (2.28)$$

Substituting into the master equation, one finds a common structure to the transition rates and operators [93], which allows easy identification of the different orders of the  $N^{-1/2}$  hierarchy. At leading order ( $N^{1/2}$ ), we find a set of deterministic equations,

$$\dot{\theta}_i(t) = \alpha_i(\boldsymbol{\theta}(t)), \quad (2.29)$$

for the macroscopic variables. Taking the example of the SIR model,  $\alpha_1 = -\beta\phi\psi - \eta\phi + \mu(1 - \phi)$ . The functions  $\alpha_i$  then depend on time through the constants and the variables  $\boldsymbol{\theta}$ . Subtracting these terms from the expansion, we are left with a proper expansion in terms of  $N^{-1/2}$  for  $\Pi(\mathbf{x}, t)$ . Thus at next to leading order ( $N^0$ ) we obtain a linear Fokker-Planck equation [94] of the form,

$$\frac{\partial \Pi}{\partial t} = - \sum_{i,j} A_{ij}(\boldsymbol{\theta}) \frac{\partial[x_j \Pi]}{\partial x_i} + \frac{1}{2} \sum_{i,j} B_{ij}(\boldsymbol{\theta}) \frac{\partial^2 \Pi}{\partial x_i \partial x_j}, \quad (2.30)$$

where  $A$  is the drift matrix, which is equal to the Jacobian of the deterministic equations (2.29), and  $B$  is the diffusion matrix, which encodes the structure of the noise. This procedure is completely general, but progress can only be easily made when we know the solutions to equation (2.29). This is usually a fixed point, but in Chapter 6 it is a limit cycle.

A number of similar techniques to the system size expansion have been developed. The most notable is the theorem due to Kurtz [95, 96], which is essentially a mathematically rigorous derivation of the van Kampen result. This result is also known colloquially as the diffusion approximation, and has been widely used in theoretical ecology [63, 97].

## 2.4.2 Langevin formalism

To quantify the fluctuations it is easier to work with the stochastic trajectories,  $\mathbf{x}(t)$ , for which  $\Pi(\mathbf{x}, t)$  is the underlying probability distribution. It can be shown that a linear Fokker-Planck equation (2.30) is equivalent to a set of first-order

stochastic differential equations of the form [78, 82],

$$\frac{dx_i}{dt} = \sum_j A_{ij}(\boldsymbol{\theta})x_j + \xi_i(t), \quad (2.31)$$

where the  $\xi_i(t)$  are noise terms which represent the aggregate effects of demographic stochasticity on the system. These are known as Langevin equations, after Paul Langevin, who originally derived them in relation to Brownian motion [82]. For a complete specification of equation (2.31) we need to know the statistics of  $\xi_i(t)$ . These statistics are Gaussian because, following from the central limit theorem, the noise is an aggregate of many independent random events. The first moment is  $\langle \xi_i(t) \rangle = 0$  as any mean motion would be included in the deterministic part of (2.31). The second moment is given by,

$$\langle \xi_i(t) \xi_j(t') \rangle = B_{ij}(\boldsymbol{\theta})\delta(t - t'). \quad (2.32)$$

where  $B_{ij}(\boldsymbol{\theta})$  is found from Eq. (2.30). Higher order odd moments are zero, due to the Gaussian nature of the noise, and even ones can be calculated in terms of Eq. (2.32). The delta function means the noise is uncorrelated in time, which is known as white noise. We can calculate the power spectrum of the noise via the Wiener-Khinchin theorem [87],

$$\begin{aligned} \langle |\tilde{\xi}(\omega)|^2 \rangle_{jk} &= \int_{-\infty}^{+\infty} e^{-i\omega t} \langle \xi_j(t) \xi_k(0) \rangle dt \\ &= B_{jk}(\boldsymbol{\theta}). \end{aligned} \quad (2.33)$$

Thus the power spectrum of white noise is flat, indicating an equal power at all frequencies, where the strength of this noise is determined by the matrix  $B$ .

Returning to the SIR model, the stochastic fluctuations are described by a pair of Langevin equations,

$$\begin{aligned} \dot{x} &= a_{11}x + a_{12}y + \xi_1(t), \\ \dot{y} &= a_{21}x + a_{22}y + \xi_2(t). \end{aligned} \quad (2.34)$$

with noise correlators  $\langle \xi_i(t) \xi_j(t') \rangle = B_{ij}\delta(t - t')$ . With reference to the Fokker-Planck equation (2.26) we can read off the Jacobian and noise correlators matrices

as,

$$a = \begin{pmatrix} -\beta\psi - \eta - \mu & -\beta\phi \\ \beta\psi + \eta & \beta\phi - \gamma - \mu \end{pmatrix}, \quad (2.35)$$

and

$$\begin{aligned} B_{11} &= \beta\phi\psi + \eta\phi + \mu(1 - \phi), \\ B_{22} &= \beta\phi\psi + \eta\phi + (\gamma + \mu)\psi, \\ B_{21} = B_{12} &= -\beta\phi\psi - \eta\phi - \mu\psi. \end{aligned} \quad (2.36)$$

To quickly recap this section: the expansion decomposes the population level dynamics of a discrete stochastic model into a macroscopic component, modelled by a set of deterministic equations which scale with  $N$ , plus a stochastic component which scales with  $N^{1/2}$  and can be modeled by a Langevin equation (2.31). In the final sections of this chapter we look at the typical dynamics which these models display and how we can use the equations derived from the expansion to quantify them.

## 2.5 Deterministic dynamics

In general, the deterministic equations describing the macroscopic behaviour are non-linear and so cannot be solved in closed form; instead they must be integrated numerically. For the models considered in this thesis the dynamics either tend to a fixed point or, as in Chapter 6, a limit cycle [98]. The analysis of both these cases share many similarities, but we leave the discussion of the limit cycle case to Chapter 6. One can easily find any macroscopic fixed points,  $\theta_i^*$  by setting the left hand side of Eq. (2.29) to zero and solving the resulting equations. Linear stability analysis is the investigation of how small perturbations to a fixed point evolve with time. Thus if perturbations decay, the fixed-point is stable. Substituting  $\theta_i = \theta_i^* + x_i$  into equation (2.29) and retaining only linear terms, we obtain the equation,

$$\dot{\mathbf{x}} = A(\boldsymbol{\theta}^*)\mathbf{x}, \quad (2.37)$$

where,

$$A_{ij}(\boldsymbol{\theta}^*) = \left[ \frac{\partial}{\partial \theta_j} \alpha_i(\boldsymbol{\theta}) \right]_{\boldsymbol{\theta}=\boldsymbol{\theta}^*}, \quad (2.38)$$

is the Jacobian evaluated at the fixed-point. By examining the eigenvalues,  $\lambda_i$ , of the Jacobian we can investigate the stability of the fixed points [98, 99].

If the dimension of  $A$  is  $S$ , there will be  $S$  complex eigenvalues. For stability,  $\text{Re}(\lambda_i) < 0$ , for all the eigenvalues. Imaginary parts indicate that perturbations return to the fixed point in a spiral manner, which is true for the SIR model, see Figure 1.4. The approximate periods of these oscillations will be equal to  $\text{Im}(\lambda_i)/2\pi$ . Note that Eq. (2.37) is the same as the Langevin equations (2.31), except for the noise terms,  $\xi_i(t)$ . This is significant and in the next section we show that the deterministic stability of a fixed point and stochastic fluctuation spectrum are intimately connected.

## 2.6 Stochastic fluctuations

As discussed in the introduction, if a deterministic system shows damped oscillations, then simulation of the corresponding IBM shows quasi-cycle oscillations [6, 68]. A deterministic solution along with two realisations of the IBM for the SIR model are shown in Figure 2.1. These oscillations are large and so clearly the stochastic corrections to the deterministic solutions are important. The periodicity of these oscillations can be quantified by calculating their power spectrum. This shows how the variance of the fluctuations is distributed over different spectral frequencies. A sharply peaked spectrum indicates structured oscillations with a dominant frequency where the spectrum is peaked.

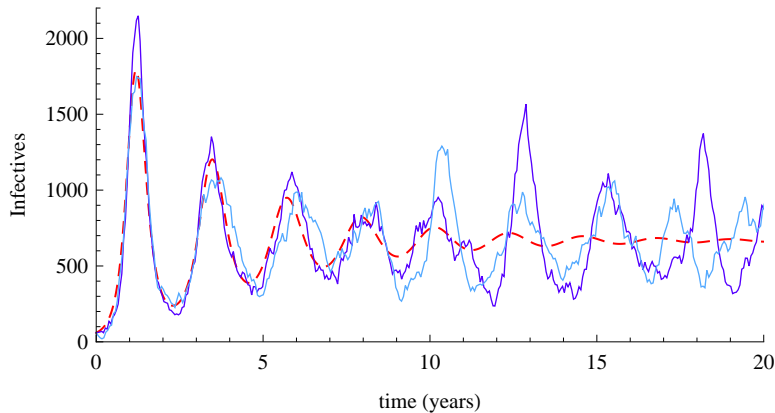


Figure 2.1: A deterministic solution (red dashed curve) and two realisations of the individual based SIR model, showing strong stochastic oscillations. Parameters:  $N = 10^6$ ,  $\beta = 1.175$ ,  $\gamma = 0.077$ . Both simulations are started with the same initial conditions. After a while they go out of phase.

We can calculate the power spectrum two ways: either directly from simulations using a standard fast Fourier transform algorithm (FFT) [32], or analytically

via the Langevin equations (2.31). Firstly, the Fourier transform is defined as,

$$\tilde{f}(\omega) = \int_{-\infty}^{+\infty} f(t)e^{-i\omega t} dt. \quad (2.39)$$

Note that because the limits are  $\pm\infty$ , we have to assume that all transients and end point effects have damped down, otherwise equation (2.39) would not apply. For the SIR model, taking the Fourier transform of Eqs. (2.34) we obtain,

$$\begin{aligned} (-i\omega - a_{11})\tilde{x} - a_{12}\tilde{y} &= \tilde{\xi}_1, \\ -a_{21}\tilde{x} + (-i\omega - a_{22})\tilde{y} &= \tilde{\xi}_2, \end{aligned} \quad (2.40)$$

where a tilde represent the Fourier transform. Solving for  $\tilde{x}$  and  $\tilde{y}$  we find,

$$\begin{aligned} \tilde{x}(\omega) &= \frac{a_{12}\tilde{\xi}_2 - a_{22}\tilde{\xi}_1 - i\omega\tilde{\xi}_1}{D(\omega)}, \\ \tilde{y}(\omega) &= \frac{a_{21}\tilde{\xi}_1 - a_{11}\tilde{\xi}_2 - i\omega\tilde{\xi}_2}{D(\omega)}, \end{aligned} \quad (2.41)$$

where the denominator,  $D(\omega)$ , is given by

$$D(\omega) = (-i\omega)^2 - (a_{11} + a_{22})(-i\omega) + [a_{11}a_{22} - a_{12}a_{21}]. \quad (2.42)$$

Next we take the Fourier transform of eq (2.32) to get,

$$\langle \xi_i(\omega)\xi_j(\omega') \rangle = 2\pi B_{ij}\delta(\omega + \omega'). \quad (2.43)$$

The power spectrum is the ensemble average of the squared moduli, so for the infective time series we obtain,

$$P_I(\omega) = \langle |\tilde{y}(\omega)|^2 \rangle = \frac{\alpha_I + B_{22}\omega^2}{|D(\omega)|^2}, \quad (2.44)$$

where  $\alpha_I = B_{22}a_{11}^2 + B_{11}a_{21}^2 - 2B_{12}a_{21}a_{11}$ . The elements of the Jacobian,  $a$ , are evaluated at the fixed point after transients have damped down. The denominator can be rewritten to give

$$P_I(\omega) = \frac{\alpha_I + B_{22}\omega^2}{(\omega^2 - \Omega_0^2)^2 + \Gamma^2\omega^2}, \quad (2.45)$$

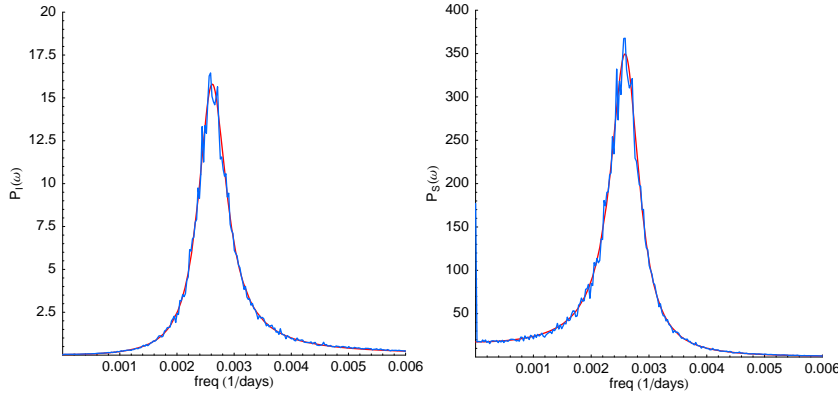


Figure 2.2: Power spectra for the stochastic SIR model. Theory from eq (2.45) (red curve) and from simulation of the stochastic model (blue curve). Parameters as in Figure 2.1.

where,  $\Gamma = \text{tr}(a)$ ,  $\Omega_0^2 = \det(a)$ . These spectra are shown in Figure 2.2, along with results from simulations and the agreement is excellent.

We use two main measures of the power spectrum: the peak frequency and the amplification. The amplification is proportional to the total area under the power spectrum curve and the spectrum is normalised so that the amplification corresponds to the mean squared amplitude of the fluctuations, i.e.,

$$A_0 = \frac{1}{2\pi} \int_0^\infty P_I(\omega) d\omega = \frac{1}{365} \int_0^\infty P_I(f) df = \langle y^2 \rangle, \quad (2.46)$$

where the frequency is in years<sup>-1</sup>. In this thesis we use the one-sided definition for the power spectrum, which assumes the range of  $\omega$  to be  $(0, \infty)$ ; Figure 2.3 shows a typical time series and power spectrum. A third measure that is sometimes useful is the coherence [7]. This measures how much power is centred around the main peak, thus a large coherence will show very regular oscillations and a low coherence more irregular oscillations.

One important point for correct normalisation is how the discrete power spectrum from the simulations and the analytic spectrum are related. Firstly we define the points of our discrete function as  $f_n = f(\Delta n)$  where  $\Delta$  is the sampling interval and  $n$  an integer. If the number of points sampled is  $N$  then the length is  $T = (N - 1)\Delta$ . To match the analytic spectrum, our discretised version must

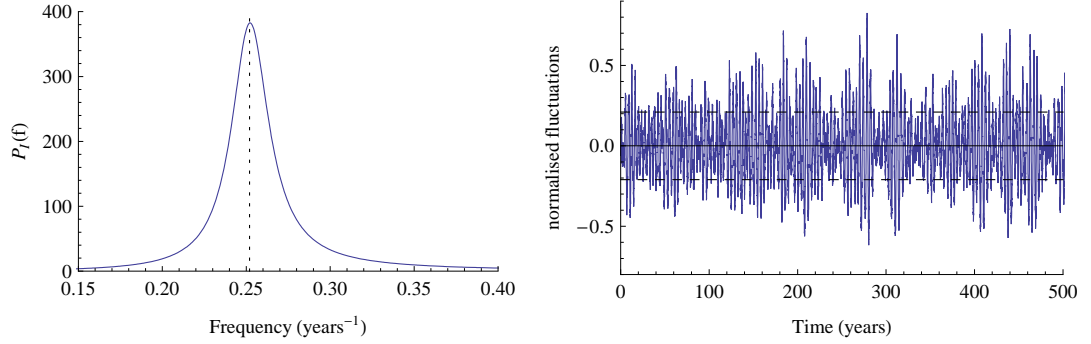


Figure 2.3: Theoretical power spectrum and the normalised fluctuations of the total infective time series. The amplification  $A_0 = 0.044$  and peak frequency is  $0.252 \text{ years}^{-1}$ . The dashed lines show the RMS value for the time series which is equal to  $\sqrt{A_0}$ .

satisfy,

$$A_0 = \frac{1}{N} \sum_{n=0}^{N-1} |f_n|^2 = \frac{1}{\Delta N} \sum_{k=0}^{N-1} P_k, \quad (2.47)$$

where  $P_k$  are the points of the power spectrum. This is essentially just restating that the area under the discrete numerical spectrum should be equal to the amplification, as in equation (2.46). The problem now is to relate the discrete Fourier coefficients from the FFT of the time-series [32],

$$C_k = \frac{1}{N} \sum_{n=0}^{N-1} f_n e^{-2\pi i kn/N}, \quad (2.48)$$

to the power spectrum. The discrete version of Parseval's theorem is [22],

$$\sum_{n=0}^{N-1} |f_n|^2 = \frac{1}{N} \sum_{k=0}^{N-1} |C_k|^2. \quad (2.49)$$

Substituting this into Eq. (2.47) we find,

$$\frac{1}{N^2} \sum_{k=0}^{N-1} |C_k|^2 = \frac{1}{\Delta N} \sum_{k=0}^{N-1} P_k. \quad (2.50)$$

Thus by inspection we see that  $P_k = \Delta/N|C_k|^2$  for correct normalisation.

### 2.6.1 General power spectra

We can learn a lot about the form of the power spectrum by considering the general case. Taking the Fourier transform of Eq. (2.31) we get,

$$\sum_j (A_{ij} - i\omega \delta_{ij}) \tilde{x}_j = \tilde{\xi}_i, \quad (2.51)$$

where  $\tilde{x}_j$  and  $\tilde{\xi}_i$  are the Fourier transforms of  $x_j$  and  $\xi_i$  respectively. If we define  $S_{ij} = (A_{ij} - i\omega \delta_{ij})$  then the solution can be written as [100],

$$\tilde{x}_i(\omega) = \sum_j S_{ij}^{-1}(\omega) \tilde{\xi}_j(\omega). \quad (2.52)$$

So the power spectrum is,

$$P_l(\omega) = \left\langle |\tilde{x}_l(\omega)|^2 \right\rangle = 2 \sum_j \sum_k S_{lj}^{-1} B_{jk} (S^{-1})_{kl}^\dagger. \quad (2.53)$$

The factor of 2 appears because we use the one-sided definition for the power spectrum, which takes the range of  $\omega$  to be  $(0, \infty)$ . This expression involves the inverse of matrix  $S$ , which is proportional to  $1/\det(S)$ . This is independent of  $l$  and equal to  $1/|J - i\omega \mathbb{I}|$ . Diagonalising the Jacobian we can then write the denominator of Eq. (2.53) as,

$$\prod_j |\lambda_j - i\omega|^2, \quad (2.54)$$

where  $\lambda_j$  are the eigenvalues of the Jacobian  $J$ . Inspection of (2.54) shows why the form of the spectrum is closely related to the eigenvalues found from a linear stability analysis. The denominator is a polynomial in  $\omega$  and if there is a complex conjugate pair of eigenvalues then we expect to see minimum in  $D(\omega)$ , and thus a peak in the spectrum when  $\omega = \text{Im}(\lambda_i)$ . At these points the relative amplitude of the spectrum will be proportional to  $1/|\text{Re}(\lambda_i)|^2$ . This is exactly what one would expect from considering only a deterministic analysis of the linearised system, although it is not exact because the numerator of (2.53) is also polynomial in  $\omega$ . In general the numerator will depend on  $l$  and this gives different shapes to the various spectra (see Figure 2.2). It also shifts the peak frequencies from that found by a purely deterministic analysis. The magnitude of this effect is usually

small for the epidemic models considered in this thesis, but can be significant in other models [68].

### 2.6.2 Stochastic amplification

There are a number of ways we can interpret the stochastic dynamics of these types of models which show large oscillations. Firstly we can understand the deterministic results as the limit of many realisations of the underlying stochastic model. This explains why the deterministic dynamics show damped oscillations. The stochastic fluctuations are quasi-cycles, which means there is a natural variability in the period of the oscillation (the power spectrum has a width), thus stochastic realisations will go out of phase after a while, see Figure 2.1. The deterministic result is obtained in the limit of many averaged realisations, so the damping reflects the fact that the oscillations go out of phase [61, 101]. The more coherent the power spectrum (the narrower the width [7]), the longer realisations will take to go out of phase, thus the deterministic result shows a longer damping time. This agrees with the discussion above on the relation between the eigenvalues and the power spectrum.

The Langevin equations afford another phenomenological view of the dynamics. We can draw a parallel between the Langevin equations for the SIR model (2.34) and a simple forced oscillator. The equation of motion for a simple mass on a spring, moving in a viscous medium and subject to a sinusoidal forcing is [102],

$$m\ddot{x} + b\dot{x} + kx = F_0 \cos(\omega t). \quad (2.55)$$

Calculating the amplitude of oscillation as a function of the forcing frequency  $\omega$  we find,

$$A(\omega) = \frac{F_0/m}{[(\omega_0^2 - \omega^2)^2 + \gamma\omega^2]^{1/2}}. \quad (2.56)$$

One can see a close correspondence with the expression for the power spectrum of the SIR model, equation (2.45). This can be made a little more clear by introducing a variable for the velocity,  $v = \dot{x}$ , in which case we find,

$$\begin{aligned} m\dot{v} + bv + kx &= F_0 \cos(\omega t) \\ \dot{x} &= v \end{aligned} \quad (2.57)$$

which are similar to the Langevin equations (2.34), except that the forcing is only

applied to one of the variables. The main difference between the two is that in the simple physics example the forcing is only applied at a single frequency; in the Langevin equations the system is driven by white noise, thus it excites *all* the frequencies of the power spectrum, not just one. This is known as stochastic amplification [68]. Another account of the same phenomenon goes by the name coherence resonance [70].

## 2.7 Summary

This chapter has set the theoretical background for the rest of this thesis. We have defined a discrete stochastic model in terms of the transitions which can occur between states and shown how the probability distribution of such a model evolves via a master equation. There are two methods of analysing such a model. Typically the easiest way is to simulate its dynamics with a computer using Monte-Carlo techniques. The second way is to derive analytically the emergent population level dynamics with the van Kampen expansion. Both methods allow one to calculate the power spectrum of the large stochastic fluctuations which are typical of the type of models we are considering. In the next chapter I go on to consider the SIR model in more detail. I also look at the validity of the van Kampen approximation when the system size is made smaller.

# Chapter 3

## Immigration in the SIR model

---

In this chapter we examine in more detail some results from the SIR model, introduced in the previous chapter, which forms the starting point for this thesis. In particular, we examine the effect of immigration on both the deterministic and stochastic dynamics. We also look at the limits of the validity of the van Kampen expansion.

In a stochastic model immigration is an important process. Because the population is finite there is a chance that the number of infectives drops to zero, which is known as fade-out of the disease [103]. Immigration represents the fact that no population is completely isolated, and there will always be some degree of spatial coupling. There is also the more practical reason that one would have to restart simulations after fade-out; including immigration not only circumvents this, but is more biologically realistic. As shown by Bartlett [104, 105], there is a critical community size, below which fade-out happens regularly, thus reintroduction of the disease is required for all but the largest cities in England and Wales. More recently it has been shown that the only way for a model to capture both the dynamical and persistence properties of measles is to include immigration [65].

There are two main ways of incorporating this into a stochastic model. One can assume a direct stream of infectious imports into the population [9, 106], or one can use a commuter formulation where susceptibles are in contact with a pool of infectives outside the main populations [7, 84, 107]. We use the second of these as it is more biologically realistic and lends itself to further extension into a fully spatial meta-population model [108]. The results tend to be similar regardless of the method used [3]. We assume that these immigration events happen at a

small rate  $\eta$ , as detailed in Section 2.2.

One advantage of the IBM approach is that the terms representing immigration are automatically included in the deterministic equations which describe the macroscopic behaviour. In the phenomenological approach which starts with macroscopic equations, these terms are easily omitted because the variables are continuous and therefore extinction cannot happen. Even though we would normally expect such small terms to be important when the number of infectious individuals is low, we show that it can have a large impact on the fluctuation spectrum. These terms are even more important when we consider the addition of seasonal forcing to these models in Chapters 5 and 6.

The stochastic model has already been defined by the set of reactions in Section 2.2. In Section 2.4 it was shown that the expansion of the resulting master equation leads to two deterministic equations (2.25) which describe the macroscopic behaviour and stochastic corrections described by the Langevin equations (2.31). The Jacobian,  $a$ , and noise correlators,  $B$ , are given by equations (2.35) and (2.36).

### 3.1 Deterministic analysis

The deterministic equations (2.25) can be solved numerically and the solutions show damped oscillations tending to a fixed point, see Figure 1.4. The fixed points are found by setting the left hand side of (2.25) to zero and solving the resulting equations. We find the two equations,

$$\begin{aligned} (\phi^*)^2 - \left[ 1 + \frac{\eta}{\mu} \frac{(\gamma + \mu)}{\beta} + \frac{(\gamma + \mu)}{\beta} \right] \phi^* + \frac{(\gamma + \mu)}{\beta} &= 0, \\ \psi^* &= \frac{\mu(1 - \phi^*)}{\gamma + \mu}. \end{aligned} \tag{3.1}$$

The stability of the fixed points is investigated by looking at the eigenvalues of the Jacobian (2.35), which satisfy the equation,

$$\lambda^2 - \text{Tr}(a)\lambda + \text{Det}(a) = 0. \tag{3.2}$$

Without immigration ( $\eta = 0$ ), the equations for the fixed-points simplify and we find a trivial solution ( $\phi_+^* = 1$ ,  $\psi_+^* = 0$ ) and a non-trivial one:

$$\phi_-^* = \frac{\gamma + \mu}{\beta} = \frac{1}{R_0}, \quad \psi_-^* = \frac{\mu(1 - \phi^*)}{\gamma + \mu}, \quad (3.3)$$

where  $R_0$  is the basic reproductive ratio defined in Section 1.2. Throughout this thesis we are interested in the parameter regime of childhood diseases, where the mean lifetime of an individual is orders of magnitude greater than the mean infectious period ( $\mu \ll \gamma$ ). This allows us to make the following approximations, valid for small  $\mu$ ,

$$\phi_-^* = \frac{\gamma}{\beta} + O(\mu), \quad \psi_-^* = \mu \left( \frac{1}{\gamma} - \frac{1}{\beta} \right) + O(\mu^2). \quad (3.4)$$

In general the eigenvalues will be a complex-conjugate pair, and for stability require  $\text{Re}(\lambda) < 0$ . If  $\eta = 0$ , the condition for stability of the non-trivial fixed point is  $R_0 > 1$  [2, 30]. If  $R_0 < 1$  then the disease free fixed-point is stable, thus  $R_0 = 1$  is a bifurcation point between these two regimes.

In the endemic region ( $R_0 > 1$ ) we will observe damped oscillations if the eigenvalues are complex. The condition for this will be:  $4 \text{Det}(a) > \text{Tr}(a)^2$ . Introducing a dimensionless parameter  $\alpha = (\gamma + \mu)/\mu$ , which is the ratio of life expectancy to the infectious period, we find,

$$\alpha > \frac{R_0^2}{4(R_0 - 1)}. \quad (3.5)$$

For childhood diseases  $\alpha \sim 10^3$  [2], so condition (3.5) is always true and the system approaches the fixed point via damped oscillations. One can also derive the approximate frequency of these oscillations by making a small  $\mu$  approximation for the magnitude of the imaginary part of the eigenvalue,

$$\begin{aligned} \text{Im}(\lambda) &= \sqrt{(\mu R_0)^2 - 4\mu(R_0 - 1)(\mu + \gamma)/2}, \\ &= \sqrt{\gamma\mu(R_0 - 1)} + O(\mu). \end{aligned} \quad (3.6)$$

The frequency of the damped oscillations is then equal to  $\text{Im}(\lambda)/2\pi$ .

If we introduce immigration ( $\eta \neq 0$ ) then this picture is changed. Only the positive root of equation (3.1) is a physical solution with  $\phi^* < 1$  and  $\psi^* > 0$ . The fixed points with and without immigration are compared in Figure 3.1. Contrary

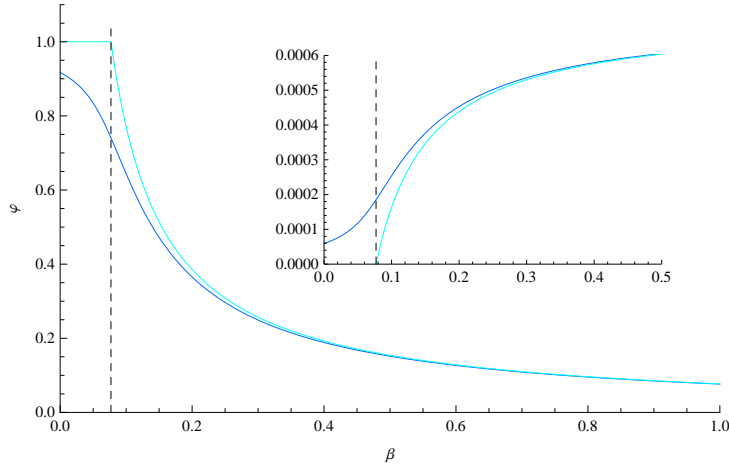


Figure 3.1: Fixed points with (dark blue curve) and without (light blue curve) immigration as a function of  $\beta$ . The dashed line marks the boundary  $R_0=1$ . Other parameters are fixed:  $\gamma = 0.077$ ,  $\mu = 5.5 \times 10^{-5}$ ,  $\eta = 5 \times 10^{-6}$ .

to the statement in [7], there is no instability boundary when immigration is included, which destroys the absorbing state on the deterministic level. Of course in the stochastic model this is not true and there is always a boundary at  $I = 0$ . We examine the effect of this boundary in more detail in Section 3.3

## 3.2 Stochastic fluctuations

The power spectrum for the stochastic fluctuations about the fixed point was derived in Section 2.6. As discussed in Section 2.6.1 the form of the spectrum is highly dependent on the eigenvalues of the Jacobian, with amplitude and frequency proportional to the real and imaginary parts respectively. If  $\eta = 0$ ,  $\text{Re}(\lambda) = \text{Tr}(a)/2 = -\mu R_0/2$ . The factor of  $\mu$  means this will be small and decreases as the bifurcation point is approached. At some point condition (3.5) will break down, but this does not affect the basic result that as we approach the bifurcation point,  $\text{Re}(\lambda) \rightarrow 0$  and the amplitude of the spectrum diverges, and thus the fluctuations increase without bound.

Figure 3.2 shows the trace of the Jacobian as a function of  $\beta$  for different values of  $\eta$ . Introducing some immigration ( $\eta \neq 0$ ) essentially acts to bound the fluctuations. We can see this more clearly by looking at the power spectra. Figure 3.3 shows power spectra with and without immigration for a range of decreasing values of  $\beta$ . As  $\beta$  is decreased, so is the endogenous frequency. The power

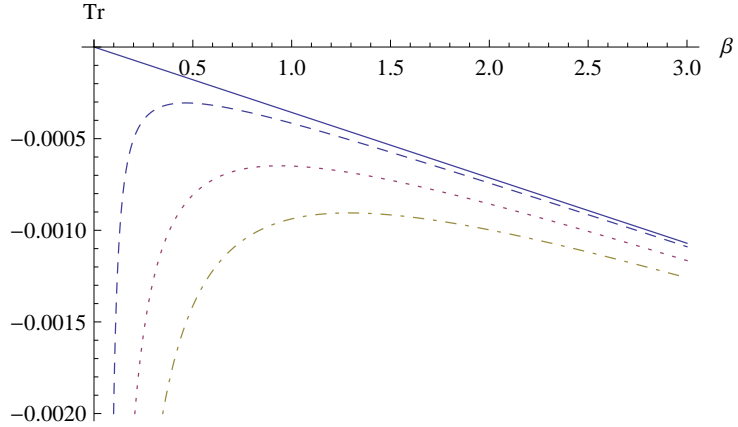


Figure 3.2: The trace of the Jacobian as a function of  $\beta$ , for different values of  $\eta$ , the immigration parameter.  $\eta = 0$  (solid line) and  $\eta = 10^{-6}$ ,  $5 \times 10^{-6}$  and  $10^{-5}$  (dashed, dotted, dot-dashed lines, respectively). Other parameters as in Figure 3.1.

spectrum with the maximum amplitude is at  $\beta = 0.9$ , which from Figure 3.2 is the maximum point of the trace for the particular value of  $\eta$ . We can imagine this as a type of damping [107], where a constant stream of new infections into the population depletes the pool of susceptibles, reducing the potential for large outbreaks. This will have a larger effect on the longer period oscillations because the pool of susceptibles is depleted over a longer time, thus the power spectrum is suppressed at smaller values of  $\beta$ .

Alonso et al. [7] hypothesise that the van Kampen expansion breaks down in this model, but we have shown that it is accurate as long as  $N$  is large enough and immigration is included. We examine this in closer detail in the next section. Figure 3.4 shows the amplification mapped into parameter space, with  $\mu$  and  $\eta$  fixed. Constant values of  $R_0$  are shown by dashed contours. We can see that the highest amplification occurs at longer infectious periods and smaller  $\beta$ .

### 3.3 Small- $N$ deviations

In the previous section we showed that when immigration is included the macroscopic equations have only one stable fixed point. This is because the macroscopic limit assumes that  $N \rightarrow \infty$ , but in the stochastic version, with a finite  $N$ , extinction or fade-out can still happen when the number of infectives drops to zero. Immigration then acts to reintroduce the disease back into the population. This

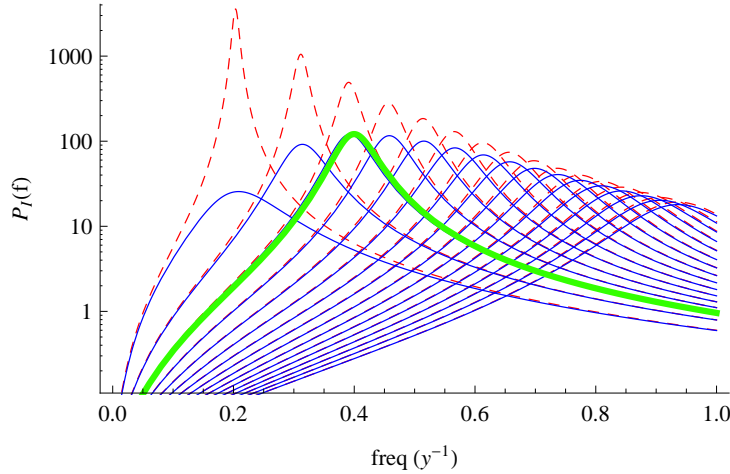


Figure 3.3: Power spectra with (blue solid curves) and without (red dashed curves) immigration as we approach the boundary  $R_0 = 1$  by decreasing  $\beta$ . As  $\beta$  is decreased the endogenous frequency is lowered. With no immigration the amplitude of the spectrum diverges as the bifurcation point is approached. With immigration ( $\eta \neq 0$ ), the fluctuations remain bounded. The spectrum with the maximum amplitude is highlighted in light green. Notice that this occurs well before the point  $R_0 = 1$ . Other parameters are fixed:  $\gamma = 0.077$ ,  $\mu = 5.5 \times 10^{-5}$ ,  $\eta = 5 \times 10^{-6}$ .

is an important boundary in the stochastic system and is the main obstacle to the accuracy of the system-size expansion. We can derive a rough estimate for the population size at which this becomes important by comparing the mean with the RMS size of the fluctuations,

$$\begin{aligned} N\psi^* &\sim N^{1/2} \sqrt{\langle y^2 \rangle}, \\ N &\sim A_0^2 / (\psi^*)^2, \end{aligned} \tag{3.7}$$

where  $A_0$  is the total amplification defined in equation (2.46). Figure 3.5 shows three time-series at decreasing values of  $N$ , together with their corresponding power spectra. Substituting the set of parameters given in Figure caption 3.5 into (3.7) gives the estimate,  $N \sim 3 \times 10^5$ . As the system size is decreased the endogenous period tends to be shifted to longer periods and a secondary harmonic peak appears [67]. The shift in frequency is due to the fact that the dynamics start to depend on the re-introduction of the disease after fade-out. This effect was first noted by Bartlett [1, 104, 109]. He categorised cities into three types: type I were populations large enough not to experience fade-out and type II did

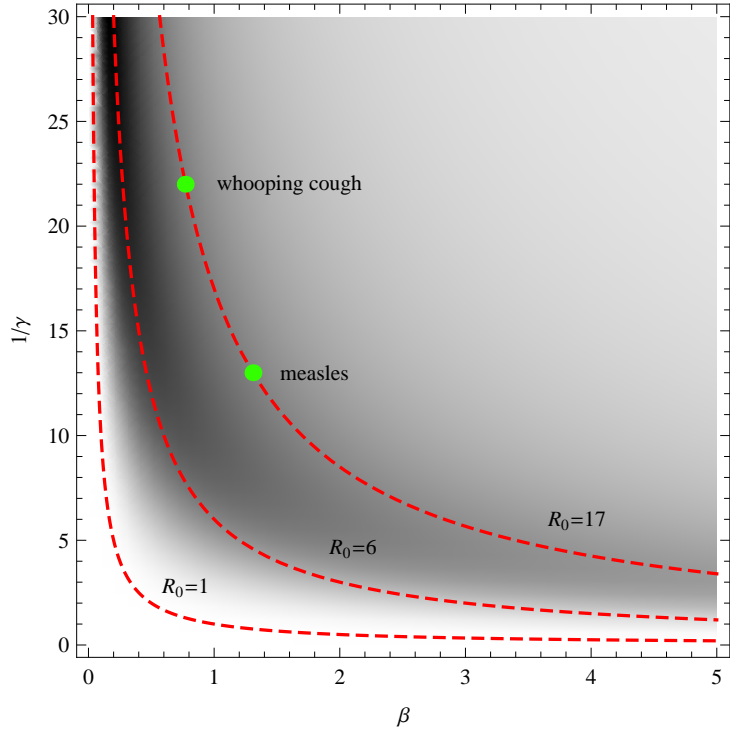


Figure 3.4: Amplification,  $A_0$ , mapped into parameter space (darker shade shows higher values).  $1/\gamma$  is the average length of the infectious period. The dashed red lines show contours of constant  $R_0$ . See Table 1.1 for disease specific parameter values:  $\mu = 5.5 \times 10^{-5}$  and  $\eta = 10^{-6}$ .

experience fade-out but immigration was large enough to spark a new epidemic as soon as the number of susceptibles (from births) was large enough. Type III were small populations, where the inter-epidemic period will depend strongly on the time to the next infectious immigration event, thus the dynamics are more irregular. These three scenarios roughly correspond to the three time-series shown in Figure 3.5. The greater irregularity in the third time-series is reflected in the broader power spectrum.

### 3.3.1 Higher-order corrections

As discussed in Section 2.4, the van Kampen expansion gives an equation for the fluctuation probability density,  $\Pi$ , in terms of powers of  $N^{-1/2}$ . Usually we only keep terms of  $O(1)$ —known as the linear-noise approximation—in which case the equation for the temporal evolution of  $\Pi$  is a Fokker-Planck equation of the form (2.30). Thus we are approximating the full probability density as a Gaussian, and at large  $N$  this is seen be good (see Figure 3.5 top). At smaller  $N$  the system can

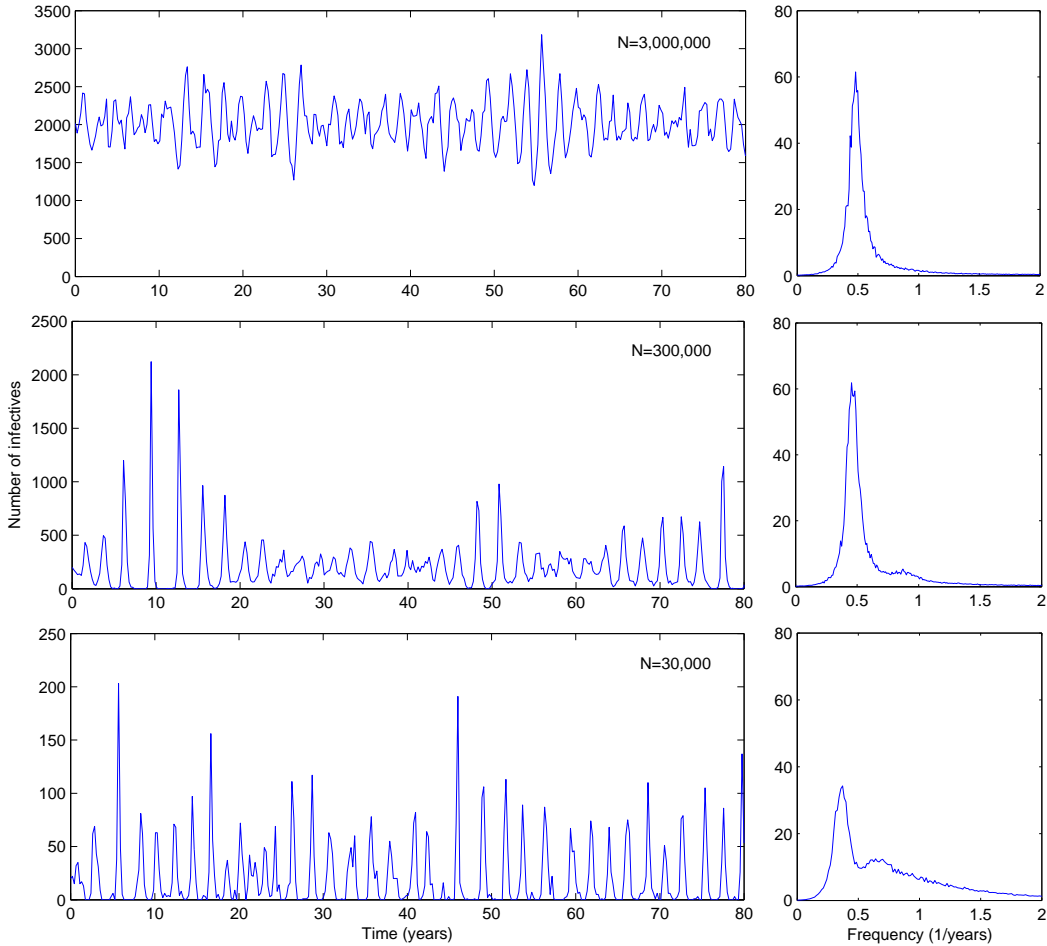


Figure 3.5: Time series (left hand panels) and corresponding power spectra (right hand panels) for decreasing populations sizes,  $N$ . The peak frequency of the power spectra are shifted to the the left at smaller values of  $N$ . These three populations illustrates the type I, II and III dynamics first described by Bartlett. Other parameters are fixed:  $\beta = 1.175$ ,  $\gamma = 0.077$ ,  $\mu = 5.5 \times 10^{-5}$ ,  $\eta = 5 \times 10^{-6}$ .

approach the fade-out boundary, the fluctuations are no longer Gaussian, and the approximation starts to break down.

One can improve the approximation and take into account the non-Gaussian behaviour by including higher-order terms in the equations for  $\Pi$ . This introduces a number of complications though. Firstly, actually carrying out the expansion becomes very tedious and prone to error because of the sheer number of terms involved, even for a very simple case such as the SIR model. The second problem is that the Fokker-Planck equation describing the probability distribution is no

longer linear and so cannot be solved directly. Instead one has to derive equations for the moments, which can then be used to construct an auto-correlation function [78]. The moments are found by multiplying the Fokker-Planck equation by various powers of the fluctuation variables, then integrating over all variables via a number of successive integration-by-parts. The equations for the moments form a set of coupled first order differential equations, which can be solved using standard routines [110].

Preliminary investigation of these ideas has been completed, but details are not included in this thesis. It is found that including terms of order  $N^{-1/2}$  in the expansion can improve the accuracy of the theoretical spectrum (the small shifts in the peak frequency as well as the harmonic peak are reproduced), but only within a limited range of  $N$ . The fundamental problem here is that in deriving the equations for the moments we make the assumption that  $\Pi(x, y, t) \rightarrow 0$  at the boundaries of the system. This is clearly false for the SIR model as there starts to be a build up of probability along the boundary  $I = 0$ , even for medium size systems. For the example shown in Figure 3.5 the theoretical result is good down to about  $N = 3 \times 10^5$ . The expansion cannot capture this small  $I$  behaviour and other methods, such as a WKB approximation [162], must be used to try to capture the effects of the boundary. A corollary to this is that because  $N$  is small, simulations are quicker, but as with all simulations, general results are difficult to establish.

## 3.4 Summary

In this chapter we have examined the role of immigration in the stochastic SIR model. One of the main problems in the literature up till now has been the heuristic treatment of this process. It is often included in simulations for practical reasons, but not in other analyses of the model. This has lead to much confusion and is discussed in greater detail in Chapter 7.

We have shown that just small amounts of immigration can have a large effect on the stochastic dynamics. In the macroscopic limit it destroys the absorbing state and we left with only one stable fixed point. This then acts to bound the fluctuations, so we do not see a divergence in the power spectrum at the boundary  $R_0 = 1$ . Immigration can be imagined as applying a sort of damping to the system, thus larger values of  $\eta$  lead to a depressed fluctuation spectrum.

# Chapter 4

## Staged epidemic models

---

There is one important assumption in the SIR model, which is clearly false: the infectious period is not exponentially distributed. In general there will be a latent period followed by an infectious period of roughly constant length [111–113]. Thus, the probability of recovery will depend strongly on the time since infection. As discussed in Section 2.1, if a process depends on its history (time since first infection) then it is not Markovian.

There are a number of models that have incorporated this aspect but they are usually formulated in terms of partial differential or integro-differential equations [80, 114]; this makes them much more difficult to analyse. The original models of Kermack and McKendrick incorporated an arbitrarily distributed infectious period (although they could only be solved when this was exponential) [28]. In deterministic models without external forcing, the inclusion of distributed periods has been shown to destabilise the equilibrium fixed point [79, 115]. In stochastic versions this leads to larger amplitude oscillations and a decrease in persistence (a measure of the number of fade-outs) [116]. If seasonal forcing is also included, one finds that a period doubling bifurcation can be induced with smaller amounts of forcing than in the SIR model with an exponential period [79, 80].

This chapter examines how we can incorporate distributed infectious periods into the stochastic SIR model via the method of stages [87]. This allows us recover the Markov property and write down a master equation. From this, through the use of the system-size expansion, we can derive the theoretical power spectrum for the fluctuations. Thus we can obtain a proper quantification of the stochastic oscillations seen in these models.

One of the primary motivations for this work is to look for a biologically realistic mechanism for inducing more coherent larger-scale stochastic oscillations. The colouring of the basic SIR model with a virtually endless palette of additional complexities does produce sustained oscillations, and more complex behaviour; some examples already mentioned are delays [39, 117] and non-linear incidence terms [40]. However, none of these modifications predicts the regular patterns of recurrent epidemics found in many data sets for a significant range of realistic parameter values [12]. In [67] the power spectrum of a stochastic SIR model with a fixed infectious period was numerically computed. For a large parameter range, the amplitude and coherence (power centred about the peak of the spectrum) of the fluctuations was found to be enhanced with respect to the standard SIR model [7], as was the frequency of the fluctuations. With this work, we can establish these results analytically and show that the amplification of demographic stochasticity is large enough for the behaviour of moderately sized systems to be akin to the self-sustained oscillations typical of the discrete versions of the model [118, 119].

## 4.1 Infectious period distributions

The infectious period distribution is defined by a probability density  $f_I(t)$  where  $f_I(t)dt$  is the probability of recovery in the interval  $(t, t + dt)$  given that an individual was infected at  $t = 0$ . We can then define the probability that an individual is still infective at time  $\tau$  (survivorship) as,

$$P(\tau) = \int_{\tau}^{\infty} f_I(t)dt. \quad (4.1)$$

Notice that we have neglected the chance of death occurring while infected. This would add a factor  $e^{-\mu t}$  to the integral, which as  $\gamma \gg \mu$ , is very small and can be neglected. As discussed in Section 2.3, simulating a stochastic model with an arbitrary infectious period distribution is straightforward as long as there exist good methods for generating random numbers according to that distribution. But, because the probability of recovery now depends on the time since infection, the process is no longer Markov and we cannot write down a master equation of the form (2.9).

The most natural way to circumvent this problem is via the method of stages,

which gives gamma-distributed infectious periods [87, 120]. We split the recovery period up into  $L$  stages which are traversed in series,

$$I = I_1 + I_2 + \cdots + I_L, \quad (4.2)$$

where the time in each stage,  $I_j$  is independently exponentially distributed with parameter  $\gamma L$ , i.e.  $f_j(t) = \gamma L e^{-\gamma L t}$ , where  $j = 1, \dots, L$ . The moment generating function for each individual stage,  $I_j$ , is given by the Laplace transform of the probability distribution,  $f_j(t)$ , [87],

$$\mathbb{M}[I_j] = \int_{-\infty}^{+\infty} f_j(t) e^{-st} dt = \frac{\gamma L}{\gamma L + s}. \quad (4.3)$$

$I$  is now the sum of  $L$  independent random variables,  $I_j$ , so

$$\mathbb{M}[I] = (\mathbb{M}[I_j])^L = \frac{(\gamma L)^L}{(\gamma L + s)^L}. \quad (4.4)$$

Transforming back,  $f_I(t)$ , the waiting time distribution for the total number of infectives, is a gamma distribution,

$$f_I(t) = \frac{(\gamma L)^L}{\Gamma(L)} t^{L-1} e^{-\gamma L t}, \quad (4.5)$$

with mean  $1/\gamma$  and variance  $1/\gamma^2 L$ . By setting  $L = 1$  we recover the original exponential distribution. As  $L$  is increased the distribution becomes more central and an individual remains infectious for a more constant amount of time. Figure 4.1 illustrates the gamma-distributions and survivorships for increasing values of  $L$ . Thus we can interpolate between the basic exponential model and one with a constant infectious period by tuning  $L$ . The gamma distribution is a practical choice as it lends itself to easy analysis. It is easy to fit to data [19, 121], and straightforward to incorporate in simulations, as opposed to say integro-differential equations, which have been used in previous studies [81, 114, 115].

## 4.2 Staged SIR model

We take the simplest case where the SIR model has a gamma-distributed infectious period. This model is exactly the same as defined in Section 2.2, but the

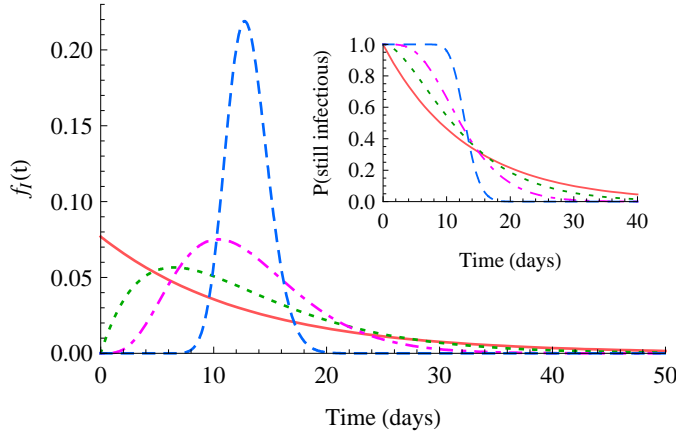


Figure 4.1: (Main) The distribution of infectious periods,  $f_I(t)$ , for  $L = 1, 2, 5$  and  $50$  (solid, dotted, dot-dashed and dashed lines respectively). The case  $L = 1$  corresponds to the exponential distribution of the standard SIR model. The inset shows the probability that an individual is still infectious at time  $t$ : for large  $L$  it approaches a step function, where all individuals remain infectious for a constant period of time. The average infectious period,  $1/\gamma = 13$  days.

infectious class is split up into  $L$  stages which are traversed sequentially, with rate  $L\gamma$ , where  $I_j$  is the number of infectives in class  $j$ . There are now two constraints on the variables,  $N = R + S + I$  and  $I = \sum_j I_j$ . We use the second of these to rewrite  $I_1$  in terms of  $I$  so the state of the system is  $\mathbf{n} \equiv \{S, I, I_2, \dots, I_L\}$ . Defining  $\mathbf{I} \equiv \{I_1, I_2, \dots, I_L\}$ , the transition rates are then:

(i) Infection:  $S + I \xrightarrow{\beta} I + I_1$

$$T(S+1, I-1, I_2, \dots | S, \mathbf{I}) = \frac{\beta SI}{N}$$

(ii) Birth / death:  $I_1 \xrightarrow{\mu} S$

$$T(S+1, I-1, I_2, \dots | S, \mathbf{I}) = \mu \left( I - \sum_{j=2}^L I_j \right)$$

(iii) Birth / death:  $I_j \xrightarrow{\mu} S \quad j = 2, \dots, L$

$$T(S+1, I-1, \dots, I_j-1, \dots | S, \mathbf{I}) = \mu I_j$$

(iv) Birth / death:  $R \xrightarrow{\mu} S$

$$T(S+1, I, \dots | S, \mathbf{I}) = \mu (N - S - I)$$

(v) Recovery:  $I_1 \xrightarrow{L\gamma} I_2$

$$T(S, I, I_2 + 1, \dots | S, \mathbf{I}) = \gamma \left( I - \sum_j I_j \right)$$

(vi) Recovery:  $I_j \xrightarrow{L\gamma} I_{j+1}$ ,  $j = 2, \dots, L - 1$

$$T(S, I, \dots, I_j - 1, I_{j+1} + 1, \dots | S, \mathbf{I}) = \gamma I_j$$

(vii) Recovery:  $I_L \xrightarrow{L\gamma} R$

$$T(S, I - 1, I_2, \dots, I_L - 1 | S, \mathbf{I}) = \gamma I_L.$$

Note that we do not include immigration in this formulation as we are mainly concerned with how the distributed periods change the spectrum of the fluctuations compared to the basic model. We get around the need for immigration in simulations by using large system sizes, where the fluctuations are not large enough to cause extinction. This system can be simulated in two ways: either by including all the subclasses and using a typical Gillespie type algorithm [86], or as discussed in Section 2.3, using a next reaction type scheme and drawing the recovery times directly from a gamma distribution [89]. This second method is the most computationally efficient, especially as  $L$  increases, and the same code can be used as for the SIR model with only minor changes.

With the transition rates defined above, the master equation is easy to write down by introducing step operators,

$$\begin{aligned} \mathbb{E}_s^{\pm 1} f(S, I, I_2, \dots, I_L) &= f(S \pm 1, I, I_2, \dots, I_L), \\ \mathbb{E}_1^{\pm 1} f(S, I, I_2, \dots, I_L) &= f(S, I \pm 1, I_2, \dots, I_L), \\ \mathbb{E}_j^{\pm 1} f(S, I, I_2, \dots, I_L) &= f(S, I, I_2, \dots, I_j \pm 1, \dots, I_L). \end{aligned}$$

The master equation for this model is then,

$$\begin{aligned} \frac{dP(\mathbf{n}; t)}{dt} = & \left\{ (\mathbb{E}_s^{+1} \mathbb{E}_1^{-1} - 1) \frac{\beta SI}{N} + (\mathbb{E}_s^{-1} \mathbb{E}_1^{+1} - 1) \mu \left( I - \sum_{j=2}^L I_j \right) \right. \\ & + \sum_{j=2}^L (\mathbb{E}_s^{-1} \mathbb{E}_1^{+1} \mathbb{E}_j^{+1} - 1) \mu I_j + (\mathbb{E}_s^{-1} - 1) \mu (N - S - I) \\ & + (\mathbb{E}_2^{-1} - 1) \gamma \left( I - \sum_{j=2}^L I_j \right) + \sum_{j=2}^{L-1} (\mathbb{E}_j^{+1} \mathbb{E}_{j+1}^{-1} - 1) \gamma I_j \\ & \left. + (\mathbb{E}_1^{+1} \mathbb{E}_L^{+1} - 1) \gamma I_L \right\} P(\sigma; t). \end{aligned}$$

The system-size expansion is applied as detailed in Section 2.4.1. We introduce the new variables:  $S = \phi N + x_0 \sqrt{N}$ ,  $I = \psi N + x_1 \sqrt{N}$  and  $I_j = \psi_j N + x_j \sqrt{N}$

with  $j \geq 2$ , where  $\phi$  is the fraction of susceptibles,  $\psi$  is the fraction of total infectives and  $\psi_j$  is the fraction of infectives in class  $j$ , with  $x_0, \dots, x_L$  describing the stochastic corrections.

To leading order we obtain a set of  $L + 1$  deterministic equations, describing the macroscopic dynamics,

$$\begin{aligned}\dot{\phi} &= -\beta\phi\psi + \mu(1 - \phi), \\ \dot{\psi} &= \beta\phi\psi - \mu\psi - L\gamma\psi_L, \\ \dot{\psi}_2 &= -(L\gamma + \mu)\psi_2 + L\gamma(\psi - \sum_{j=2}^L \psi_j), \\ \dot{\psi}_j &= -(L\gamma + \mu)\psi_j + L\gamma\psi_{j-1}, \quad j = 3, \dots, L.\end{aligned}\tag{4.6}$$

The fixed points are given by the equations,

$$\begin{aligned}\phi^* &= \frac{\mu/\beta}{1 - \left(1 + \frac{\mu}{L\gamma}\right)^{-L}}, \\ \psi^* &= \left(1 - \frac{\mu}{\beta}\right) - \left(1 + \frac{\mu}{L\gamma}\right)^{-L}, \\ \psi_j^* &= \frac{\frac{\mu}{L\gamma} \left(1 + \frac{\mu}{L\gamma}\right)^{-j}}{\left(1 + \frac{\mu}{L\gamma}\right)^L - 1} \left[ \left(1 - \frac{\mu}{\beta}\right) \left(1 + \frac{\mu}{L\gamma}\right)^L - 1 \right], \quad j = 2, \dots, L.\end{aligned}\tag{4.7}$$

To compare with the fixed points of the basic SIR model, we note that  $\mu \ll 1$ . Thus carrying out a binomial expansion we find,

$$\left(1 + \frac{\mu}{L\gamma}\right)^{-L} = 1 - \frac{\mu}{\gamma} + O(\mu^2)\tag{4.8}$$

Expanding (4.7) for the fixed points in powers of  $\mu$  we find,  $\phi^* = \gamma/\beta + O(\mu)$ ,  $\psi^* = \mu(1/\gamma - 1/\beta) + O(\mu^2)$  and  $\psi_j^* = \psi^*/L + O(\mu^2)$ . Comparing with Eq. (3.3) we see that these are the same as the exponentially distributed model, to lowest order in  $\mu$ . Thus, changing the infectious period distribution has only a very small effect on the deterministic fixed points [79, 115]. Numerical integration of the equations (4.6) shows that the total number of infected,  $\psi(t)$ , approaches the fixed point via damped oscillations, as expected.

### 4.3 Power spectrum

At next-to-leading order the fluctuations obey an  $L+1$  dimensional linear Fokker-Planck equation, which as shown in Section 2.4.2, is equivalent to the Langevin equations of the form,

$$\frac{dx_i}{dt} = \sum_{j=0}^{L+1} A_{ij}x_j + \xi_i(t), \quad (4.9)$$

where,  $\xi_i(t)$  are Gaussian noise terms with zero mean and satisfying  $\langle \xi_i(t)\xi_j(t') \rangle = B_{ij}\delta(t-t')$ . The explicit form of the Jacobian,  $A_{ij}$ , and noise correlator matrix,  $B_{ij}$ , are given in Appendix A. We evaluate these at the fixed point after transients have damped down, and so they are time independent. By taking the Fourier transform of equation (4.9) we obtain

$$\sum_{j=0}^{L+1} S_{ij}\tilde{x}_j + \tilde{\eta}_i = 0, \quad (4.10)$$

where  $S_{ij} = A_{ij} - i\omega\delta_{ij}$ . The power spectrum for the total number of infectives can then be written as,

$$P_L(\omega) = \frac{\sum_{ij} B_{ij}C_i(\omega)C_j^*(\omega)}{D(\omega)D^*(\omega)}, \quad (4.11)$$

where  $C_i(\omega)$  is the co-factor of the matrix  $S$  in row  $i$  and column  $j = 1$ , and  $D(\omega)$  is the determinant of the full  $S$  matrix. In practice the matrices are computed numerically, and  $P_L(\omega)$  is computed from these using the symbolic package Mathematica [110].

The theoretical power spectra resulting from the infectious period distributions in Fig. 4.1 are presented in Fig. 4.2. The case considered in the previous chapter corresponds to  $L = 1$ , and it is clear that both the enhancement of the amplitude and the coherence of the power spectrum increases as  $L$  increases. The change is more pronounced for low values of  $L$  following the large changes of the recovery profile at those low values. Therefore for the values of  $L$  which are usually thought to be applicable ( $L$  of the order of 10 or 20 [64, 121]) an enhancement of 3 or 4 times that found with exponential recovery ( $L = 1$ ) can be seen. The position of the peak (given by the fixed points of the mean field equations) also shifts with  $L$ . Fig. 4.3 is a plot of the amplification (which is proportional to the amplitude [7]) and position of the peak (endogenous frequency) of the power

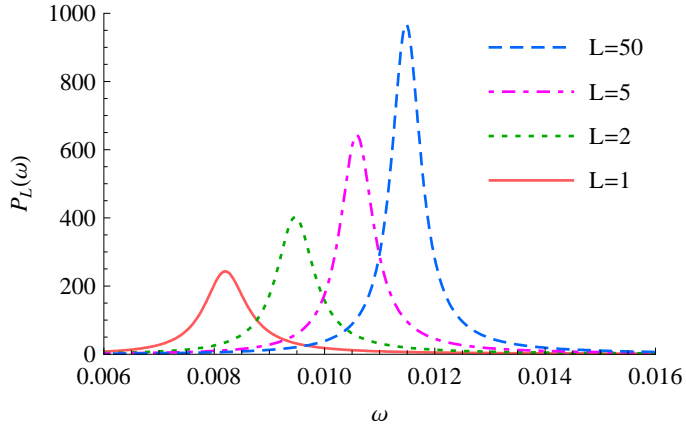


Figure 4.2: Analytical power spectra for fluctuations in the total number of infectives for the distributions shown in Figure 4.1. Other parameters are:  $\beta = 1.3$ ,  $1/\gamma = 13$  and  $\mu = 5.5 \times 10^{-5}$

spectrum as a function of  $L$ . The change of these quantities with  $L$  is smooth and appears to approach a fixed limit for large  $L$ . They are well-fitted by an expression of the form  $a - b/(c + L)$ , where  $a, b$  and  $c$  are constants.

In general  $A_{ij}$  will have  $L + 1$  eigenvalues. We expect to see a peak in the spectrum for every pair of complex eigenvalues, at frequencies equal to the imaginary parts of the eigenvalues (see Section 2.4.1). Both the analytical calculation and numerical simulations show only one peak (Figures 4.2 and 4.4). Numerical determination of the eigenvalues of  $A$  for small  $L$  shows that there are typically more than one pair of complex eigenvalues, but that there is always one dominant pair, with a real part roughly four orders of magnitude smaller than the others. This implies that this dominant eigenvalue is very close to the real axis and so will give a large peak and therefore large amplitude fluctuations. The imaginary part of the dominant eigenvalue is also orders of magnitude smaller than those of the others, and therefore the tiny peaks resulting from these other complex eigenvalues will be at much higher frequencies.

We can also derive an expression for the power spectrum in the limit  $L \rightarrow \infty$  and small  $\mu$ . Since the position and peak of the power spectrum change little for values of  $L$  of the order of 10 or above, this results is a good approximation. By considering the form of the matrices  $A$  and  $B$  to first order in  $\mu$ , the numerator and denominator of Eq. (4.11) can be shown to have a finite limit as  $L \rightarrow \infty$ ; see appendix of [122] for more details. Specifically, if we define  $\hat{\mu} = \mu/\gamma$  and

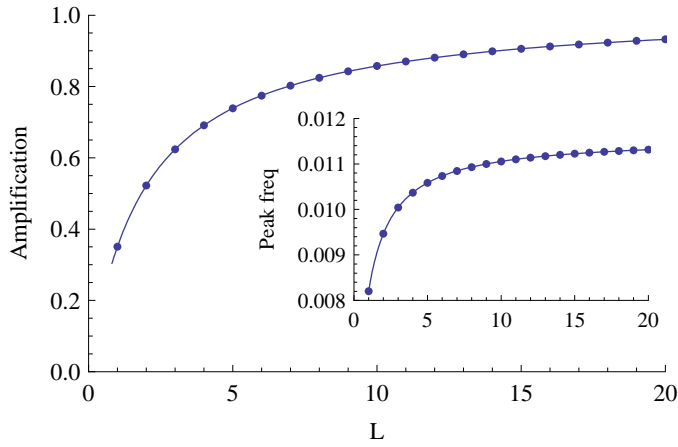


Figure 4.3: (Main) Increase in amplification (see Eq. (2.46)) of  $P_L(\omega)$  with increasing  $L$ , where amplification is defined as the area under the power spectrum, which is equal to the mean squared variance of the time series  $x_1$ . (Inset) Drift of the peak position of  $P_L(\omega)$  for increasing  $L$ . In both cases  $\beta = 1.32$ ,  $\gamma = 1/8$  and  $\mu = 6 \times 10^{-4}$ . Both curves are perfectly fitted by an expression of the kind:  $a - b/(c + L)$  (continuous line), which shows that the underlying dependence on  $L$  is simple and that the power spectrum converges to a definite shape as  $L \rightarrow \infty$ .

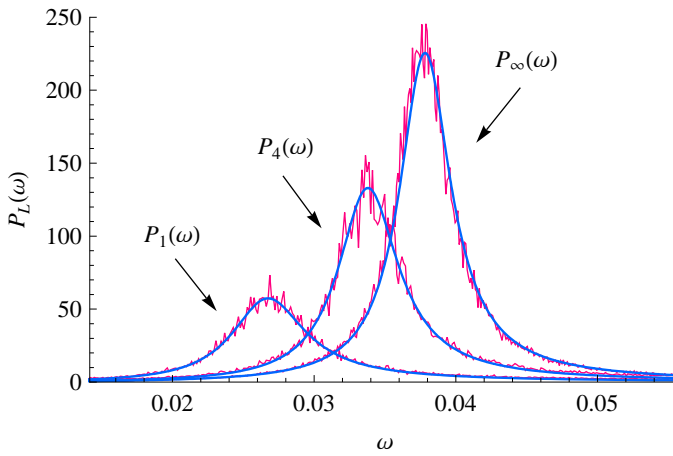


Figure 4.4: Comparison between the analytic power spectra (solid blue lines) given by (4.11) and numerical simulations of the SIR model (noisy red lines) for  $L = 1, 4$  and  $\infty$ , for which there is perfect agreement. Other parameter values are  $\beta = 1.32$ ,  $\mu = 6 \times 10^{-4}$ ,  $\gamma = 1/8$  and a population size of  $N = 10^6$  individuals. The numerical curves were obtained by averaging the power spectra of 200 realisations for each of the three cases considered.

$\hat{\beta} = \beta/\gamma$ , the numerator of Eq. (4.11) is

$$\begin{aligned} \sum_{i=0}^L \sum_{j=0}^L C_i(\omega) B_{ij} C_j^*(\omega) &= \hat{\mu} \left(1 - \frac{1}{\hat{\beta}}\right) (\hat{\mu}^2 + \omega^2)^{-1} \\ &\quad \times \left[ \hat{\mu}^2 (\hat{\beta}^2 - 2\hat{\beta} + 2) + \omega^2 \right] (e^{2\hat{\mu}} - 2e^{\hat{\mu}} \cos \omega + 1), \end{aligned} \quad (4.12)$$

and the denominator is,

$$\begin{aligned} D(\omega) D^*(\omega) &= e^{2\hat{\mu}} \left[ \left( \hat{\beta}\hat{\mu} - 1 - \frac{\hat{\mu}}{2} \right)^2 + \omega^2 \right] + \left( 1 + \frac{\hat{\mu}}{2} \right)^2 \\ &\quad + e^{\hat{\mu}} (2 + \hat{\mu}) \left[ \cos \omega \left( \hat{\beta}\hat{\mu} - 1 - \frac{\hat{\mu}}{2} \right) - \omega \sin \omega \right]. \end{aligned} \quad (4.13)$$

The analytically derived spectra are compared to those obtained numerically in Figure 4.4. The limit  $L \rightarrow \infty$  corresponds to the case where recovery occurs at a fixed period of time after infection and is the case considered in [67]. The numerical spectra have been left relatively noisy to help distinguish them from the analytic results, otherwise agreement is excellent.

## 4.4 Discussion

In this chapter we have analysed the SIR model with a distributed infectious period. By using the method of stages we have shown that the SIR model with a much more realistic recovery profile, can be analysed almost as simply as the standard SIR model (which has  $L = 1$ ). The sustained, and amplified oscillations found in the standard SIR model [7] are even more evident for  $L > 1$ , with the frequency of the oscillations and their amplitude increasing with  $L$ . Typical values of  $L$  estimated from data lie between 10 and 20 [64, 121], and for these values the frequency and amplitude of the oscillations are already near to the asymptotic limit  $L \rightarrow \infty$ . In this limit the power spectrum may be obtained in closed form, verifying the small changes that occur in the nature of the spectrum for large  $L$ .

Some aspects of the staged SIR model have been investigated previously. Grossman [79] studied the deterministic SIR model incorporating a fixed infectious period. Later this work was elaborated by Lloyd [80, 116] who expanded the

results to include gamma-distributed infectious periods and studied the stochastic version of the model numerically. He found that the fixed points became less stable with increasing  $L$ , which he interpreted as a “destabilisation” of the SIR model. Our result that the total amplification (which is proportional to the mean variance of the time series) increases with  $L$ , is consistent with Lloyd’s earlier result that the damping time of the deterministic system increased with  $L$ . However the frequency of the damped oscillations of the deterministic system is only approximately the same as the frequency of the sustained oscillations, due to the additional frequency dependence in the numerator of the power spectrum.

While destabilisation has been discussed previously, the increase in the endogenous frequency of the system with increasing  $L$  has received comparatively little attention. For example, the exponentially distributed model, parametrised for measles, predicts a natural period of oscillation of 2 years, whereas the fixed infectious period version ( $L \rightarrow \infty$ ) predicts 1.5 years. We have not included seasonal forcing in this analysis, but we would expect that a system with a higher endogenous frequency would be more unstable to seasonal forcing. This would be in line with the findings of previous authors [64, 116], in the context of deterministic SIR models. Inclusion of explicit time-dependence in the SIR model is the topic of Chapter 6 and this issue is discussed more in Chapter 7.

In principle the framework set out in this chapter can be made even more general to include arbitrary distributions, or by weighting different stages to represent different level of infectiousness [87]. For these epidemic models there is little to be gained by using arbitrarily distributed periods, as the gamma distribution is a very good fit to data. For other systems such as biochemical [100] or gene-regulatory networks this might be more important. The more complex these models become the larger the two matrices,  $A$  and  $B$ , become. This in itself is not too big an obstacle as long as good methods exist for handling large matrices and the expansion can be automated to generate them accurately from a given set of reactions.

## Chapter 5

# Whooping cough model

---

In this chapter we use our analytic techniques to help understand the oscillations seen in the time-series of whooping cough cases. In England and Wales, before mass vaccination, the time-series of case reports shows dynamics which are strongly multiennial, but after vaccination in the 1950s, quite regular 3.5-4 year epidemic cycles occur [20]. These also appear very synchronised across the whole country [16]. As discussed in the introduction, the modelling of whooping cough has thrown up many interesting points to do with the interaction of stochastic and seasonal forces.

Unlike measles, all suitably parametrised deterministic models, which include seasonal forcing, fail to capture the correct dynamics; they only ever produce annual oscillations. On the other hand, IBMs produce qualitatively correct patterns [16, 24]. Stochasticity is therefore important, but its precise role has been hard to quantify [5]. The work which has been carried out has been an amalgam of analytical work on the PLM and simulations of the IBM [45, 46]. While this has yielded valuable insights, fundamentally one is left with the problem of interpreting stochastic simulations in terms of deterministic results. The broad consensus arising from such studies is that the dynamics come from the interaction of the stochasticity with the non-linearity which cannot be captured with deterministic models alone. Thus noise is of the active type, as defined by Coulson *et al.* [5].

To make headway with this problem, we build on the work from the previous chapter and derive the analytic power spectrum for an SEIR model with distributed latent and infectious periods. The main motivation for going beyond the basic SIR model is to connect with the recent work by Nguyen and Rohani

[19]. For whooping cough there is a long incubation period of roughly a week, thus it can be dynamically significant to include this. Their work suggests that an essentially deterministic SEIR model with realistically distributed periods, *can* capture the qualitative dynamics of whooping cough. They believe the mechanism behind the dynamics is multiple co-existing attractors [35]; noise plays a secondary role of switching the system between these different deterministic states.

With the use of a suitable approximation for the time dependence in the master equation, we apply the formalism developed for the unforced model, to analyse this model which includes seasonal forcing. This allows us to more accurately interpret the results of simulations and to make a more quantitative assessment of the predictions of the model. We show that the observed dynamics are a result of a macroscopic limit cycle induced by the external forcing and resonant stochastic oscillations about this cycle. The inclusion of more realistically distributed infectious periods only acts to change the endogenous frequency of the stochastic oscillations. We do not observe co-existing attractors.

## 5.1 Staged SEIR model

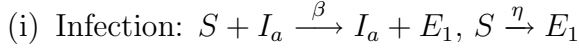
A latent period is included in the model by introducing a new exposed class, E. We define  $f_E(t)$  so that the probability that an individual *becomes* infectious is  $f_E(t)dt$  in the time interval  $(t, t + dt)$ . The probability of being infectious at time  $\tau$ , after initial infection at time  $\tau = 0$  is then,

$$P(\text{infectious}) = \int_0^\tau f_E(t)[1 - P_I(\tau - t)]dt \quad (5.1)$$

where the second factor,  $[1 - P_I(\tau - t)]$ , is the probability that having become infectious at time  $t$  they have not yet recovered at time  $\tau$ ; with  $P_I(t)$  given in Eq. (4.1). As in the previous chapter we ignore the chance of death, *not* due to the disease, during this period. If we assume that the infectious period distribution,  $f_I(t)$ , and the latent period distribution,  $f_E(t)$ , are gamma distributions with means  $1/\gamma$  and  $1/\sigma$  respectively, then we can again use the method of stages [87] to incorporate these into the stochastic model while still retaining the Markov property.

Individuals within the population now belong to one of four compartments:

susceptible, exposed, infectious or recovered,  $\{S, E, I, R\}$ . The latent and infectious periods are split up into  $M$  and  $L$  stages respectively, which are traversed sequentially. Figure 5.1 shows the probability of being infections for three choices of  $M$  and  $L$ . Apart from these changes the model is formulated exactly as in Section 2.2. The reactions and transition rates are presented below where  $\mathbf{E} = (E_1, E_2, \dots, E_M)$ ,  $\mathbf{I} = (I_1, I_2, \dots, I_L)$  and  $\mathbf{n} \equiv \{S, \mathbf{E}, \mathbf{I}\}$ :

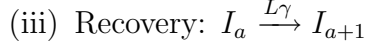


$$T(S - 1, E_1 + 1, \dots, \mathbf{I}|S, \mathbf{E}, \mathbf{I}) = \frac{\beta S}{N} \sum_{a=1}^L I_a + \eta S$$



$$T(S, E_\alpha - 1, E_{\alpha+1} + 1, \mathbf{I}|S, \mathbf{E}, \mathbf{I}) = M\sigma E_\alpha, \quad \alpha = 1, \dots, M - 1,$$

$$T(S, E_M - 1, I_1 + 1|S, \mathbf{E}, \mathbf{I}) = M\sigma E_M,$$

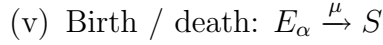


$$T(S, \mathbf{E}, I_a - 1, I_{a+1} + 1, \dots |S, \mathbf{E}, \mathbf{I}) = L\gamma I_a, \quad a = 1, \dots, L - 1,$$

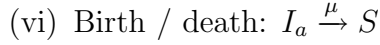
$$T(S, \mathbf{E}, \dots, I_L - 1|S, \mathbf{E}, \mathbf{I}) = L\gamma I_L,$$



$$T(S + 1, \mathbf{E}, \mathbf{I}|S, \mathbf{E}, \mathbf{I}) = \mu \left( N - S - \sum_{\alpha=1}^M E_\alpha - \sum_{a=1}^L I_a \right),$$



$$T(S + 1, E_\alpha - 1, \mathbf{I}|S, \mathbf{E}, \mathbf{I}) = \mu E_\alpha, \quad \alpha = 1, \dots, M,$$



$$T(S + 1, \mathbf{E}, I_a - 1|S, \mathbf{E}, \mathbf{I}) = \mu I_a, \quad a = 1, \dots, L,$$

This is a slightly different formulation to the one considered in the previous chapter as we do not introduce a variable for the total number of infected at this stage in the derivation and we also include immigration. As before we introduce step operators,

$$\begin{aligned} \mathbb{E}_S^{\pm 1} f(S, \mathbf{E}, \mathbf{I}) &= f(S \pm 1, \mathbf{E}, \mathbf{I}), \\ \mathbb{E}_{E_\alpha}^{\pm 1} f(S, E_1, \dots, E_\alpha, \dots, E_M, \mathbf{I}) &= f(S, E_1, \dots, E_\alpha \pm 1, \dots, E_M, \mathbf{I}), \\ \mathbb{E}_{I_a}^{\pm 1} f(S, \mathbf{E}, I_1, \dots, I_a, \dots, I_L) &= f(S, \mathbf{E}, I_1, \dots, I_a \pm 1, \dots, I_L), \end{aligned}$$

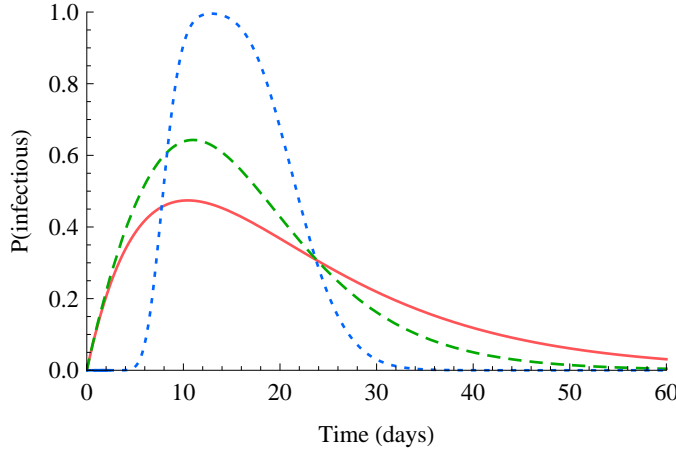


Figure 5.1: Probability that an individual is infectious as a function of time in the staged-SEIR model for  $(L, M) = (1, 1)$ ,  $(1, 5)$  and  $(30, 15)$  (solid, dashed and dotted lines respectively). The case  $(1, 1)$  corresponds to the standard SEIR model. Average latent period,  $1/\sigma = 8$  days, average infectious period,  $1/\gamma = 14$  days (typical for whooping cough).

which allow us to write the master equation as,

$$\begin{aligned} \frac{d}{dt}P(S, \mathbf{E}, \mathbf{I}; t) = & \left\{ \left( \mathbb{E}_S^{+1} \mathbb{E}_{E_1}^{-1} - 1 \right) \left( \frac{\beta S}{N} \sum_{a=1}^L I_a + \eta S \right) \right. \\ & + \sum_{\alpha=1}^{M-1} \left( \mathbb{E}_{E_\alpha}^{+1} \mathbb{E}_{E_{\alpha+1}}^{-1} - 1 \right) M \sigma E_\alpha + \left( \mathbb{E}_{E_M}^{+1} \mathbb{E}_{I_1}^{-1} - 1 \right) M \sigma E_M \\ & + \sum_{a=1}^{L-1} \left( \mathbb{E}_{I_a}^{+1} \mathbb{E}_{I_{a+1}}^{-1} - 1 \right) L \gamma I_a + \left( \mathbb{E}_{I_L}^{+1} - 1 \right) L \gamma I_L \\ & + \left( \mathbb{E}_S^{-1} - 1 \right) \mu \left( N - S - \sum_{\alpha=1}^M E_\alpha - \sum_{a=1}^L I_a \right) \\ & + \sum_{\alpha=1}^M \left( \mathbb{E}_{E_\alpha}^{+1} \mathbb{E}_S^{-1} - 1 \right) \mu E_\alpha \\ & \left. + \sum_{a=1}^L \left( \mathbb{E}_{I_a}^{+1} \mathbb{E}_S^{-1} - 1 \right) \mu I_a \right\} P(S, \mathbf{E}, \mathbf{I}; t). \end{aligned} \quad (5.2)$$

We define our new variables,  $S = N\phi + N^{1/2}x$ ,  $E_\alpha = N\rho_\alpha + N^{1/2}z_\alpha$  and  $I_a = N\psi_a + N^{1/2}y_a$ , where  $\phi$  is the fraction of susceptibles,  $\rho_\alpha$  the fraction of exposed in class  $\alpha$  and  $\psi_a$  the fraction of infected in class  $a$ . The master equation is then expanded in the usual way, as detailed in Section 2.4.1. To leading order we find

a set of  $M + L + 1$  deterministic equations describing the macroscopic behaviour of the system,

$$\begin{aligned}\dot{\phi} &= -\beta\phi \sum_{a=1}^L \psi_a - \eta\phi + \mu(1 - \phi), \\ \dot{\rho}_1 &= \beta\phi \sum_{a=1}^L \psi_a + \eta\phi - (M\sigma + \mu)\rho_1, \\ \dot{\rho}_\alpha &= M\sigma\rho_{\alpha-1} - (M\sigma + \mu)\rho_\alpha, \quad \alpha = 2, \dots, M \\ \dot{\psi}_1 &= M\sigma\rho_M - (L\gamma + \mu)\psi_1, \\ \dot{\psi}_a &= L\gamma\psi_{a-1} - (L\gamma + \mu)\psi_a, \quad a = 2, \dots, L.\end{aligned}\tag{5.3}$$

The fixed points are found by setting the right hand sides of Eqs. (5.3) to zero and solving the resulting equations. Defining  $r = \frac{L\gamma}{L\gamma + \mu}$  and  $q = \frac{M\sigma}{M\sigma + \mu}$ , the susceptible component of the fixed point is found from the negative root of the quadratic equation,

$$(\phi^*)^2 - \left[ 1 + \frac{\eta + \mu}{\beta(1 - r^L)q^M} \right] \phi^* + \frac{\mu}{\beta(1 - r^L)q^M} = 0.\tag{5.4}$$

If  $\eta = 0$  then this reduces to  $\phi^* = 1$  or,

$$\phi^* = \frac{\mu}{\beta} \frac{1}{(1 - r^L)q^M}.\tag{5.5}$$

The other components of the fixed point are then given by,

$$\rho_1^* = \frac{\mu(1 - \phi^*)}{\sigma M + \mu}, \quad \psi_1^* = \frac{\mu(1 - \phi^*)q^M}{\gamma L + \mu},\tag{5.6}$$

and

$$\psi_a^* = r^{a-1}\psi_1^*, \quad \rho_\alpha^* = q^{\alpha-1}\rho_1^*, \quad \sum_{a=1}^L \psi_a^* = \psi_1^* \left( \frac{1 - r^L}{1 - r} \right).\tag{5.7}$$

Firstly, as before, we can approximate  $q^M = 1 - \mu/\sigma + O(\mu^2)$  and  $r^L = 1 - \mu/\gamma + O(\mu^2)$ . Substituting these into the above we see that the fixed points are:  $\phi^* = \beta/\gamma + O(\mu)$ ,  $\sum \psi^* = \mu(1/\gamma - 1/\beta) + O(\mu^2)$  and  $\sum \rho^* = \gamma/\sigma \sum \psi^* + O(\mu^2)$ , which are to leading order in  $\mu$  the same as the basic SEIR model, which are again the same as the SIR model [2, 3]. Thus, as with the SIR model, adding distributed latent and infectious periods has only a minor effect on the deterministic fixed points [115]. Numerical integration of Eqs. (5.3) shows the total number of

infectives approaches the fixed point via damped oscillations.

## 5.2 Power spectrum

At next-to-leading order in the expansion of the master equation we obtain an  $M + L + 1$  dimensional, linear Fokker-Planck equation, which is equivalent to the Langevin equations (see Section 2.4.2),

$$\dot{X}_A = \sum_B J_{AB} X_B + \xi_A, \quad (5.8)$$

where  $X = (x, z_1, \dots, z_M, y_1, \dots, y_L)$ , and the noise correlators obey  $\langle \xi_A(t) \xi_B(t') \rangle = G_{AB} \delta(t - t')$ . The elements of matrices  $J$  and  $G$  are given in Appendix A. This is solved, as before, by Fourier transform, in which case we obtain the solution,

$$\tilde{X}_A(\omega) = \sum_B S_{AB}^{-1}(\omega) \tilde{\xi}_B(\omega), \quad (5.9)$$

where  $S_{AB} = (-J_{AB} - i\omega \delta_{AB})$  and  $\tilde{X}_A$  and  $\tilde{\xi}_A$  are the Fourier transforms of  $X_A$  and  $\xi_A$ . We are interested in the power spectrum of the total number of infectives so we need take the sum of the solutions  $\tilde{y}_a$ ,

$$\sum_{a=1}^L \tilde{y}_a = \sum_{A=2+M}^P \tilde{X}_A = \sum_{A=2+M}^P \sum_{B=1}^P S_{AB}^{-1}(\omega) \tilde{\xi}_B(\omega), \quad (5.10)$$

where  $P = M + L + 1$ . The power spectrum is then,

$$P_I(\omega) = 2 \left\langle \left| \sum_{a=1}^L \tilde{y}_a \right|^2 \right\rangle = 2 \sum_{A=2+M}^P \sum_B^P \sum_{C=2+M}^P \sum_D^P S_{AB}^{-1}(\omega) G_{BD} (S_{CD}^{-1})^\dagger(\omega). \quad (5.11)$$

Again the matrices  $J$  and  $G$  are computed numerically and then the power spectrum is computed symbolically using Mathematica [110].

We can now examine the effect of the parameters  $M$  and  $L$  on the form of the power spectrum, which control the variances of the gamma-distributions. The behaviour is obviously parameter dependent, but if we hold the intrinsic parameters  $\{\beta, \sigma, \gamma, \mu, \eta\}$  fixed, then we can make a number of observations.

Independent of the other parameters, changing  $M$  has a simple effect on the power spectrum. Increasing  $M$  (decreasing the variance of the exposed period

distribution) increases the amplitude of the spectrum with a negligible change to its frequency. This is illustrated in Figure 5.2. The longer the exposed period, as compared with the infectious period, and the larger  $L$ , the larger the increase in amplitude. The biggest changes happen for the smaller values of  $M$ , typically less than 10, where the exposed period distribution changes the most.

The effect of  $L$  on the power spectrum is more complicated and can change both the peak frequency and amplitude. Firstly, independent of  $M$ , increasing  $L$  shifts the peak frequency of the spectrum to higher values. The effect on the amplitude depends on whether the infectious period is longer, approximately equal or shorter than the exposed period. When the infectious period is longer than the exposed period ( $\sigma > \gamma$ ) then the results are similar to that of the SIR model with gamma distributed infectious periods, as discussed in the previous chapter. Thus increasing  $L$ , increases both the amplitude and the peak frequency of the spectrum, see Figure 5.3. Again the largest changes are seen for smaller values of  $L$ .

If the exposed period is longer than the infectious period ( $\gamma > \sigma$ ), as with measles [2], then there is still an increase in frequency with increasing  $L$ , but a decrease in amplitude; see Figure 5.2. When the two average periods are approximately equivalent ( $\gamma \approx \sigma$ ) the behaviour is not as easy to quantify and the amplitude is not necessarily an increasing function of  $L$  [80], however any shifts tend to be small.

## 5.3 Whooping cough analysis

In this section we apply our analysis to the seasonally forced, staged SEIR model, proposed by Nguyen & Rohani [19] as an explanation for the long term dynamics of whooping cough before and after mass vaccination. Their model includes seasonal forcing by assuming that the contact rate,  $\beta(t)$ , follows a term-time pattern [37, 45],

$$\beta(t) = \beta_0(1 + \beta_1 \text{term}(t)), \quad (5.12)$$

where  $\beta_0$  is the baseline contact rate,  $\beta_1$  the magnitude of forcing and  $\text{term}(t)$  is a periodic function that switches between +1 during school terms and -1 during

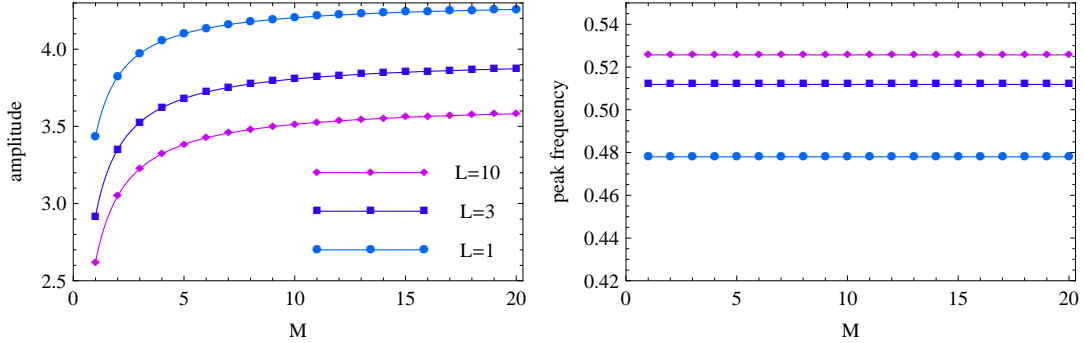


Figure 5.2: The amplitude and peak frequency of the analytic power spectrum as a function of  $M$ , the exposed period variance parameter. Increasing  $M$  (decreasing the variance of the exposed period distribution) increases the amplitude of the spectrum, while having negligible effect on the peak frequency. Parameters are typical of measles:  $\beta = 3.4 \text{ d}^{-1}$ ,  $\sigma = 1/8 \text{ d}$ ,  $\gamma = 1/14 \text{ d}$ ,  $\mu = 5.5 \times 10^{-5} \text{ d}^{-1}$  and  $\eta = 10^{-6} \text{ d}^{-1}$ . In this example the exposed period is longer than the infectious period so the spectra with larger  $L$  have smaller amplitudes.

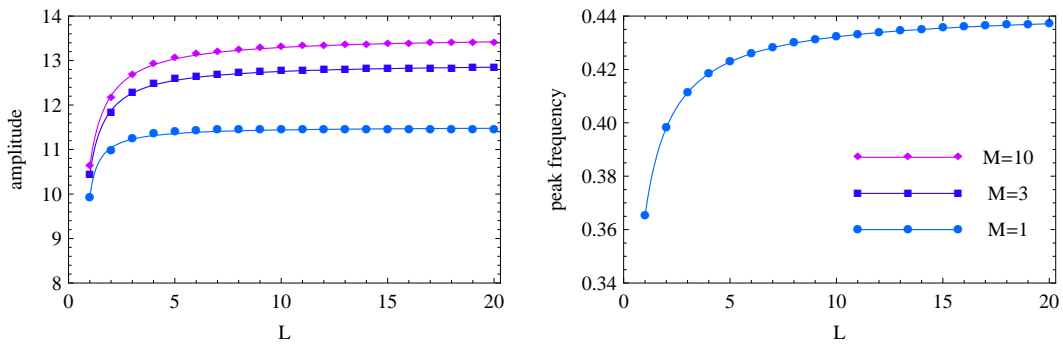


Figure 5.3: The amplitude and peak frequency of the analytic power spectrum as a function of  $L$ , where the infectious period is longer than the exposed period. Increasing  $L$  leads to an increase in the peak frequency and amplitude of the spectrum. The change in frequency is independent of  $M$ . Parameters are typical of whooping cough:  $\beta = 1.2 \text{ d}^{-1}$ ,  $\sigma = 1/8 \text{ d}$ ,  $\gamma = 1/14 \text{ d}$ ,  $\mu = 5.5 \times 10^{-5} \text{ d}^{-1}$  and  $\eta = 10^{-6} \text{ d}^{-1}$ .

holidays. We use the England and Wales term dates as set down in [45],

$$\text{term}(t) = \begin{cases} +1 & \text{days } 7 - 99, 116 - 199, 252 - 299, 308 - 355 \\ -1 & \text{days } 365 - 6, 100 - 115, 200 - 251, 300 - 307 \end{cases}. \quad (5.13)$$

The problem now explicitly includes time-dependence which is simple to include in simulations with appropriate changes to the Gillespie algorithm, detailed in Section 2.3. We consider the full time-dependent master equation in the next chapter, but here we replace  $\beta(t)$  in the master equation with the average effective  $\beta$ , defined as,

$$\langle \beta \rangle = \beta_0 [p_s(1 + \beta_1) + (1 - p_s)(1 - \beta_1)], \quad (5.14)$$

where  $p_s$  is the time spent in school, as opposed to on holiday; for the term dates given in (5.13),  $p_s = 0.75$ . As we show in the next section, for this particular model, simulations confirm this as a good approximation.

All other parameters are taken from [19]. Before vaccination  $R_0 = 17$ , from which we find  $\langle \beta \rangle \approx \gamma R_0 = 1.21$ . After vaccination,  $p = 0.6$  so  $\langle \beta \rangle^{\text{vac}} \equiv (1 - p)\langle \beta \rangle = 0.48$  [35]. Assuming  $\beta_1 = 0.25$  and using Eq. (5.14) we find that  $\beta_0 = 1.075$  pre-vaccination and  $\beta_0^{\text{vac}} = 0.427$ . These are lower than  $\langle \beta \rangle$  because children spend more time in school when  $\beta(t)$  is higher. The intrinsic parameters, estimated from household incubation data, are:  $1/\sigma = 8$  days,  $M = 1$ ,  $1/\gamma = 14$  days,  $L = 4$  and  $\mu = 5.5 \times 10^{-5}$  per day.

These authors assume a small rate of infectious imports of  $\delta = 10$  per million per year. We can convert this to our commuter model formulation of immigration by noticing that to a good approximation  $\eta \approx (\delta/N)R_0$  [3, p. 210]. This gives  $\eta = 5 \times 10^{-7}$  per day.

### 5.3.1 Results

Figure 5.4 shows the predicted analytic spectra before and after vaccination. The results of using a gamma distributed infectious period, as compared with a standard exponential, is to shift the peak frequencies, while only slightly increasing the amplitudes of the power spectra. Further increases to  $L$  have much smaller effects on the power spectrum, see Figure 5.3. Figure 5.4 also shows the peak frequencies from simply carrying out a deterministic analysis of the imaginary part of the eigenvalues. As can be seen for this choice of parameters, demographic stochasticity causes only very small shifts in frequency away from those

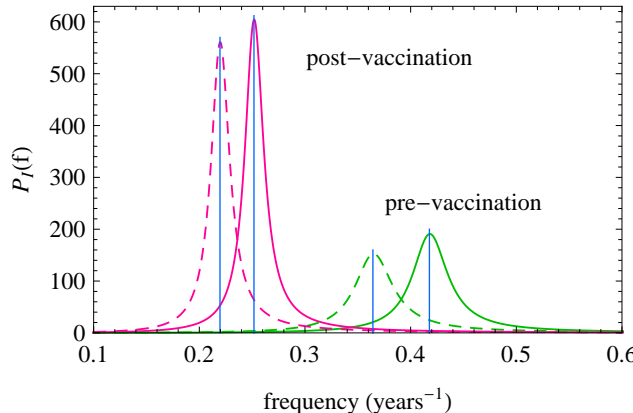


Figure 5.4: Comparison of the analytic power spectra for whooping cough using the SEIR (dashed curves) and staged-SEIR (solid curves) models. Parameters are given in the main text. Using the staged version shifts the peak periods from 2.7 to 2.4 years pre-vaccination and from 4.5 to 4 years post-vaccination. The blue line show the peak frequencies from an analysis of just the deterministic model.

predicted by the deterministic theory [7].

Figure 5.5 shows power spectra from simulations of the staged-SEIR model which include the time-dependent  $\beta$ , along with the analytic predictions. The simulations were initialised near to the fixed point of the unforced system, and transients were allowed to damp down before the data for the power spectra was collected. Other initial conditions were tried, but it was found that the dynamics always settled into the annual attractor. As the transients have essentially the same frequency as the stochastic oscillations, it is important to make sure these have damped down, otherwise the stochastic peak in the power spectrum will appear enhanced. The length of each time series was about 700 years; this is certainly very large, but was chosen to facilitate a good resolution on the power spectrum without aliasing [22]. The simulations show an annual peak at 1 year, which comes from the macroscopic limit cycle induced by the external seasonal forcing, and a stochastic peak at lower frequencies. In general there are more harmonic peaks at  $1/2, 1/3$ , etc. years, but these are much smaller and not shown for clarity.

Pre-vaccination the analytic prediction is good at lower frequencies, but there is enhancement, giving a higher amplitude and very slight shift in frequency. This is in contrast to the post-vaccination model where the analytic curve provides a very good fit, but still somewhat enhanced. The amount of power under each peak depends on the population size. The annual macroscopic peak scales with

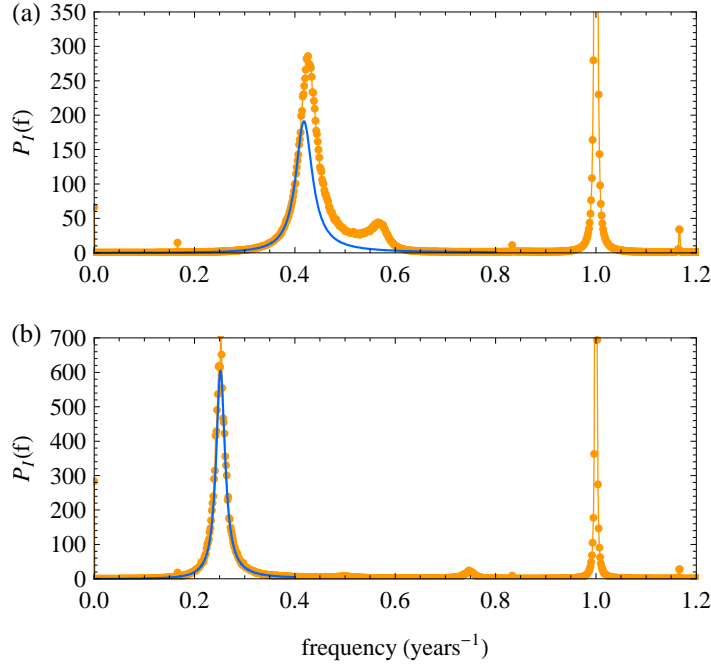


Figure 5.5: Theoretical and numerical power spectra for the whooping cough model: (a) pre-vaccination, and (b) post-vaccination. The light orange dotted lines are the average of 2000 realisations of the stochastic simulation, including seasonal forcing. The dark blue curves are the theoretical predictions. The forcing slightly shifts the frequency and amplitude of the stochastic peaks from the analytic prediction, but is otherwise good. The value of  $N$  is  $5 \times 10^6$ , with other parameters being given in the main text. The annual peaks in the numerical spectra are cropped for clarity in the comparison.

$N^2$ , while the stochastic part scales with  $N$ . In the post-vaccination case the stochastic peak is larger and the annual peak smaller by a factor of a third than in the pre-vaccination simulations. The sub-dominant peaks seen in the numerical power spectra are not predicted by the time-independent analytical calculation. They are predicted in the full time-dependent theory which is developed in the next chapter.

In the time series the dominant period can appear to change. This is due to the superposition of the macroscopic limit cycle and stochastic fluctuations. The power of the stochastic oscillations is spread out over a range of frequencies. Although there is a dominant frequency, at certain times the stochastic oscillations will be of a much longer/shorter frequency, with a much reduced amplitude. This allows the macroscopic signal to be seen more strongly, thus generating the effect

of a changing period.

Simulating the system at smaller population sizes results in small shifts to the peak frequencies [67], but does not alter the qualitative picture. For the whooping cough model, significant shifts occurs at  $N < 10^6$ . Taking a smaller, more biologically realistic [21], forcing magnitude (eg,  $\beta_1 = 0.15$ ), results in significantly better agreement with the analytic predictions at lower population sizes.

## 5.4 Discussion

In this chapter we have derived the power spectrum for the staged SEIR model and used this to quantify the stochastic oscillations in a model of whooping cough. The ability to derive the exact power spectrum gives considerable insight, especially with regards to the effects of the parameters  $M$  and  $L$  on the form of the spectrum. Having the analytical method is especially useful for this model as it allows us to generate results valid over a large range of parameters (Section 5.2). To compute these using simulations would be very time consuming and still not offer the insight which is available from analysis.

In the previous chapter we discussed that gamma-distributed models are much more sensitive to seasonal forcing, in the sense that the bifurcation to biennial dynamics happens at lower forcing magnitudes, than in the basic exponential model. Lloyd [80] attributes this increased sensitivity to a destabilisation of the model, but our analysis goes further to show that a distributed infectious period also tends to increase the natural frequency of the system. We conjecture that it is this effect rather than the decreased stability that makes these models more sensitive to seasonal forcing. This should be easy to test within the SEIR framework as, with the appropriate choice of parameters, we can tune the size and frequency of the power spectrum. It should be possible to see whether a model with only a distributed exposed period is more sensitive to forcing, as this would be destabilised but with the same natural frequency. This is discussed more in Chapter 7.

The stochastic dynamics of models of whooping cough have been the source of debate for long time [16, 19, 45, 46]. Our approach, which allows us to be much more quantitative, can encompass both older SEIR results and the newer staged-SEIR model of Nguyen & Rohani [19]. External forcing creates a macroscopic

annual limit cycle with stochastic oscillations about it. For the case of whooping cough, the oscillations about the limit cycle are very similar to those of the unforced model and the two components of the power spectrum, the macroscopic (from the limit cycle) and the stochastic, can be viewed as approximately independent of each other. Using the staged-SEIR model changes this picture only in that it shifts the frequency of the stochastic oscillations; it does not change the basic nature of the dynamics.

Our results argue against multiple coexisting attractors in the stochastic whooping cough system. Further investigation has shown that the bifurcation diagrams of Nguyen & Rohani [19] are not robust to the inclusion of immigration. Even small amounts as used in the simulations depress the onset of period three attractors which only appear at significantly higher magnitudes of forcing. This effect, whereby immigration can destroy longer period attractors, has been reported before [7, 84, 123]. One can speculate that the lack of immigration in the deterministic analysis of Nguyen & Rohani [19] might explain their findings, alternatively there may be other stable solutions of the deterministic equations, but that the noise is never strong enough to move the system towards them.

In this analysis we used  $\beta_1 = 0.25$ , which is a comparatively large value for this parameter. Most other studies find a smaller value,  $\beta_1 = 0.15$  [21]. Nguyen & Rohani only use the larger value because it puts their deterministic system into a regime with co-existing attractors. In light of our work, there would seem to be even less evidence to support such a large value of  $\beta_1$  for whooping cough. One aspect we have ignored is the importance of waning immunity in whooping cough [124]. This is where a recovered losses their immunity and becomes susceptible again (effectively  $R \xrightarrow{\kappa} S$ ). This would be very easy to include in the model, but we do not expect it to alter our results significantly as the time scale for this is of the order of tens of years [124].

It is surprising that the predictions from the unforced model remain so good in the presence of forcing—there is no *a priori* reason to expect this to be true. In the next chapter we develop the full time-dependent theory, which sheds more light on this and can account for the deviations seen in power spectrum shown in Figure 5.5.

# Chapter 6

## Seasonal forcing

---

The model of whooping cough, presented in the previous chapter, included seasonal forcing, but that case we chose to approximate the time dependence in the master equation by a constant value. Results from simulations confirmed this as a good approximation. For whooping cough models the forcing has only limited consequences for the deterministic dynamics; there are only ever found to be annual limit cycles [19]. For a disease such as measles this is not the case and forcing can, among other things, induce period doubling in the deterministic dynamics. In this chapter we analyse the full time-dependent master equation for the SIR model with term-time seasonal forcing. We use this to confirm the results from the previous chapter and to help understand the dynamics and large-scale temporal transitions in measles epidemic patterns [35].

The theory we develop in this chapter unifies much of the previous work on these models. It encompasses the influential work of Earn *et al.* [35] in understanding the transitions in measles epidemics, the later work of Bauch & Earn [21] relating to the transient fluctuations close to cyclic attractors for different diseases and the more recent work on stochastic amplification in epidemic models, which has been presented in the last three chapters. Up till now the most successful synthesis, by Bauch & Earn [21], showed that a simple SEIR model can accurately predict the positions of peaks in the power spectrum of a number of different disease time series. The picture that emerges from our work is close to that proposed by Bauch & Earn [21], but goes beyond it in two important respects. Firstly, we calculate the exact power spectrum for the forced model. Secondly, we show how the forcing changes the form of the fluctuations, and

how in a stochastic model these are intimately related to the period doubling bifurcation, which is vital for explaining the dynamics of measles.

The SIR model is exactly the same as presented in Section 2.2 except that  $\beta$  is now a function of time following the term-time pattern as in Eq. (5.12). We use the SIR model for technical simplicity; extending this analysis to the staged-SEIR model is computationally difficult and adds no real further insight. The expansion of the master equation follows exactly as in Section 2.4 except that now both the Jacobian and correlator matrices depend on time through  $\beta$ ,  $\phi$  and  $\psi$ . We repeat the main results here for reference, using slightly modified notation to make clear the time dependence. The deterministic equations are,

$$\begin{aligned}\dot{\phi} &= -\beta(t)\phi\psi - \eta\phi + \mu(1 - \phi), \\ \dot{\psi} &= \beta(t)\phi\psi + \eta\phi - (\mu + \gamma)\psi.\end{aligned}\tag{6.1}$$

At next-to-leading order the Langevin equations for the stochastic corrections are,

$$\dot{\mathbf{x}} = K(t)\mathbf{x}(t) + \mathbf{f}(t),\tag{6.2}$$

where  $\mathbf{x} \equiv \{x, y\}$ , and  $\mathbf{f}(t)$  are Gaussian white-noise terms with correlation function  $\langle \mathbf{f}(t)\mathbf{f}(t')^T \rangle = G(t)\delta(t-t')$ . The matrices  $K(t)$  and  $G(t)$  are determined from carrying out the expansion and are given by

$$K(t) = \begin{pmatrix} -\beta\bar{\psi} - \eta - \mu & -\beta\bar{\phi} \\ \beta\bar{\psi} + \eta & \beta\bar{\phi} - \gamma - \mu \end{pmatrix},\tag{6.3}$$

and

$$\begin{aligned}G_{11} &= \beta\bar{\phi}\bar{\psi} + \eta\bar{\phi} + \mu(1 - \bar{\phi}), \\ G_{22} &= \beta\bar{\phi}\bar{\psi} + \eta\bar{\phi} + (\gamma + \mu)\bar{\psi}, \\ G_{12} &= G_{21} = -\beta\bar{\phi}\bar{\psi} - \eta\bar{\phi} - \mu\bar{\psi},\end{aligned}\tag{6.4}$$

where a bar indicates that the solutions are evaluated on the limit cycle.

## 6.1 Deterministic dynamics

The mean behaviour is found by integrating the deterministic equations (6.1). As discussed in Chapter 3, when  $\beta_1 = 0$ , solutions show damped oscillations tending to a fixed point [2]. For non-zero  $\beta_1$ , this model can display a rich set of dynamics

including chaos [9, 55], but for realistic parameter values the most common long-time solution is a limit cycle with a period that is an integer multiple,  $n$ , of a year [33, 52]. As the forcing is a step function in time (see Eq. (5.12)), we can visualise this as the system alternately switching between two spiral fixed-points [45] resulting in a piecewise continuous limit cycle, illustrated in Figure 6.1. Any other periodic forcing function, for instance a sinusoidally varying one, could be used without more difficulty, and would typically lead to a limit cycle which is smooth. As  $\beta_1$  is increased, the limit cycle grows (although typically not linearly with  $\beta_1$ ) and at critical values bifurcations are induced to longer period solutions [53, 54].

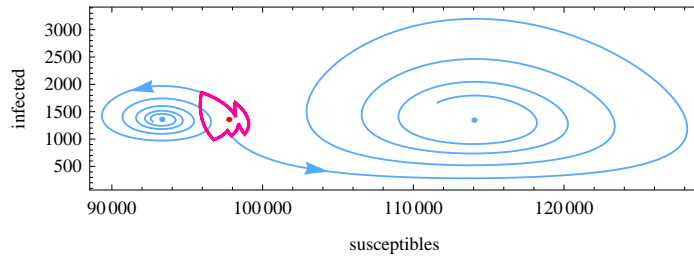


Figure 6.1: Phase portrait illustrating a deterministic solution of the forced SIR model. The term-time forcing creates a limit cycle (red curve) as the system alternately spirals between the two fixed points defined by  $\beta_H = \beta_0(1 + \beta_1)$  and  $\beta_L = \beta_0(1 - \beta_1)$ . The light blue solutions show the behaviour if the forcing was switched off, to illustrate the two spiral attractors. The red dot shows the fixed point calculated using the approximation where  $\beta(t)$  is replaced by  $\langle \beta \rangle$ .

The stability of these limit-cycle solutions can be investigated with the use of Floquet theory [125, 126]. This quantifies how perturbations to the trajectory of the limit cycle behave and is analogous to linear stability analysis about a fixed point [127]. The variational equation describing these small perturbations  $\mathbf{x} \equiv \{x, y\}$  is

$$\dot{\mathbf{x}} = K(t)\mathbf{x}, \quad (6.5)$$

where  $K(t)$  is the time-dependent Jacobian (6.3). A fundamental matrix or propagator  $X(t)$ , is formed from the linearly independent solutions of Eq. (6.5). Thus one can write the general solution to Eq. (6.5) as  $\mathbf{x}(t) = X(t)\mathbf{c}$ , where  $\mathbf{c}$  is a vector of constants. If we have an initial condition,  $\mathbf{x}(0) = \mathbf{x}_0$ , then  $\mathbf{c} = X^{-1}(0)\mathbf{x}_0$ . It follows that any fundamental matrix satisfies the relation,

$$\dot{X}(t) = K(t)X(t). \quad (6.6)$$

Floquet theory states that for any periodic solution of Eq. (6.1) there exists a matrix  $B$  which satisfies the relation,

$$X(t + T_n) = X(t)B, \quad (6.7)$$

where  $X(t)$  is the fundamental matrix [127] and  $T_n$  is the period of the limit cycle. The eigenvalues of  $B$  are called the Floquet multipliers,  $\rho_i$ ; a related set of quantities are the Floquet exponents  $\lambda_i = \ln(\rho_i)/T_n$  (since we will be discussing frequencies rather than angular frequencies, these exponents will be divided by a factor of  $2\pi$ ). The matrix  $X(t)$  is not unique and will depend on the initial conditions used to solve Eq. (6.6), but the multipliers are unique for a given limit-cycle.

Another way to think of this is as linear stability analysis of the fixed points of the  $n$ -cycle Poincare map of the system [21, 125]. This is where a section is taken of the deterministic system every  $n$  years. Thus a 2 year limit cycle sampled every 2 years will produce a a fixed point in phase space. A limit-cycle solution will be stable if  $|\rho_i| < 1$ . When the multipliers are complex, perturbations to the trajectories return to the limit-cycle in a damped oscillatory manner, analogous to a stable spiral fixed point [127]. Similar ideas have been used to investigate the transients in forced epidemic systems in the past, but only in a deterministic setting [21, 128]. Here we will explore how the nature of the fluctuations can be quantified using Floquet theory.

## 6.2 Annual limit cycle

In this section we present results where there is only an annual limit-cycle ( $n = 1$ ). The case where we also have a period doubling is examined in Section 6.3. Figure 6.2 shows a simulation of the full stochastic system together with the deterministic limit-cycle solution, using whooping cough parameters, which we know generates an annual limit-cycle. We can see that even for large populations the stochastic corrections to the deterministic solution are important. The noise due to demographic stochasticity excites the natural oscillatory modes about the limit cycle, creating a resonance and giving rise to large scale coherent oscillations. As described in Appendix B, by solving the Langevin equations (6.2) using aspects

of Floquet theory, we can express the auto-correlation function,

$$C(\tau) = \frac{1}{T_n} \int_0^{T_n} \langle \mathbf{x}(t + \tau) \mathbf{x}^T(t) \rangle dt, \quad \mathbf{x} \equiv \{x, y\}, \quad (6.8)$$

as an integral without further approximation [126]. Taking the Fourier transform of this expression then gives an exact expression for power spectrum of these stochastic oscillations.

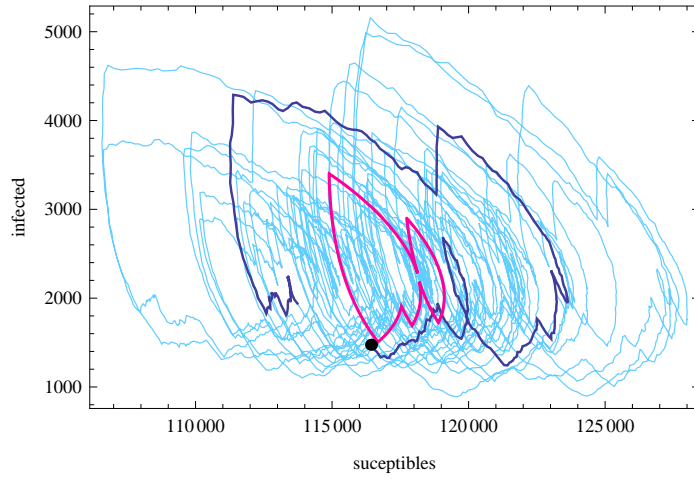


Figure 6.2: Phase portrait of the stochastic SIR system. A time-series of 100 years duration is shown in light blue. The first two years are highlighted in dark blue, with the dot showing the start point. The macroscopic limit-cycle (red) is also superimposed. Parameters are those relevant for whooping cough [19]:  $R_0 = 17$ ,  $\gamma = 1/22$ ,  $\beta_1 = 0.25$ ,  $\mu = 5.5 \times 10^{-5}$ ,  $\eta = 10^{-6}$  and  $N = 2 \times 10^6$ .

Figure 6.3 shows simulated and analytic power spectra for the system shown in Figure 6.2. We observe a sharp peak at 1 year due to the deterministic annual limit-cycle and a number of broader peaks due to the stochastic amplification of the transients. In general there are other harmonics of the deterministic peak at higher integer frequencies, but these are much smaller and not shown for clarity. We would expect on general grounds that the stochastic peaks would be observed at frequencies,

$$m/T_n \pm \text{Im}(\lambda), \quad (6.9)$$

where  $m$  is an integer and  $\lambda$  is the Floquet exponent [126, 129], and this is indeed what is seen. For the annual limit-cycle the dominant peak is at  $0 + \text{Im}(\lambda)$ , with the other peaks being much smaller. Near bifurcation points these minor peaks become important and are treated in more detail in the following section.

Looking back to Section 5.3 we can see the same structure in the numerical power spectrum shown in Figure 5.5 for the staged whooping cough model.

The area under the peaks in the power spectrum is proportional to the root-mean-square amplitude of the oscillations. Away from any deterministic bifurcation points the amplitude is proportional to  $\text{Re}(\lambda)$ , as in the unforced model. Thus the spectrum is close in form to that predicted from the unforced model by substituting  $\langle \beta \rangle$  for the time-independent transmission rate [130], as shown in Chapter 5.

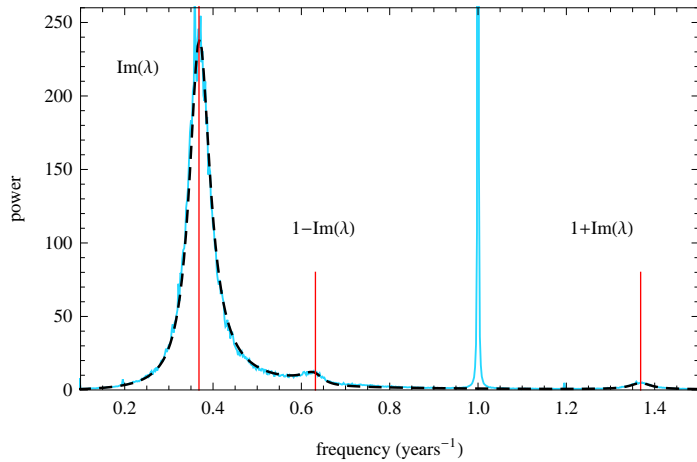


Figure 6.3: Power spectra for the number of infectives from simulation (light blue solid curve) and analytic calculation (black dashed curve). From the simulations, we observe a sharp peak at 1 year from the deterministic annual-limit cycle. The other peaks, marked by the red lines, are from stochastic amplification, with the peak frequencies given by  $m \pm \text{Im}(\lambda)$ , where  $\text{Im}(\lambda) = 0.36$ . The dominant stochastic period is therefore  $1/0.36 = 2.7$  years. Parameters are as in Figure 6.2.

There is good agreement between analytical calculations and simulations. Although calculations give the power spectrum as an integral, it must be evaluated numerically because the deterministic equations (6.1) cannot be solved in closed form; this is all carried out using the symbolic package Mathematica [110]. This analysis about an annual limit cycle corresponds to that of Bauch & Earn [21] except that we can derive the full power spectrum. They term the ‘resonant peak’ what we describe as the deterministic or annual peak, and the ‘non-resonant peak’ what we describe as the stochastic peaks. Their terminology is somewhat misleading, as the stochastic peak is generated by a resonance phenomena whereas the macroscopic peak is not.

## 6.3 Period doubling and measles transitions

We can use our analytic methods to help understand the dynamics and large-scale temporal transitions in measles epidemic patterns, first investigated by Earn *et al.* [35]. The main force in driving these transitions is changes in the susceptible recruitment (a mixture of changes in birth rates and vaccination), which, as shown in Chapter 5 can be mapped onto  $R_0$ . Thus a knowledge of the model dynamics as a function of  $R_0$  can be used to explain the changes in epidemic patterns. Although the analysis of Earn *et al.* [35] is in good qualitative agreement with time-series data, there are a number of outstanding questions with regard to the interpretation of the mechanisms for the dynamics. We first provide a brief review of the original analysis and then go on to show how the stochastic dynamics of this model can be understood within the framework we have laid out in the previous section.

### 6.3.1 Review of Earn's original analysis

It is acknowledged that stochasticity plays a role in the dynamics of measles, which can only be captured through simulation of the individual-based model. Fundamentally though, the analysis of these mechanisms by Earn *et al.* is deterministic. Figure 6.4 shows the bifurcation diagram derived from the SIR equations (6.1), as a function of  $R_0$ , with parameters corresponding to measles and no immigration ( $\eta = 0$ ). This shows the incidence sampled annually on the 1st of January each year, thus stable limit cycles are shown by different numbers of (colour coded) curves. The single curve, beginning at small  $R_0$ , shows an annual cycle which bifurcates at  $R_0 = 15.5$  into two curves giving a biennial cycle. For values of  $R_0$  lying between about 5 and 15, there are several sets of  $n$  curves representing  $n$ -year cycles.

For large  $R_0$  (e.g.  $R_0 \approx 30$ ) only an annual limit cycle exists. As  $R_0$  is reduced a biennial limit-cycle is found; before vaccination was introduced in England and Wales, most cities would be in this region. Higher birth-rates might move the system back into the region with only an annual attractor, whereas vaccination would act to reduce  $R_0$ , moving it into the region with multiple co-existing longer period attractors. The interpretation put forward by Earn et al, is that stochasticity will then cause the system to jump between these different deterministic states [72], giving rise to irregular patterns. Thus, in this description, noise plays

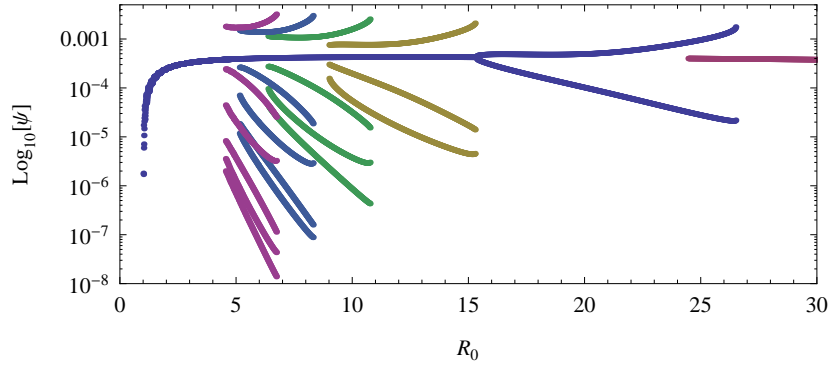


Figure 6.4: Bifurcation diagram showing the SIR dynamics as a function of  $R_0$ . Fixed parameters:  $\beta_1 = 0.29$ ,  $\gamma = 1/13$ ,  $\mu = 5.5 \times 10^{-5}$  and  $\eta = 0$ . The different period limit cycles are shown in different colours, which are produced by different initial conditions.

a passive role [5].

Although peaks were seen in power spectra from simulations, which *appear* to confirm this view, there are a number of problems with this interpretation. As with the whooping cough model, the crucial aspect that is neglected is that there are no infectious imports included in the deterministic analysis (although presumably they are included in simulations). When this factor is introduced ( $\eta \neq 0$ ) then most of the additional structure disappears, see Figure 6.5a; we are left with an annual limit cycle and a period doubling [7, 84, 123].

When  $\eta = 10^{-6}$ , there is only a small region in the range  $24 < R_0 < 25$  where there are coexisting annual and biennial limit-cycles. As the immigration parameter is reduced some of the additional structure reappears; for example at  $\eta = 10^{-7}$  some of the period 3 attractors can be found in the range  $9 < R_0 < 11$ . As  $\eta$  is decreased further still, more of the structure is found [61, 107].

Immigration is an important aspect in the simulation because without it the disease would fade out as the minimum number of infections can go far below a single individual [65, 104, 107]. In a deterministic analysis this term is easily omitted because the variables are continuous and therefore fadeout cannot happen [63]. This raises the question: do these longer period solutions have an effect on the stochastic dynamics? If not, how can we describe the nature of the stochastic dynamics? We can use our analytic method to help clarify these questions. The power spectrum is especially useful as it can show up anomalous peaks from simulations.

### 6.3.2 Analytic predictions

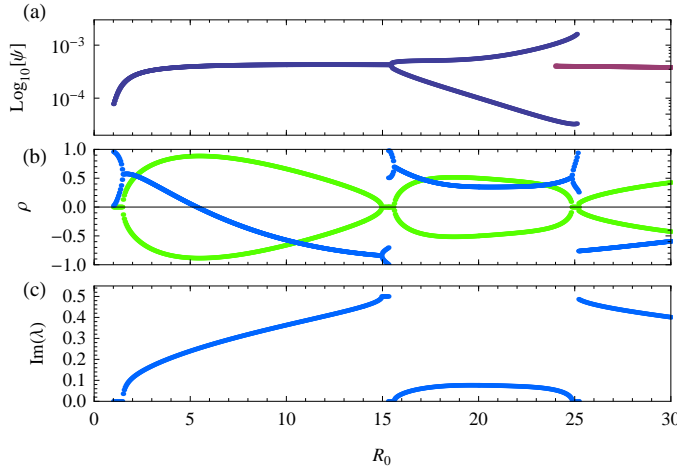


Figure 6.5: (a) Bifurcation diagram for the SIR model with  $\beta_1 = 0.29$  and  $\eta = 10^{-6}$ . (b) The Floquet multipliers are in general a complex conjugate pair, thus we plot the real (dark blue) and imaginary (light green) parts separately. (c) Imaginary parts of the Floquet exponents. Note that in the region where there are the coexisting limit cycles ( $24 < R_0 < 25$ ), only the multipliers/exponents for the biennial cycle are shown for clarity.

Figure 6.5 shows the bifurcation diagram for the model presented in the previous section, but with  $\eta = 10^{-6}$ , along with the Floquet multipliers and exponents. These parameter values will be used for the rest of this section. Figure 6.6 shows the Floquet multipliers on a larger scale near the period doubling bifurcation point and Figure 6.7 shows the analytical and numerical power spectra for various values of  $R_0$  with  $N = 5 \times 10^6$ . Away from any bifurcation points there is good agreement between the analytic and the simulated spectra.

As we approach the period-doubling bifurcation point from below, the stochastic oscillations follow a virtual-Hopf pattern [129, 131]. This is where the oscillations first show the precursor characteristics of a Hopf bifurcation (peaks in the power spectrum at  $m/T_n \pm \text{Im}(\lambda)$ , as in the previous section) before changing into the precursor characteristics of a period-doubling (a broad peak in the spectrum centered at double the frequency of current deterministic limit cycle). This is clearly seen in the power spectra shown in Figure 6.7. In the Hopf-like regime ( $R_0 < 14.94$ ), the Floquet multipliers are a complex conjugate pair, giving rise to two peaks in the spectrum: a major one at frequency  $\text{Im}(\lambda)$  and a minor one at  $1 - \text{Im}(\lambda)$ , as in Section 6.2. Therefore in Figure 6.7a the two peaks are most

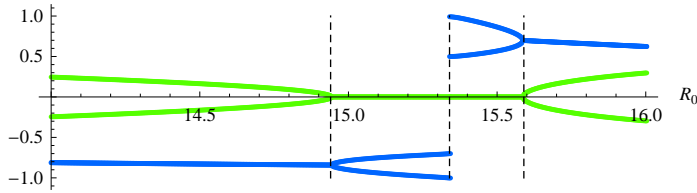


Figure 6.6: Floquet multipliers near to the period doubling bifurcation point, showing the virtual-Hopf pattern. For  $R_0 < 14.94$  the multipliers are a complex conjugate pair, with a negative real part (dark blue line); this is the Hopf-like region. The actual period-doubling bifurcation occurs at  $R_0^{\text{bif}} = 15.34$ , where one of the multipliers becomes equal to  $-1$ .

widely separated for  $R_0 = 4$ .

As we increase  $R_0$ ,  $\text{Im}(\lambda)$  also increases, and the major and minor peaks move closer together, converging at  $0.5 \text{ years}^{-1}$  when the multipliers become real and negative; this marks the onset of the period doubling regime, see Figure 6.6. In this regime ( $14.94 < R_0 < 15.34$ ), as the multipliers are negative, so their phase is  $\pm\pi$  and so the imaginary part of the Floquet exponents is  $\pm\pi/2\pi T_1 = \pm 0.5$ . Therefore the peak stays fixed at  $0.5 \text{ years}^{-1}$  as we increase  $R_0$  further within this range, but the amplitude increases quickly. At  $R_0^{\text{bif}} = 15.34$  one of the multipliers reaches  $-1$  and we see a deterministic period doubling [125], and the size of the fluctuations grows to order  $N$ . Figure 6.8 shows how in this way the oscillations smoothly turn into the macroscopic biennial limit cycle. The same pattern is seen if we hold  $R_0$  fixed and increase  $\beta_1$  to induce a period doubling.

When the system is in the biennial regime we can still calculate the fluctuations about the limit cycle and get a good correspondence with analytic predictions (Figure 6.7b). The positions of the peaks are now at  $m/2 \pm \text{Im}(\lambda)$  and the spectrum changes little within this parameter range. The peaks at  $m/2 + \text{Im}(\lambda)$  are barely visible, as compared to the prominent peaks at  $m/2 - \text{Im}(\lambda)$ . In the annual regime after the doubling ( $R_0 > 25$ ), the analytic results are again very accurate, with stochastic peaks at frequencies  $m \pm \text{Im}(\lambda)$  (Figure 6.7c). Here as well, the set of peaks at  $m + \text{Im}(\lambda)$  are much smaller. Note that in both of these regions the time-series will be dominated by the deterministic signal as the stochastic oscillations are much smaller than in the pre-bifurcation region ( $R_0 < 15$ ).

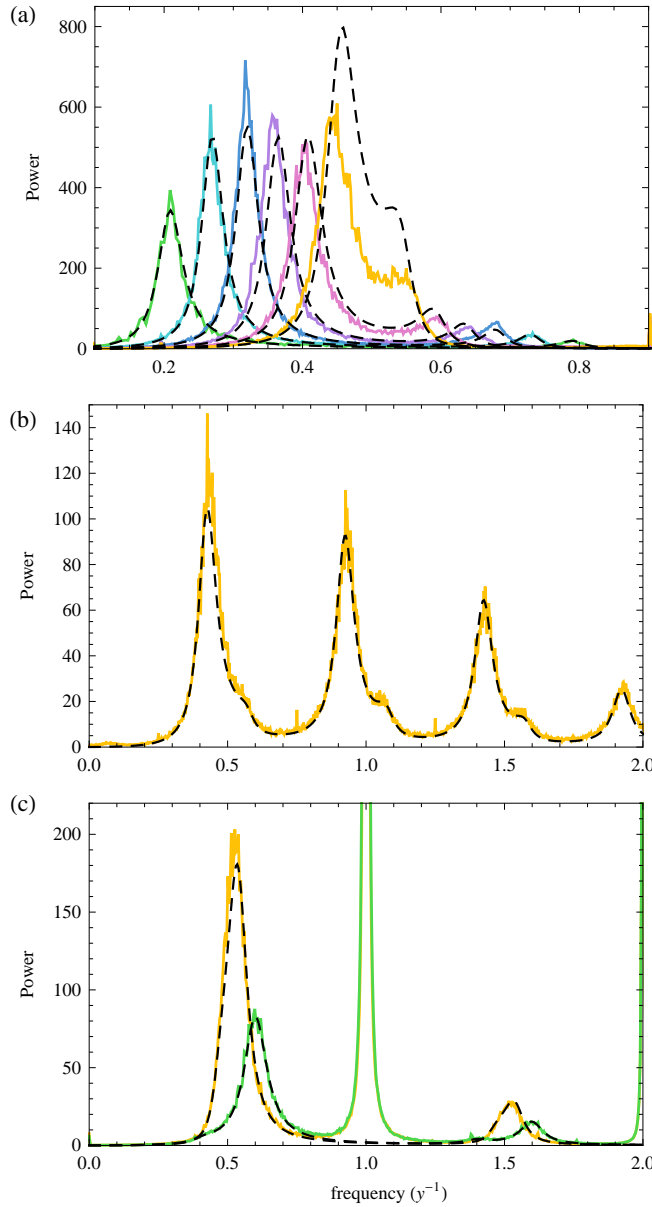


Figure 6.7: Analytic (black dashed curves) and numerical (coloured) power spectra for a range of  $R_0$  with  $N = 5 \times 10^6$ . In most cases the analytic and numerical spectra are virtually indistinguishable, apart from  $R_0 = 14$ . (a) Spectra before the bifurcation,  $R_0 = 4, 6, 8, 10, 12, 14$ . As  $R_0$  is increased the dominant frequency moves towards  $0.5 y^{-1}$ . (b) Typical biennial regime,  $R_0 = 20$ . Note that the stochastic peaks have been made clearer by subtracting the deterministic dynamics before calculating the power spectrum. The spectrum would otherwise be dominated by the peak at  $0.5 y^{-1}$ . (c) The major and minor peaks in the large  $R_0$  annual regime:  $R_0 = 26, 30$ , with the larger peaks corresponding to  $R_0 = 26$  for both the major and minor peaks.

### 6.3.3 Near the bifurcation point

For values of  $R_0$  near the bifurcation point, the deviations between the analytic and simulated spectra become larger (see for example Figure 6.7a;  $R_0 = 14$ ). This is expected: the analysis developed here is essentially linear and thus predicts an unbounded increase in the fluctuations as we approach the bifurcation point [132]. As the fluctuations become larger the linear approximation breaks down and non-linear effects become important and act to bound the fluctuations. Going to larger system sizes can result in better agreement between analytic results and simulation, but this will always break down at some point.

Although the analytic approximation breaks down near the bifurcation point, the structure we have uncovered is still visible. Figure 6.8 shows stochastic power spectra from simulations for  $14 < R_0 < 18$ , as we move though the bifurcation point. The virtual-Hopf pattern is still clear, as predicted by the analysis, but the fluctuations remain bounded, growing to the same order as the system size [78, 133]. Within this region the macroscopic dynamics cannot be split into a deterministic and stochastic part and it is not in general possible to reconstruct the deterministic part by averaging over many realisations. Thus, determining exactly where the bifurcation takes place is difficult [129]. At  $R_0 = 16$  the deterministic biennial peak should be observed, but is not clearly visible until  $R_0 = 18$ . It is possible that the bifurcation point is shifted in the stochastic system, but more analysis is required to determine that this is so.

### 6.3.4 Smaller populations

The results presented in the previous sections were for  $N = 5 \times 10^6$ , which roughly corresponds to the largest populations we would be interested in modelling. Simulations of smaller populations tend to show regular deviations from the analytic calculations and results are sensitive to  $N$ ,  $\eta$  and  $\beta_1$ . The forcing pushes the system close to the fade-out boundary ( $I = 0$ ), where fluctuations are non-Gaussian, and so large deviations from the theory are expected. Figure 6.9 shows the stochastic power spectra from simulations, within the range  $4 \leq R_0 \leq 30$  and with  $N = 5 \times 10^6, 10^6$  and  $5 \times 10^5$ .

For smaller values of  $R_0$  we still clearly observe the virtual-Hopf pattern, but a visual inspection of the time-series shows much more irregular dynamics. This is due to the increased stochasticity in the smaller systems, but also the closeness

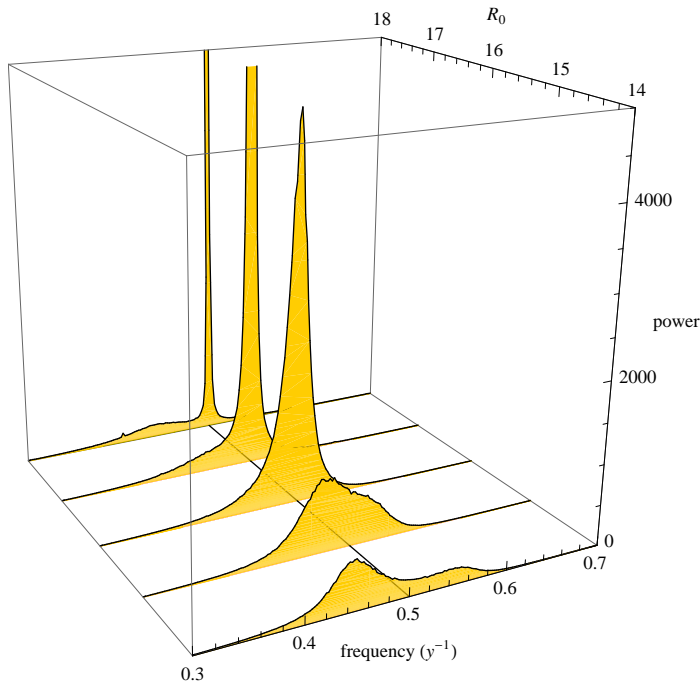


Figure 6.8: Simulation results showing the power spectrum of stochastic oscillations as the period doubling bifurcation point is crossed. The peaks for  $R_0 = 17$  and  $18$  have been cropped for clarity.

of the fade-out boundary, where extinction and re-colonisation events start to have an impact on the dynamics [134]. This has an effect on the power spectra in two ways: firstly as a broadening of the power spectra, showing a greater range or amplified frequencies and thus a more irregular dynamics. Secondly the endogenous period is systematically shifted higher, as in unforced versions of this model, detailed in Section 3.3. This reflects the fact that the period of oscillations also depends on the re-introduction of the disease after fade-out [104].

The most important effect is on the fluctuations in the biennial regime after the period doubling. For  $N = 5 \times 10^6$  the peaks are sharp, indicating a deterministic limit cycle, and the stochastic oscillations are much smaller (Figure 6.7b), hence the good predictability of these larger systems. For the two smaller populations this is not the case. We do not observe the deterministic biennial limit cycle, but instead see an enhanced stochastic peak and a broadening of the spectrum. The range of this enhanced region is also reduced.

Although there are large deviations, having an analytical description still helps us interpret the dynamics at smaller  $N$ . Taking the average of Eq. (2.21) we

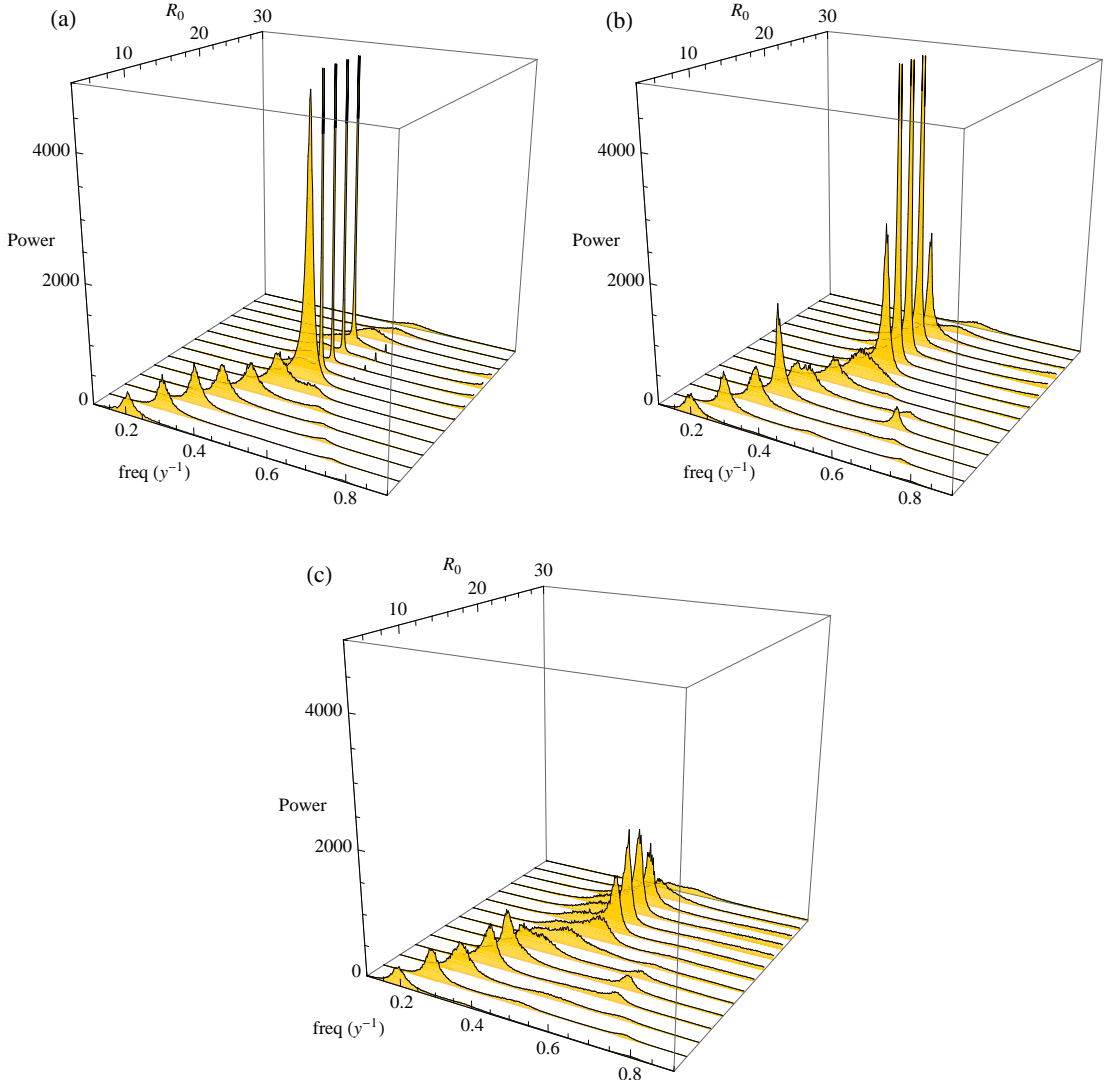


Figure 6.9: Power spectrum through the bifurcation point for different size populations. (a)  $N = 5 \times 10^6$ , (b)  $N = 10^6$ , (c)  $N = 5 \times 10^5$ . Some of the peaks are cropped for clarity. Notice the anomalously enhanced peak for  $N = 10^6$ ,  $R_0 = 10$ , see section 6.3.5 for discussion of this.

obtain

$$\langle I \rangle = N\psi(t) + N^{1/2}\langle y \rangle. \quad (6.10)$$

In the linear noise approximation, which we have used throughout this thesis, the fluctuations are Gaussian and therefore  $\langle y \rangle = 0$ . At some point this will break down and we must include the next-order corrections. These will be of the order  $N^{1/2}$  to the macroscopic equations. It will no longer be true that the macroscopic value,  $\psi(t)$ , is equal to the average,  $\langle I \rangle$  [78, 135]. This effect of the fluctuations

on the deterministic dynamics could be enough to retard the onset of the biennial limit cycle and is the subject of further research.

### 6.3.5 Switching between attractors

As seen from the bifurcation diagram in Figure 6.5, where  $\eta = 10^{-6}$ , the only region where deterministically there are predicted to be two coexisting states is when  $24 < R_0 < 25$ . This can be detected in simulations and the period of switching depends strongly on the system size. If the system is large it will tend to stay in the state it started in, because the fluctuations are not large enough compared to the mean to kick the system into the other state. Decreasing the system size makes this possible, and we see periods of annual dynamics followed by biennial and back to annual, where the period of switching depends on the system size.

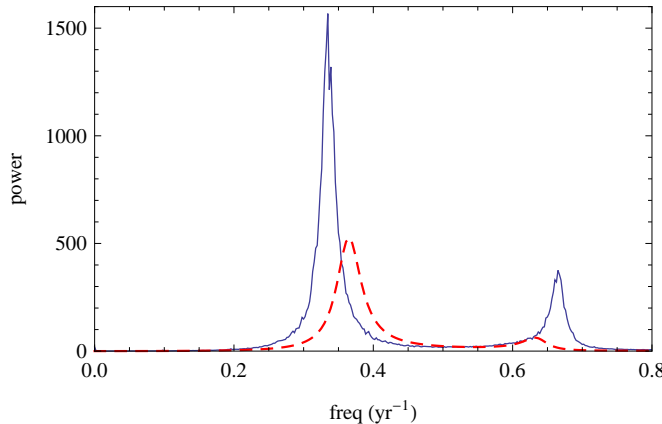


Figure 6.10: Anomalous enhancement of the power spectrum for  $R_0 = 10$ ,  $N = 10^6$ . Solid curve is from simulation, red dashed curve is the theoretical prediction.

There is another intriguing region where we see signs of this type of behaviour. For  $N = 10^6$  and  $R_0 = 10$  (Figure 6.9b and 6.10), we observe an enhanced stochastic peak in the spectrum with a period of 3 years. Visual inspection of the time series (Figure 6.11) shows regions of irregular annual oscillations interspersed with very regular triennial oscillations. Note that this is not observed in the larger or smaller systems and the power spectrum is shifted by the proximity to the fade-out boundary from its infinite system size limit. Very similar behaviour is observed for measles data from Baltimore between 1928 and 1935 (see Figure 1.2), which has similar parameter values [21]. This phenomenon is discussed further

in Chapter 7.

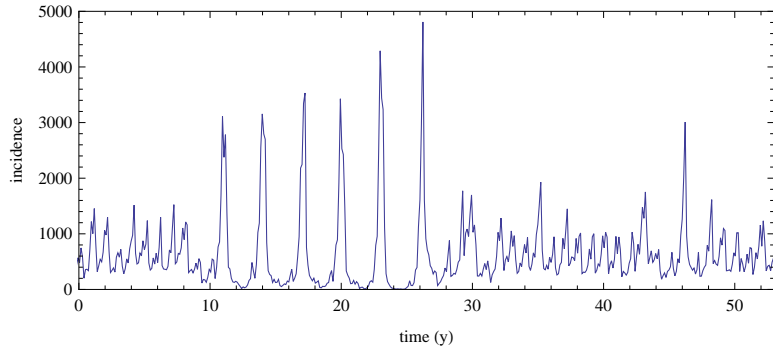


Figure 6.11: Time series from the forced SIR model showing switching between triennial and annual patterns.

## 6.4 Discussion

In this chapter we have extended the analytic approach, to include the time dependence explicitly instead of by using an approximation as in the previous chapter. Because this model has a finite population, and therefore is inherently stochastic, it can only be studied ‘exactly’ by simulation. The system-size expansion, which we use to derive approximate analytic solutions for this model suggests that we should view the population-level dynamics as being composed of a deterministic part and a stochastic part, where the spectrum of the stochastic fluctuations is intimately related to the stability of the deterministic level dynamics. Power spectra of these models have been known for some time, but it has not always been clear what the mechanisms that generate the peaks are. This is the main advantage of being able to calculate the power spectrum of the stochastic fluctuations analytically; by comparison with the simulations we can gain insight into the mechanisms at work.

Our analysis suggests a simple explanation for the differences seen in the epidemic patterns of measles and whooping cough in England and Wales both before and after vaccination [16], and which are representative of the two main parameter regimes for childhood diseases. The generic situation occurs when we are far away from a bifurcation point. Here we observe a deterministic annual limit cycle with stochastic oscillations, as in Figures 6.2 and 6.3. In general the form of the spectrum is close to that predicted by the unforced model. As already

shown in the previous chapter, this situation can account for the dynamics of whooping cough pre- and post-vaccination [136]. Pre-vaccination the stochastic oscillations are centred on 2-3 years. Vaccination acts to shift the endogenous frequency lower and increases the amplitude of these fluctuations giving large four yearly outbreaks. Even though it uses the staged-SEIR model, we observe in the power spectrum shown in Figure 5.5 the same structure described in Section 6.2, i.e. major and minor peaks at frequencies  $\text{Im}(\lambda)$  and  $1 - \text{Im}(\lambda)$ . This confirms our view that the deviations in that spectrum are caused by the proximity to the period doubling bifurcation point and not by something else such as switching between attractors.

Measles epidemics show a contrasting behaviour and represent the second important parameter regime, where the deterministic dynamics are near to a bifurcation point. Pre-vaccination, large cities such as London are in the regime with a deterministic biennial limit-cycle. Vaccination acts to lower  $R_0$  and shift the system into the regime where there is an annual limit cycle with large stochastic oscillations. As vaccination coverage is increased, the endogenous period of these oscillations is also increased [18]. Measles dynamics show a strong dependence on population size [1, 104]. Our analysis also offers some insight into this: in large populations the stochastic oscillations are very small compared with the deterministic biennial limit-cycle. This accounts for the regularity and explains why purely deterministic models capture this aspect so well [52]. For smaller populations the deterministic biennial limit-cycle is not observed, just enhanced stochastic oscillations, thus accounting for the more irregular dynamics seen in these smaller populations.

The bifurcation diagrams for SEIR and SIR models are very similar, which justifies our use of the SIR model in this chapter. The extension to uncoupled births and deaths would be straightforward, but would offer no further insight [3]. There are technical difficulties in extending the method to the SEIR model because of the difference in time scales between the collapse onto the centre manifold [33] and the period of forcing; this creates difficulties in computing the Floquet multipliers. These could in principle be overcome either by calculating the multipliers by a different method [137, 138], or by carrying out a centre-manifold reduction before doing the van-Kampen expansion [139]. Recently a new study has calculated the power spectrum for the stochastic SEIR model [140], which took a brute-force approach to calculating the Floquet multipliers.

This work supports our findings, in that they found no evidence of co-existing attractors in their stochastic model. The breakdown of the linear theory near the bifurcation point is discussed in more detail in the next chapter.

## Chapter 7

# Conclusions and further work

---

A number of conclusions have already been drawn throughout this thesis. In this chapter we draw some broader conclusions with reference to previous results and give directions for potential further research.

The first stochastic simulations of an epidemic model were carried out by Bartlett [62] in 1957 on the then new Manchester electronic computer. Since then, further studies have shown that relatively simple models can capture the complex oscillatory dynamics displayed by childhood diseases. The two main ingredients that must be included are seasonal forcing, from the aggregation of children in schools, and demographic stochasticity, due to the individual nature of the population. Up till now such models have only been investigated by computer simulations. One of the major obstacles to a better understanding of these models is that the mathematics required to analyse them is much more technical and has lagged behind that used to study non-linear differential equations. This has led to the dominance of deterministic approaches, even where their validity is questionable.

We have approached this problem by starting with an individual-based model formulated as a continuous-time Markov process. The main advantage of this approach is that the dynamics can be modelled by a master equation. This is inherently stochastic: we do not have to make any assumptions about the form or strength of the noise the system is subject to, as this is encoded naturally in the model definitions and the master equation. The only way to obtain exact solutions to the master equation is by simulation, but through the use of the system-size expansion we can derive approximate analytic solutions. This suggests that we

should view the full stochastic dynamics as being composed of a macroscopic part plus stochastic fluctuations about this, where the spectrum of the stochastic fluctuations is intimately related to the stability of the deterministic dynamics. The master equation approach has the advantage that both the macroscopic behaviour and the stochastic fluctuations about it both emerge from the same integer based description.

Power spectra derived from the stochastic output of these models have been known for some time, but it has not always been clear what the mechanisms are that generate the various observed peaks. The main advantage of the master equation approach is that we are able to calculate the power spectrum of the stochastic fluctuations analytically; by comparison with the simulations we can then gain insight into the mechanisms at work. In this thesis we have considered two main extensions to the basic SIR model first described by Alonso *et al.* [7]: distributed infectious periods and the inclusion of explicit seasonal forcing. This has allowed us to make contact with a number of existing studies [16, 35] and give a clear quantification of the stochastic dynamics of these models.

## Measles and whooping cough

One of the main aims of this thesis has been to understand the contrasting dynamics of whooping cough and measles, which up till now has been rather unclear. Stochastic models can capture both patterns but explaining the dynamics of the model has proved to be difficult. Our work allows us to give a much clearer explanation why these two diseases display such different dynamics, even though their  $R_0$  values are similar. Of the two diseases, the dynamics of whooping cough are the simplest to explain. The forcing induces an annual limit cycle in the deterministic dynamics with large stochastic oscillations, via a resonant amplification of the transients. These dynamics are relatively straightforward because the annual limit-cycle is the only possible solution of the deterministic equations for all realistic parameter values.

Vaccination acts to lower the effective  $R_0$ . For whooping cough this does not effect the deterministic dynamics, but has a large effect on stochastic corrections: the spectrum is amplified and the peak is shifted to a higher period. Including the more realistic latent and infectious periods does not qualitatively change this picture, it only acts to change the endogenous frequencies of the spectra. Alonso *et al.* [7] detailed the increase in endogenous period in the unforced model, but found

that the spectrum was suppressed by vaccination. This was because they used a much larger value for  $\eta$ . As discussed in Chapter 3 whether the amplitude of the spectrum increases or decreases with decreasing  $\beta$  depends on the magnitude of  $\eta$ . The value we used in Section 5.3 was much smaller ( $\eta = 5 \times 10^7$  compared with  $10^{-5}$  in [7]), so that the amplitude of the spectrum increases as  $R_0$  is decreased. We return to the question of the value for this parameter later.

In the case of measles, discussed in Chapter 6, the dynamics are more complicated because the forcing can induce a period doubling in the deterministic dynamics, which is the dominant feature of the dynamics. That this strong biennial oscillation is observed in much of the data has often been taken as good evidence for the correctness of a simple deterministic approach. There are a number of observations which a deterministic approach cannot capture, such as the more irregular dynamics of medium size to smaller populations and after vaccination. To understand these aspects we need a better understanding of the relationship between the deterministic dynamics and the stochastic dynamics, which our work provides. Our analysis shows that vaccination acts to move the system out of the biennial regime and into a parameter space where there is an annual limit cycle and large stochastic oscillations, as with whooping cough. For smaller populations the biennial limit cycle is suppressed and we observe a region of high stochastic amplification, in the power spectrum, instead. This accounts for the much more irregular behaviour observed for smaller systems.

Our work has shown that the sensitivity to seasonal forcing is the primary reason why these two diseases display contrasting dynamics. Measles is a highly infectious disease with a short infectious period; whooping cough is less infectious, but with a much longer infectious period [2]. This means that the unforced endogenous period of whooping cough is longer than that of measles (using Eq. (3.6) roughly 2.7 and 2 years respectively). When forcing is applied it is much easier to excite a period doubling in the measles system. This point arises again later in relation to the gamma distributed models. Other childhood diseases, such as chickenpox, rubella and mumps are in a parameter regime similar to that of whooping cough [21].

All previous work on characterising these two stochastic systems has relied on an ad hoc collection of methods. Mostly, these have revolved around perturbing the deterministic system to try and understand transients and stability properties. This has led to the use of confusing concepts such as invasion orbits [19, 46, 55] to

try and quantify the dynamics. Fundamentally though, these are all deterministic methods to try and understand stochastic results. The mechanisms of stochastic amplification allows for a more elegant understanding of the stochastic dynamics. The importance of critical points and bifurcations has been highlighted in the literature for a number of ecological systems [4, 132, 141]. The work presented in this thesis extends these results to epidemiological systems and provides some of the best examples of these mechanisms in action in a large biological system.

One further avenue for potential research is in comparing our results with the large data sets which exist for these two diseases. Obviously the models are too simple to make a direct comparison with data, but the power spectra from time series should scale in certain ways over a range of community sizes. The data for whooping cough should prove the easiest to test, due to the simpler dynamics.

## Immigration and spatial models

One of the areas highlighted throughout this thesis is the importance of immigration in these stochastic models, even for large populations. Finite-size effects and immigration / imports are closely related in a stochastic individual-based model because the population is finite. Immigration reflects the basic fact that no population is isolated and there must be reintroduction of the disease if it fades out. One advantage of the approach which starts from an individual based model and derives the population level model, is that the immigration terms from the stochastic model are automatically included in the deterministic equations which describe the macroscopic behaviour. These terms are easily omitted in a deterministic analysis because the system size is an innocent parameter [63].

In the unforced model immigration acts to bound the size of the fluctuations. As discussed in Chapter 3, with no immigration there is a bifurcation point in the SIR model at  $R_0 = 1$ . This marks the boundary between a disease-free and endemic equilibrium. Without immigration the fluctuation spectrum diverges as the bifurcation point is approached. Adding immigration destroys the absorbing state on the macroscopic level, so there is no longer a bifurcation point and the spectrum does not diverge. The slow stream of new infectious cases, caused by immigration events, acts analogously to a damping force on an oscillatory system.

Immigration is again vital when working with the forced model. As discussed in both Chapters 5 and 6, many of the longer period solutions and chaotic behaviour are no longer seen in the deterministic dynamics when immigration is

included. This removes much of the speculation as to the influence of multiple co-existing attractors on the stochastic dynamics [5]. It is interesting to note the similarities between immigration and the inclusion of age-structure [37] in these forced models. Adding age-structure creates a constant pool of infectives in the infant class which acts to damp the dynamics [59, 60], exactly analogous to how we model immigration.

Clearly the value of  $\eta$  is important to the overall dynamics, but it is the hardest parameter to estimate by any measure. This is because it depends on a number of factors such as longer range mobility [142, 143] and contact patterns [144–146] which are intrinsically hard to measure, as well as changing over longer periods of time [147]. In our implementation we have assumed that the rate of imports scales with the number of susceptibles and hence the total population. There is some evidence that the rate of imports might actually scale with  $N^{1/2}$  [1, 12], thus there are relatively more imports into smaller populations than larger. But because such a process is non-linear in  $N$  it is impossible to perform a system-size expansion of the resulting master equation [78]. In a strict derivation, vaccination should have an effect on  $\eta$ , so that,  $\eta \rightarrow (1 - p)\eta$  [7]. This is assuming that mixing on the global scale, between population centres, follows the mass action law as within cities; this is unrealistic for the same reasons as given above. Being wholly ignorant of its correct scaling we have followed Alonso *et al.* [7] and taken  $\eta$  as a constant throughout this thesis. Another relevant outstanding question is: what form should the immigration parameter take when forcing is included? As measles dynamics can be highly synchronised it could be argued that the immigration parameter should reflect this [107, 109, 145]. On the other hand for larger cities, this parameter can be viewed as an aggregate of many infectious encounters from varied sources and could be approximated as a constant. Clearly these are all complicated issues, which can only be addressed by further research into explicitly spatial models.

Previous work has hinted at the sort of effects that can arise in spatial epidemic models, such as synchronisation, coupling and increased persistence [148–152], but not within a rigorous stochastic framework [153]. Some work has been done on this area, but has not been presented in this thesis. One model that was considered was a lattice type very similar to that presented in [93], where susceptibles and infected could move between lattice sites at different rates. One of the motivations for this was to look for Turing instabilities which lead to patterns

on the spatial scale [154]. It was found that these do not exist in the basic SIR system, but it has since been shown that with an added constant removal rate of infectives [155] they can be found. The system presented in [155] should be possible to analyse with the system size expansion, using a master equation with delay terms [156].

One reason for not pursuing further that line of research was because it was unrealistic for human infections (although might be suitable for plant diseases [36, 73]). A more fruitful avenue of research would be the use of stochastic meta-population model [157] which can be used to examine spatial effects on both the global and local level [13, 144]. In such scheme the population is split up into a number of equal size patches, then we can define a force of infection in the  $i$ 'th patch as,

$$\lambda_i = \sum \beta_{ij} I_j, \quad (7.1)$$

where  $\beta_{ij}$  is the transmission rate between patch  $i$  and  $j$ . This matrix then encodes the structure of the meta-population. The infection transmission rate in the  $i$ 'th patch is then,

$$T(S_i - 1, I_i + 1 | S_i, I_i) = \frac{\lambda_i S_i}{N}, \quad (7.2)$$

where  $N$  is the population of the patch. This sort of scheme is not only much more realistic for human diseases, but easier to manage than a model where individuals are moving around lattice sites. Simulation is simpler as there is no movement between patches to take into account. To theoretically analyse this using a master equation we can treat this in a similar way to the staged model discussed in Chapter 4. One would not be able to calculate the power spectrum in an individual patch, unless the population is large enough, but could calculate an average over many patches.

## Gamma-distributed models

One of the major criticisms of epidemic models in the past has been the overly simplistic assumptions made in the derivation of ordinary differential equation models [80]. The assumption of exponentially distributed infectious periods, although convenient from a mathematical point of view, is very unrealistic. In Chapters 4 and 5 I described how gamma distributed latent and infectious periods can be incorporated and analysed within the master equation framework. In

general non-exponential distributions only have a minor effect on the macroscopic dynamics, but can have a larger effect on the stochastic corrections, usually acting to shift and amplify the power spectrum.

It would be interesting to extend these models to include explicit forcing, but this might be problematic considering the difficulty in extending the analysis to the forced SEIR model. A recent study has managed to carry out a full analysis of the sinusoidally forced SEIR model [140]. This was only possible by a brute force numerical approach to calculate the Floquet multipliers down to  $O(10^{-178})$ . It is not known how well such an approach would scale to systems with a larger number of species. Alternative methods might be to calculate the multipliers via a different approach [137, 138], or to carry out a centre manifold reduction before doing the system size expansion [139]. One point to note is that although the Floquet multiplier are very small for these systems, the characteristic exponents are well behaved. This might offer a potential different route to deriving the canonical fundamental matrix and hence the multipliers.

In Chapter 4 we discussed the hypothesis that models with distributed infectious periods are more sensitive to seasonal forcing because the stochastic oscillations have a higher endogenous period. This could only be tested conclusively with the analysis described above, but the whooping cough model considered in Chapter 5 lends weight to this hypothesis. In this model the distributed infectious period only acts to increase the frequency of the oscillations. Inspection of the power spectrum (Figure 5.5) shows deviations consistent with the findings from the work on the forced model presented in Chapter 6. We can be confident that the observed deviations are caused by the proximity to the period doubling bifurcation point, and not any other stochastic effects.

One issue that needs to be addressed in the future is how distributed periods effect the bifurcation diagram for the measles model (Figure 6.5a). Nyguyen & Rohani [19] report that from preliminary research it does make a large difference. This could also have implications for estimating  $\beta_1$  and  $R_0$  values [3, 121]. Extrapolating from our results it is likely to be found that a qualitatively similar bifurcation diagram can be generated with a smaller value of  $\beta_1$ . Such models have been used to investigate persistence properties of measles [65, 158], but have not considered dynamical properties.

## Switching between attractors

I have already discussed how the introduction of immigration removes most of the co-existing attractor structure that is otherwise found in the bifurcation diagram for the measles model. Although this work has answered many of the questions regarding noise induced switching between attractors, it has also raised some new ones. Small periods of coherent triennial oscillations are seen in the data (for example Baltimore shown in Figure 1.2) and similar oscillations are detected in simulations, as discussed in Section 6.3.5. One thing we can say is that this behaviour appears to result from a strong interaction with the fade-out boundary, so the current methods (system size expansion) are inadequate to analyse it.

The recent work by Rozhnova & Nunes [140] on the stochastic SEIR model has examined more closely the role of higher period attractors by not including immigration. They find that the deterministic period three attractors are only found in very large simulations ( $N > 10^8$ ). This contrasts with our work where we find switching behaviour only within a limited range of  $N$ , where the system can approach the boundary. One other possibility is that although overall the triennial limit cycle is unstable, this could be because a small part is unstable with rest being stable. This type of behaviour has been noted before with regard to measles by analysing the local Lyapunov exponents around the attractor [1].

There are some parallels here with the work of Stone *et al.* [159]. They derive a new threshold condition for a skip year (a year with no outbreak) to occur in a given time-series. This happens when the number of infected goes below a certain threshold, but there is also a condition on the phase relative to the limit cycle. Although their work is completely deterministic, it could point the direction for a similar stochastic mechanism. Thus if the system is pushed near the boundary by a fluctuation at the right time it could enter onto a new deterministic trajectory.

It should also be noted that a similar sort of behaviour can be seen in the unforced SIR model where we observe short bursts of very coherent oscillations. A time-series and associated power spectrum are shown in Figure 7.1, which illustrates this. Although there is no change in frequency, as with the example shown in Figure 6.11, there is clearly an interaction with the boundary. Understanding this phenomena in the unforced model could hopefully act as a stepping stone to a better understanding of the switching phenomena in the forced model.

One aspect we have not considered in this thesis is the role of transients. All power spectra have been evaluated about a steady state solution (either a

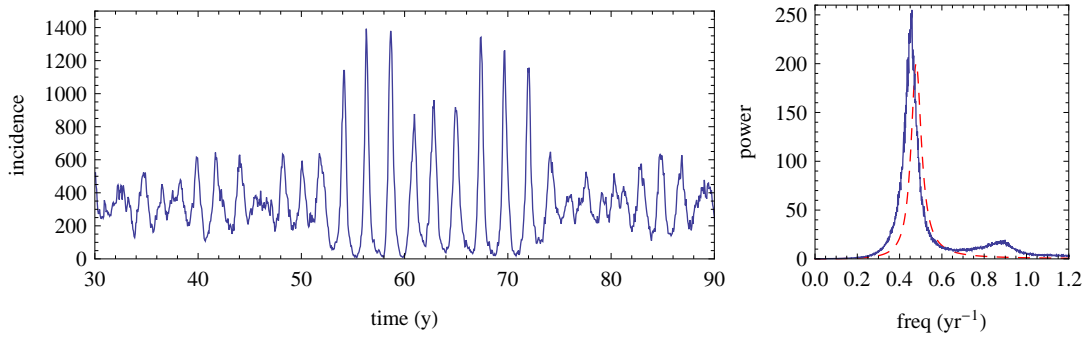


Figure 7.1: Short bursts of coherent oscillations in the unforced SIR model; time series and associated power spectrum. Parameters:  $N = 5 \times 10^5$ ,  $R_0 = 17$ ,  $\gamma = 0.077$  and  $\eta = 10^{-6}$ .

fixed point or limit cycle). Of course the observed time-series are almost never in a steady state. The question of transients after vaccination is also important. Vaccination can cause large transients [44], which could contribute to the observed fluctuations. But these transients will be at the same frequency as the stochastic oscillations. The magnitude of any induced transients depend strongly on how the process of vaccination is implemented [24], or indeed at what time of the year it is induced compared to the limit cycle [16]. Sudden jumps in parameters tend to induce large transients and most studies take this to be the case [44]. This is mainly because this produces oscillatory behaviour, but there is little evidence that the change is so sudden.

## Methodology

In Section 3.3 we showed that there are definite limits to the expansion of the master equation. Including higher-order terms in the expansion does not improve the accuracy much because the basic assumption at the heart of the expansion, that the probability distribution has one peak at a macroscopic value, breaks down. At smaller system sizes there is a build up of probability along the fade-out boundary and so the distribution essentially has two peaks. The breakdown of the linear theory near the bifurcation point can be remedied by including next-to-leading order terms from the expansion of the master equation [78], although this would result in a much more complex calculation. Unlike the examples of a small system where we approach the fade-out boundary, this would be a more appropriate place to apply this theory. Extending the higher-order expansion to

also include time dependence would essentially involve solving similar equations to the time-dependent Langevin equations presented in Chapter 6. These could be solved using a Floquet formalism, although it is likely there would be problems with small multipliers, but as already discussed these can be overcome in principle [140].

There are two broad areas of interest within mathematical epidemiology: dynamics (which we have been concerned with in this thesis) and extinction and persistence properties [103], which we have not addressed. As discussed in Chapter 3 these methods are not suitable to address the question of persistence for the reasons outlined above, even though attempts have been made in this direction [63, 75, 160]. There is a clear need for a good analytical understanding of the boundary effects in these systems if we are to ever make any progress with questions of persistence or to try and answer some of the questions raised with respect to switching between attractors. There are a few possibilities for using different methods to try and make headway with this problem. Linearisation of the master equation at the boundary and WKB methods [161–163] are but two examples.

# Appendix A

## Staged model matrices

---

### Staged SIR model

The staged SIR model as defined in Section 4.2. Both matrices are of dimension  $L + 1$ , where  $L$  is the number of stages. Defining some new constants  $\hat{\mu} = \mu/\gamma$  and  $\hat{\beta} = \beta/\gamma$ , the Jacobian,  $A_{ij}$  is of the form,

$$A = \begin{pmatrix} -\hat{\beta}\psi - \hat{\mu} & -\hat{\beta}\phi & 0 & 0 & 0 & \dots & 0 \\ \hat{\beta}\psi & \hat{\beta}\phi - \hat{\mu} & 0 & 0 & 0 & \dots & -L \\ 0 & L & -(2L + \hat{\mu}) & -L & -L & \dots & -L \\ 0 & 0 & L & -(L + \hat{\mu}) & 0 & \dots & 0 \\ 0 & 0 & 0 & L & -(L + \hat{\mu}) & \dots & 0 \\ \vdots & & & & & \ddots & \end{pmatrix} \quad (\text{A.1})$$

The noise-correlator matrix is of the form,

$$B = \begin{pmatrix} 2\hat{\mu}(1 - \phi) & \hat{\mu}(\phi - \psi_0 - 1) & -\hat{\mu}\psi_2 & -\hat{\mu}\psi_3 & \dots & -\hat{\mu}\psi_L \\ \hat{\mu}(\phi - \psi_0 - 1) & 2\hat{\mu}(1 - \phi) & \hat{\mu}\psi_2 & \hat{\mu}\psi_3 & \dots & (L + \hat{\mu})\psi_L \\ -\hat{\mu}\psi_2 & \hat{\mu}\psi_2 & 2(L + \hat{\mu})\psi_2 & -L\psi_2 & \dots & 0 \\ -\hat{\mu}\psi_3 & \hat{\mu}\psi_3 & -L\psi_2 & 2(L + \hat{\mu})\psi_3 & \dots & 0 \\ \vdots & & & & & \ddots \end{pmatrix} \quad (\text{A.2})$$

Both of these are evaluated at the deterministic fixed point,  $(\phi^*, \psi^*, \psi_j^*)$ , given by Eqs. (4.7).

## Staged SEIR model

Here I give the matrices for the staged SEIR model described in Chapter 5. The matrices are dimension  $M + L + 1$ . The matrix  $J$  can be split up into nine parts which are shown below,

$$J = \left( \begin{array}{c|c|c} J_{11}^{(1)} & J_{1\beta}^{(2)} & J_{1b}^{(3)} \\ \hline J_{\alpha 1}^{(4)} & J_{\alpha\beta}^{(5)} & J_{\alpha b}^{(6)} \\ \hline J_{a1}^{(7)} & J_{a\beta}^{(8)} & J_{ab}^{(9)} \end{array} \right), \quad \begin{aligned} \alpha, \beta &= 1, \dots, M, \\ a, b &= 1, \dots, L. \end{aligned}$$

$$\begin{aligned} J_{11}^{(1)} &= -\beta \sum_{a=1}^L \psi_a - \eta - \mu, \\ J_{1\beta}^{(2)} &= J_{a1}^{(7)} = 0 \quad \text{for all } a, \beta. \\ J_{1b}^{(3)} &= -\beta\phi, \quad \text{for all } \alpha. \\ J_{\alpha 1}^{(4)} &= \begin{cases} \beta \sum_{a=1}^L \psi_a + \eta & \text{if } \alpha = 1, \\ 0 & \text{otherwise.} \end{cases} \\ J_{\alpha b}^{(6)} &= \begin{cases} \beta\phi, & \text{if } \alpha = 1, \\ 0 & \text{otherwise.} \end{cases} \\ J_{\alpha\beta}^{(5)} &= \begin{cases} -(M\sigma + \mu), & \text{if } \alpha = \beta, \\ M\sigma\delta_{\beta, \alpha-1}, & \text{if } \alpha > 1, \\ 0 & \text{otherwise.} \end{cases} \\ J_{a\beta}^{(8)} &= \begin{cases} M\sigma & \text{if } a = 1, \beta = M, \\ 0 & \text{otherwise.} \end{cases} \\ J_{ab}^{(9)} &= \begin{cases} -(L\gamma + \mu), & \text{if } a = b, \\ L\gamma\delta_{b, a-1}, & \text{if } a > 1, \\ 0 & \text{otherwise.} \end{cases} \end{aligned} \tag{A.3}$$

where  $\delta_{a,b}$  is the Kronecker delta. The form of the matrix  $G$  is the same as for  $J$  except that it is symmetric,  $G_{AB} = G_{BA}$ .

The elements of  $G$  are,

$$\begin{aligned}
G_{11}^{(1)} &= \beta\phi \sum_{a=1}^L \psi_a + \eta\phi + \mu(1 - \phi), \\
G_{1\beta}^{(2)} &= \begin{cases} -\beta\phi \sum_{a=1}^L \psi_a - \eta\phi - \mu\rho_1 & \text{if } \beta = 1, \\ -\mu\rho_\beta & \text{if } \beta \neq 1. \end{cases} \\
G_{1b}^{(3)} &= -\mu\psi_b. \\
G_{\alpha\beta}^{(5)} &= \begin{cases} \beta\phi \sum_{a=1}^L \psi_a + \eta\phi + (\mu + M\sigma)\rho_1 & \text{if } \alpha = \beta = 1 \\ (\mu + M\sigma)\rho_\alpha + M\sigma\rho_{\alpha-1} & \text{if } \alpha = \beta > 1, \\ -M\sigma\rho_\alpha & \text{if } \beta = \alpha + 1, \alpha = 1, \dots, M-1 \\ 0 & \text{otherwise} \end{cases} \\
G_{\alpha b}^{(6)} &= \begin{cases} -M\sigma\rho_M & \text{if } \alpha = M, b = 1 \\ 0 & \text{otherwise} \end{cases} \\
G_{ab}^{(9)} &= \begin{cases} (\mu + L\gamma)\psi_1 + M\sigma\rho_M, & \text{if } a = b = 1 \\ (\mu + L\gamma)\psi_a + L\gamma\psi_{a-1}, & \text{if } a = b > 1 \\ -L\gamma\psi_a & \text{if } b = a + 1, a = 1, \dots, L-1 \\ 0 & \text{otherwise} \end{cases}
\end{aligned} \tag{A.4}$$

## Appendix B

# Floquet theory

---

In this appendix we detail the procedure for calculating the time dependent power spectrum. In general, Floquet theory states that if  $K(t + T_n) = K(t)$ , then there exists a canonical fundamental matrix which can be expressed in the form  $X_0(t) = P(t)Y(t)$  [127]. It has the property that the Floquet matrix, defined by  $B_0 = X_0^{-1}(0)X_0(T_n)$ , is diagonal, with elements which are the Floquet multipliers,  $\rho_i$ . The matrix  $P(t)$  carries the periodicity of the limit cycle, while  $Y(t) = \text{diag}[e^{\lambda_1 t}, e^{\lambda_2 t}]$ , where  $\lambda_i$  are the Floquet exponents.

The procedure for calculating the matrices  $P(t)$  and  $Y(t)$  is as follows:

- (i) Numerically integrate equation (6.6), with initial condition  $X(0) = \mathbb{I}$ , to obtain a fundamental matrix  $X(t)$ .
- (ii) Calculate the Floquet matrix  $B = X(T_n)$ , from which one can calculate the eigenvalues and eigenvectors of  $B$ .
- (iii) The eigenvalues are the multipliers  $\rho_i$ , from which we calculate the characteristic exponents  $\lambda_i = \ln(\rho_i)/T$ .
- (iv) Next construct  $S$ , the columns of which are the eigen vectors of  $B$ . Then use this to get the canonical fundamental matrix  $X_0(t) = X(t)S$ . In general  $S$  and  $X_0(t)$  will be complex.
- (v) Form the matrix  $Y(t) = \text{diag}[e^{\lambda_1 t}, e^{\lambda_2 t}]$ .
- (vi) Finally, calculate the matrix of periodic functions  $P(t) = X_0(t)Y(-t)$ .

Next we look at the derivation of the power spectrum. The Langevin equation (2.31) is an inhomogeneous linear equation with periodic coefficients. We can use Floquet theory to construct a solution to this by adding a particular solution to the general solution of the corresponding homogeneous equation (6.5) [127]. This gives,

$$\mathbf{x}(t) = X(t)X^{-1}(t_0)\mathbf{x}_0 + X(t) \int_{t_0}^t X^{-1}(s)\mathbf{f}(s)ds, \quad (\text{B.1})$$

with initial condition  $\mathbf{x}(t_0) = \mathbf{x}_0$ . We are interested in the steady state solutions, when transients have damped down, thus we can ignore the first part of Eq. (B.1) and set the initial time to the infinite past,  $t_0 \rightarrow -\infty$ . Taking the case where  $X(t)$  is  $X_0(t) = P(t)Y(t)$ , one finds using the properties of the diagonal matrix  $Y(t)$ , that

$$\mathbf{x}(t) = P(t) \int_{-\infty}^t Y(t-s)P(s)^{-1}\mathbf{f}(s)ds. \quad (\text{B.2})$$

The correlation matrix is defined as  $C(t+\tau, t) = \langle \mathbf{x}(t+\tau)\mathbf{x}^T(t) \rangle$ , where,

$$\begin{aligned} \mathbf{x}(t+\tau) &= P(t+\tau) \int_{-\infty}^{t+\tau} Y(t+\tau-s)P(s)^{-1}\mathbf{f}(s)ds, \\ \mathbf{x}^T(t) &= \int_{-\infty}^t \mathbf{f}^T(s')(P^{-1}(s'))^T Y(t-s')^T ds' P(t)^T. \end{aligned} \quad (\text{B.3})$$

Substituting these expressions we find,

$$\begin{aligned} C(t+\tau, t) &= P(t+\tau) \int_{-\infty}^{t+\tau} \int_{-\infty}^t Y(t+\tau-s)P(s)^{-1}G(s) \\ &\quad \times \delta(s-s')(P^{-1}(s'))^T Y(t-s')^T ds' ds P(t)^T, \end{aligned} \quad (\text{B.4})$$

where  $\langle \mathbf{f}(s)\mathbf{f}^T(s') \rangle = G(s)\delta(s-s')$ , is the noise correlator. Integrating over the delta function, the result will depend on the sign of  $\tau$ . If we take  $\tau \geq 0$  then the integration region is  $-\infty < s < t$ , giving

$$C(t+\tau, t) = P(t+\tau) \int_{-\infty}^t Y(t+\tau-s)\Gamma(s)Y(t-s)^T ds P(t)^T, \quad (\text{B.5})$$

where we have defined

$$\Gamma(s) = P(s)^{-1}G(s)(P^{-1}(s))^T, \quad (\text{B.6})$$

which will have the periodicity of the limit cycle. Next we make a change of

variables,  $s \rightarrow t - s'$ , which gives

$$C(t + \tau, t) = P(t + \tau) \int_0^\infty Y(\tau + s') \Gamma(t - s') Y(s')^T ds' P(t)^T. \quad (\text{B.7})$$

The form of  $Y$  means we may write  $Y(\tau + s') = Y(\tau)Y(s')$ , and so the integral that we need to evaluate is given by

$$\Phi(t) \equiv \int_0^\infty Y(s) \Gamma(t - s) Y^T(s) ds. \quad (\text{B.8})$$

Using the periodicity of the matrix  $\Gamma(t - s)$ , this integral can be recast as a finite one over the period of the limit cycle:

$$\Phi_{ij} = \frac{1}{1 - \rho_i \rho_j} \int_0^{T_n} \Gamma_{ij}(t - s) e^{(\lambda_i + \lambda_j)s} ds. \quad (\text{B.9})$$

Therefore, the final expression for the correlation matrix is

$$C(t + \tau, t) = P(t + \tau) Y(\tau) \Phi(t) P(t)^T. \quad (\text{B.10})$$

So we can obtain the correlation matrix as an integral, but this has to be evaluated numerically because neither the limit-cycle solutions nor  $P(t)$  can be obtained in closed form.

Finally the auto-correlation function will be given by the average of  $C$  over one period,

$$C(\tau) = \frac{1}{T} \int_0^T C(t + \tau, t) dt \quad (\text{B.11})$$

where  $C(-\tau)^T = C(\tau)$ . This can be proved by going back to Eq. (B.3), assuming  $\tau < 0$  and doing the other integration. The power spectrum is the Fourier transform of the auto-correlation,

$$P(\omega) = \int_{-\infty}^{+\infty} C(\tau) e^{-i\omega\tau} d\tau = 2 \int_0^\infty C(\tau) \cos(\omega\tau) d\tau, \quad (\text{B.12})$$

Instead of this integral we sample the auto-correlation function and use a discrete cosine transform (DCT-I in Mathematica [110]) to calculate the power spectrum.

# Bibliography

---

- [1] Grenfell, B. T., Bjornstad, O. N., and Finkenstadt, B. F. (2002) Dynamics of measles epidemics: scaling noise, determinism and predictability with the TSIR model. *Eco. Monographs*, **72**, 185–202.
- [2] Anderson, R. M. and May, R. M. (1991) *Infectious diseases of humans: dynamics and control*. Oxford University Press.
- [3] Keeling, M. J. and Rohani, P. (2007) *Modelling infectious diseases in humans and animals*. Princeton University Press.
- [4] Bjornstad, O. N. and Grenfell, B. T. (2001) Noisy clockwork: time series analysis of population fluctuations in animals. *Science*, **293**, 638–643.
- [5] Coulson, T., Rohani, P., and Pascual, M. (2004) Skeletons, noise and population growth: the end of an old debate? *Trends Ecol. Evol.*, **19**, 359–364.
- [6] Nisbet, R. M. and Gurney, W. S. C. (1982) *Modelling fluctuating populations*. Wiley.
- [7] Alonso, D., McKane, A. J., and Pascual, M. (2007) Stochastic amplification in epidemics. *J. R. Soc. Interface*, **4**, 575–582.
- [8] Bauch, C. T. (2008) The role of mathematical models in explaining recurrent outbreaks of infectious childhood diseases. *Mathematical Epidemiology*, pp. 297–319, Springer.
- [9] Olsen, L. F., Truty, G. L., and Schaffer, W. M. (1988) Oscillations and chaos in epidemics: a nonlinear dynamic study of six childhood diseases in Copenhagen, Denmark. *Theo. Pop. Bio.*, **33**, 344–370.
- [10] London, W. P. and York, J. A. (1973) Recurrent outbreaks of measles, chickenpox and mumps I: Seasonal variation in contact rates. *Am. J. Epidemiology*, **98**, 453–468.
- [11] Fine, P. E. M. and Clarkson, J. A. (1982) Measles in England and Wales I: An analysis of underlying seasonal patterns. *Int. J. Epidem.*, **11**, 5–14.
- [12] Bjornstad, O. N., Finkenstadt, B. F., and Grenfell, B. T. (2002) Dynamics of measles epidemics: estimating scaling of transmission rates using a time series SIR model. *Eco. Monographs*, **72**, 169–184.
- [13] Grenfell, B. and Harwood, J. (1997) (Meta)population dynamics of infectious diseases. *Trends Ecol. Evol.*, **12**, 395–399.

- [14] Anderson, R. M., Grenfell, B. T., and May, R. M. (1984) Oscillatory fluctuations in the incidence of infectious disease and the impact of vaccination: time series analysis. *J. Hyg. Camb.*, **93**, 587–608.
- [15] Bolker, B. M. and Grenfell, B. T. (1996) Impact of vaccination on the spatial correlation and persistence of measles dynamics. *Proc. Natl. Acad. Sci. USA*, **93**, 12648–12653.
- [16] Rohani, P., Earn, D. J. D., and Grenfell, B. T. (1999) Opposite patterns of synchrony in sympatric disease metapopulations. *Science*, **286**, 968–971.
- [17] Grenfell, B. and Bolker, B. (1998) Cities and villages: infection hierarchies in a measles metapopulation. *Eco. Lett.*, **1**, 63–70.
- [18] Grenfell, B., Bjornstad, O. N., and Keppey, J. (2001) Travelling waves and spatial hierarchies in measles epidemics. *Nature*, **414**, 716–723.
- [19] Nguyen, H. T. H. and Rohani, P. (2008) Noise, nonlinearity and seasonality: the epidemics of whooping cough revisited. *J. R. Soc. Interface*, **5**, 403–413.
- [20] Fine, P. E. M. and Clarkson, J. A. (1986) Seasonal influences on pertussis. *Int. J. Epidemiol.*, **15**, 237–247.
- [21] Bauch, C. T. and Earn, D. J. D. (2003) Transients and attractors in epidemics. *Proc. R. Soc. Lond. B*, **270**, 1573–1578.
- [22] Priestley, M. B. (1982) *Spectral analysis and time series*. Academic Press.
- [23] Metcalf, C. J. E., Bjornstad, O. N., Grenfell, B. T., and Andreasen, V. (2009) Seasonality and comparative dynamics of six childhood infections in pre-vaccination Copenhagen. *Proc. R. Soc. B*, **276**, 4111–4118.
- [24] Hethcote, H. W. (1998) Oscillations in an endemic model for pertussis. *Can. Appl. Math. Quart.*, **6**, 61–88.
- [25] Serfling, R. E. (1952) Historical review of epidemic theory. *Human Biology*, **24**, 145–166.
- [26] Hamer, W. H. (1906) Epidemic disease in England - the evidence of variability and of persistency of type. *Lancet*, **1**, 733–739.
- [27] Bailey, N. T. J. (1985) *The mathematical theory of infectious diseases and its application*. Griffin.
- [28] Kermack, W. O. and McKendrick, A. G. (1927) A contribution to the mathematical theory of epidemics. *Proc. R. Soc. Lond. A*, **115**, 700–721.
- [29] Kermack, W. O. and McKendrick, A. G. (1932) A contribution to the mathematical theory of epidemics II. The problem of endemicity. *Proc. R. Soc. Lond. A*, **138**, 58–83.
- [30] Brauer, F. and Castillo-Chavez, C. (2001) *Mathematical models in population biology and epidemiology*. Springer.

- [31] de Jong, M. C. N., Diekmann, O., and Heesterbeek, H. (1995) How does transmission of infection depend on population size. *Epidemic models: their structure and relation to data*, Cambridge University Press.
- [32] Press, W. H., Teukolsky, S. A., Vetterling, W. T., and Flannery, B. P. (1997) *Numerical recipes in C*. Cambridge University Press, 2nd edn.
- [33] Schwartz, I. B. and Smith, H. L. (1983) Infinite subharmonic bifurcation in an SEIR epidemic model. *J. Math. Biol.*, **18**, 233–253.
- [34] Anderson, R. M. and May, R. M. (1982) Directly transmitted infectious diseases: control by vaccination. *Science*, **215**, 1053–1060.
- [35] Earn, D., Rohani, P., Bolker, B., and Grenfell, B. (2000) A simple model for complex dynamical transitions in epidemics. *Science*, **287**, 667–670.
- [36] Murray, J. D. (2002) *Mathematical Biology I: An Introduction*. Springer, 3rd edn.
- [37] Schenzle, D. (1985) An age-structured model of pre- and post-vaccination measles transmission. *Math. Med. Biol.*, **1**, 169–191.
- [38] Hethcote, H. W. (1997) An age-structured model for pertussis transmission. *Math. Biosci.*, **145**, 89–136.
- [39] Heathcoat, H. and van den Driessche, P. (2000) Two SIS epidemiological models with delays. *J. Math. Biology*, **40**, 3.
- [40] Heathcoat, H. and van den Driessche, P. (1991) Some epidemiological models with nonlinear incidence. *J. Math. Biology*, **29**, 271.
- [41] Bartlett, M. S. (1960) *Stochastic population models in ecology and epidemiology*. Methuen.
- [42] Durrett, R. and Levin, S. A. (1994) The importance of being discrete and spatial. *Theo. Pop. Biol.*, **46**, 363–394.
- [43] Altizer, S., Dobson, A., Hosseini P., Hudson, P., Pascual, M., and Rohani, P. (2006) Seasonality and the dynamics of infectious diseases. *Ecol. Lett.*, **9**, 467–484.
- [44] Grassly, N. C. and Fraser, C. (2006) Seasonal infectious disease epidemiology. *Proc. R. Soc. B*, **273**, 2541–2550.
- [45] Keeling, M., Rohani, P., and Grenfell, B. (2001) Seasonally forced dynamics explored as switching between attractors. *Physica D*, **148**, 317–335.
- [46] Rohani, P., Keeling, M. J., and Grenfell, B. T. (2002) The interplay between determinism and stochasticity in childhood diseases. *Am. Nat.*, **159**, 469–481.
- [47] Soper, H. (1929) The interpretation of periodicity in disease prevalence. *J. R. Stat. Soc.*, **92**, 34–73.

- [48] Fine, P. E. M. and Clarkson, J. A. (1982) Measles in England and Wales II: The impact of the measles vaccination programme on the distribution of immunity in the population. *Int. J. Epidem.*, **11**, 15–25.
- [49] Finkenstadt, B. and Grenfell, B. (2000) Time series modelling of childhood diseases: a dynamical systems approach. *Appl. Statist.*, **49**, 187–205.
- [50] Finkenstadt, B., Bjornstad, O., and Grenfell, B. (2002) A stochastic model for extinction and recurrence of epidemics: estimation and inference for measles outbreaks. *Biostatistics*, **3**, 493–510.
- [51] Morton, A. and Finkenstadt, B. F. (2005) Discrete time modelling of disease incidence time series by using Markov chain Monte Carlo methods. *Appl. Statist.*, **54**, 575–594.
- [52] Dietz, K. (1976) The incidence of infectious diseases under the influence of seasonal fluctuations. *Lecture Notes in Biomathematics*, vol. 11, pp. 1–15, Springer-Verlag.
- [53] Aron, J. L. and Schwartz, I. B. (1984) Seasonality and period-doubling bifurcations in an epidemic model. *J. Theo. Biol.*, **110**, 665–679.
- [54] Kuznetsov, Y. A. and Piccardi, C. (1994) Bifurcation analysis of periodic SEIR and SIR epidemic models. *J. Math. Biol.*, **32**, 109–121.
- [55] Rand, D. A. and Wilson, H. B. (1991) Chaotic stochasticity - a ubiquitous source of unpredictability in epidemics. *Proc. R. Soc. Lond. B*, **246**, 179–184.
- [56] Bartlett, M. S. (1990) Chance or chaos? *J. R. Stat. Soc. A*, **153**, 321–347.
- [57] Olsen, L. F. and Schaffer, W. M. (1990) Chaos versus noisy periodicity: alternative hypotheses for childhood epidemics. *Science*, **249**, 499–504.
- [58] Pool, R. (1989) Is it chaos, or is it just noise? *Science*, **243**, 25–28.
- [59] Bolker, B. M. and Grenfell, B. T. (1993) Chaos and biological complexity in measles dynamics. *Proc. R. Soc. Lond. B*, **251**, 75–81.
- [60] Bolker, B. M. (1993) Chaos and complexity in measles models: a comparative numerical study. *IMA J. Math. Appl. Med. Biol.*, **10**, 83–95.
- [61] Nasell, I. (2002) Measles outbreaks are not chaotic. *Mathematical Approaches for Emerging and Reemerging Infectious Diseases: Models, Methods and Theory*, pp. 85–114, Springer-Verlag.
- [62] Bartlett, M. S. (1956) Deterministic and stochastic models for recurrent epidemics. *Proc. Third Berkeley Symposium on Mathematical Statistics and Probability*, pp. 81–109, University of California Press.
- [63] Nasell, I. (1999) On the time to extinction in recurrent epidemics. *J. R. Stat. Soc. B*, **61**, 309–330.

- [64] Keeling, M. J. and Grenfell, B. T. (2002) Understanding the persistence of measles: reconciling theory, simulation and observation. *Proc. R. Soc. Lond. B*, **269**, 335–343.
- [65] Conlan, A. J. K., Rohani, P., Lloyd, A. L., Keeling, M., and Grenfell, B. T. (2010) Resolving the impact of waiting time distributions on the persistence of measles. *J. R. Soc. Interface*, **7**, 623–640.
- [66] Aparicio, J. P. and Solari, H. G. (2001) Sustained oscillations in stochastic systems. *Math. Biosciences*, **169**, 15–25.
- [67] Simoes, M., Telo da Gama, M. M., and Nunes, A. (2008) Stochastic fluctuations in epidemics on networks. *J. R. Soc. Interface*, **5**, 555–566.
- [68] McKane, A. J. and Newman, T. J. (2005) Predator-prey cycles from resonant amplification of demographic stochasticity. *Phys. Rev. Lett.*, **94**, 218102.
- [69] Risau-Gusman, S. and Abramson, G. (2007) Bounding the quality of stochastic oscillations in population models. *Eur. Phys. J. B*, **60**, 515–520.
- [70] Kuske, R., Gordillo, L. F., and Greenwood, P. (2007) Sustained oscillations via coherence resonance in SIR. *J. Theo. Bio.*, **245**, 459–469.
- [71] Greenman, J., Kamo, M., and Boots, M. (2004) External forcing of ecological and epidemiological systems: a resonance approach. *Physica D*, **190**, 136–151.
- [72] Schwartz, I. B. (1985) Multiple stable recurrent outbreaks and predictability in seasonally forced nonlinear epidemic models. *J. Math. Biol.*, **21**, 347–361.
- [73] Renshaw, E. (1991) *Modelling biological populations in space and time*. Cambridge University Press.
- [74] McKane, A. J. and Newman, T. J. (2004) Stochastic models in population biology and their deterministic analogs. *Phys. Rev. E*, **70**, 041902.
- [75] Nasell, I. (2002) Stochastic models of some endemic infections. *Math. Biosci.*, **179**, 1–19.
- [76] Keeling, M. J. and Ross, J. V. (2008) On methods for studying stochastic disease dynamics. *J. R. Soc. Interface*, **5**, 171–181.
- [77] Keeling, M. J. and Ross, J. V. (2009) Efficient methods for studying stochastic disease and population dynamics. *Theo. Pop. Biol.*, **75**, 133–141.
- [78] van Kampen, N. G. (1992) *Stochastic processes in physics and chemistry*. Elsevier.
- [79] Grossman, Z. (1980) Oscillatory phenomena in a model of infectious disease. *Theo. Pop. Biol.*, **18**, 204–243.
- [80] Lloyd, A. L. (2001) Destabilization of epidemic models with the inclusion of realistic distributions of infectious periods. *Proc. R. Soc. Lond. B*, **268**, 985–993.

- [81] Keeling, M. and Grenfell, B. (1998) Effect of variability in infection period on the persistence and spatial spread of infectious disease. *Math. Biosci.*, **147**, 207–226.
- [82] Gardiner, C. W. (2003) *Handbook of stochastic methods*. Springer, 3rd edn.
- [83] Gillespie, D. T. (1992) *Markov processes: an introduction for physical scientists*. Academic Press.
- [84] Engbert, R. and Drepper, F. (1994) Chance and chaos in population biology - models of recurrent epidemics and food chain dynamics. *Chaos, Solitons & Fractals*, **4**, 1147–1169.
- [85] Jacquez, J. A. and Simon, C. P. (1993) The stochastic SI model with recruitment and deaths. I. Comparison with the closed SIS model. *Math. Biosci.*, **117**, 77–125.
- [86] Gillespie, D. (1976) A general method for numerically simulating the stochastic time evolution of coupled chemical reactions. *J. Comp. Phys.*, **22**, 403–434.
- [87] Cox, D. R. and Miller, H. D. (1965) *The theory of stochastic processes*. Chapman and Hall.
- [88] Gibson, M. and Bruck, J. (2000) Efficient exact stochastic simulation of chemical systems with many species and many channels. *J. Phys. Chem. A*, **104**, 1876–1889.
- [89] Anderson, D. F. (2007) A modified next reaction method for simulating chemical systems with time dependent propensities and delays. *J. Chem. Phys.*, **127**, 214107.
- [90] Cormen, T. H., Leiserson, C. E., and Rivest, R. L. (1990) *Introduction to algorithms*. The MIT Press.
- [91] McCollum, J. M., Peterson, G. D., Cox, C. D., Simpson, M. L., and Samatova, N. F. (2006) The sorting direct method for stochastic simulation of biochemical systems with varying reaction execution behavior. *J. Comp. Biol. Chem.*, **30**, 39–49.
- [92] van Kampen, N. G. (1976) The expansion of the master equation. *Adv. Chem. Phys.*, **34**, 245.
- [93] Lugo, C. A. and McKane, A. J. (2008) Quasicycles in a spatial predator-prey model. *Phys. Rev. E*, **78**, 051911.
- [94] Risken, H. (1989) *The Fokker-Planck equation: methods of solution and applications*. Springer-Verlag, 2nd edn.
- [95] Kurtz, T. (1970) Solutions of ordinary differential equations as limits of pure jump Markov processes. *J. Appl. Probab.*, **7**, 49–58.
- [96] Kurtz, T. (1971) Limit theorems for sequences of jump Markov processes approximating ordinary differential processes. *J. Appl. Probab.*, **8**, 344–356.

- [97] Ross, J. V. (2006) A stochastic metapopulation model accounting for habitat dynamics. *J. Math. Biol.*, **52**, 788–806.
- [98] Jordan, D. and Smith, P. (1999) *Nonlinear ordinary differential equations*. Oxford University Press, 3rd edn.
- [99] Strogatz, S. (1994) *Nonlinear dynamics and chaos: with applications to physics, biology, chemistry, and engineering*. Persueus Books.
- [100] McKane, A. J., Nagy, J. D., Newman, T. J., and Sefanini, M. O. (2007) Amplified biochemical oscillations in cellular systems. *J. Stat. Phys.*, **128**, 165–191.
- [101] Lloyd, A. L. (2004) Estimating variability in models for recurrent epidemics: assessing the use of moment closure techniques. *Theo. Pop. Biol.*, **65**, 49–65.
- [102] French, A. P. (2000) *Vibrations and waves*. CRC Press.
- [103] Keeling, M. (1997) Modelling the persistence of measles. *Trends Micro.*, **5**, 513–518.
- [104] Bartlett, M. S. (1957) Measles periodicity and community size. *J. R. Stat. Soc. Ser. A*, **120**, 48–70.
- [105] Bartlett, M. S. (1960) The critical community size for measles in the United States. *J. R. Stat. Soc. A*, **123**, 37–44.
- [106] Grenfell, B. (1992) Chance and chaos in measles dynamics. *J. R. Statist. Soc. B*, **54**, 382–393.
- [107] Bolker, B. and Grenfell, B. (1995) Space, persistence and dynamics of measles epidemics. *Phil. Trans. R. Soc. Lond. B*, **348**, 309–320.
- [108] Lloyd, A. L. and Jansen, V. A. A. (2004) Spatiotemporal dynamics of epidemics: synchrony in metapopulation models. *Math. Biosci.*, **188**, 1–16.
- [109] Lloyd, A. L. and Sattenspiel, L. (2009) Spatiotemporal dynamics of measles: synchrony and persistence in a disease metapopulation. *Spatial Ecology*, pp. 251–272, CRC Press.
- [110] Wolfram Research (2008) *Mathematica*. Wolfram Research Inc.
- [111] Sartwell, P. E. (1950) The distribution of incubation periods of infectious disease. *Am. J. Hyg.*, **51**, 310–318.
- [112] Hope-Simpson, R. E. (1952) Infectiousness of communicable diseases in the household (measles, chickenpox and mumps). *Lancet*, **260**, 549–554.
- [113] Bailey, N. J. T. (1956) On estimating the latent and infectious periods of measles: 1. Families with two susceptibles only. *Biometrika*, **43**, 15–22.
- [114] Keeling, M. and Grenfell, B. (1997) Disease extinction and community size: modeling the persistence of measles. *Science*, **275**, 65–67.

- [115] Hethcote, H. and Tudor, D. (1980) Integral equation models for endemic infectious diseases. *J. Math. Biol.*, **9**, 37–47.
- [116] Lloyd, A. L. (2001) Realistic distributions of infectious periods in epidemic models: changing patterns of persistence and dynamics. *Theo. Pop. Bio.*, **60**, 59–71.
- [117] Green, D. (1978) Self-oscillation for epidemic models. *Math. Biosci.*, **38**, 91–111.
- [118] Kuperman, M. and Abramson, G. (2001) Small world effect in an epidemiological model. *Phys. Rev. Lett.*, **86**, 2909.
- [119] Litvak-Hinenzon, A. and Stone, L. (2009) Epidemic waves, small worlds and targeted vaccination. *J. R. Soc. Interface*, **6**, 749.
- [120] Anderson, D. and Watson, R. (1980) On the spread of a disease with gamma distributed latent and infectious periods. *Biometrika*, **67**, 191–198.
- [121] Wearing, H., Rohani, P., and Keeling, M. (2005) Appropriate models for the management of infectious diseases. *PLoS Med.*, **2**, 621–627.
- [122] Black, A. J., McKane, A. J., Nunes, A., and Parisi, A. (2009) Stochastic fluctuations in the susceptible-infectious-recovered model with distributed infectious periods. *Phys. Rev. E.*, **80**, 021922.
- [123] Ferguson, N. M., Anderson, R. M., and Garnett, G. P. (1996) Mass vaccination to control chickenpox: The influence of zoster. *Proc. Natl. Adac. Sci. USA*, **93**, 7231–7235.
- [124] Wearing, H. J. and Rohani, P. (2009) Estimating the duration of pertussis immunity using epidemiological signatures. *PLoS Pathogens*, **5**, e1000647.
- [125] Kuznetsov, Y. A. (2004) *Elements of applied bifurcation theory*. Springer, 3rd edn.
- [126] Boland, R. P., Galla, T., and McKane, A. J. (2009) Limit cycles, complex Floquet multipliers and intrinsic noise. *Phys. Rev. E*, **79**, 051131.
- [127] Grimshaw, R. (1990) *Nonlinear ordinary differential equations*. Blackwell, 1st edn.
- [128] He, D. and Earn, D. J. D. (2007) Epidemiological effects of seasonal oscillations in birth rates. *Theo. Pop. Biol.*, **72**, 274–291.
- [129] Wiesenfeld, K. (1985) Virtual Hopf phenomenon: a new precursor of period-doubling bifurcations. *Phys. Rev. A*, **32**, 1744–1751.
- [130] Bauch, C. T. and Earn, D. J. D. (2003) Interepidemic intervals in forced and unforced SEIR models. *Fields Inst. Comm.*, **36**, 33–44.
- [131] Wiesenfeld, K. (1985) Noisy precursors of nonlinear instabilities. *J. Stat. Phys.*, **38**, 1071–1097.

- [132] Greenman, J. V. and Benton, T. G. (2005) The impact of environmental fluctuations on structured discrete time population models: resonace, synchrony and threshold behaviour. *Theo. Pop. Biol.*, **68**, 217–235.
- [133] Kravtsov, Y. A. and Surovyatkina, E. D. (2003) Nonlinear saturation of prebifurcation noise amplification. *Phys. Lett. A*, **319**, 348–351.
- [134] Griffiths, D. (1973) The effect of measles vaccination on the incidence of measles in the community. *J. R. Statist. Soc. A*, **136**, 441.
- [135] Grima, R. (2009) Noise-induced breakdown of the Michaelis-Menten equation in steady-state conditions. *Phys. Rev. Lett.*, **102**, 218103.
- [136] Black, A. J. and McKane, A. J. (2010) Stochasticity in staged models of epidemics: quantifying the dynamics of whooping cough. *J. R. Soc. Interface*, **7**, 1219–1227.
- [137] Fairgrieve, T. F. and Jepson, A. D. (1991) O.K. Floquet multipliers. *SIAM J. Numer. Anal.*, **28**, 1446–1462.
- [138] Lust, K. (2001) Improved numerical Floquet multipliers. *Int. J. Bifurcation and Chaos*, **11**, 2389–2410.
- [139] Forgoston, E., Billings, L., and Schwartz, I. B. (2009) Accurate noise projection for reduced stochastic epidemic models. *Chaos*, **19**, 043110.
- [140] Rozhnova, G. and Nunes, A. (2010) Stochastic effects in a seasonally forced epidemic model. *Phys. Rev. E*, **82**, 041906.
- [141] Higgins, K., Hastings, A., Sarvela, J. N., and Botsford, L. W. (1997) Stochastic dynamics and deterministic skeletons: population behavior of Dungeness crab. *Science*, **276**, 1431–1435.
- [142] Viboud, C., Bjornstad, O. N., Smith, D. L., Simonsen, L., Miller, M. A., and Grenfell, B. T. (2006) Synchrony, waves, and spatial hierarchies in the spread of influenza. *Science*, **312**, 447.
- [143] Colizza, V., Barrat, A., Barthelemy, M., Valleron, A., and Vespignani, A. (2007) Modeling the worldwide spread of pandemic influenza: baseline case and containment interventions. *PLOS Medicine*, **4**, 95–110.
- [144] Finkenstadt, B. and Grenfell, B. (1998) Empirical determinants of measles metapopulation dynamics in England and Wales. *Proc. R. Soc. Lond. B*, **265**, 211–220.
- [145] Xia, Y., Bjornstad, O. N., and Grenfell, B. T. (2004) Measles metapopulation dynamics: a gravity model for epidemiological coupling and dynamics. *Am. Nat.*, **164**, 267–281.
- [146] Bansal, S., Grenfell, B. T., and Ancel Meyers, L. (2007) When individual behaviour matters: homogeneous and network models in epidemiology. *J. R. Soc. Interface*, **4**, 879–891.

- [147] Riley, S. (2007) Large-scale spatial-transmission models of infectious disease. *Science*, **316**, 1298.
- [148] Grenfell, B., Bolker, B., and Kleczkowski, A. (1995) Seasonality and extinction in chaotic metapopulations. *Proc. R. Soc Lond. B*, **259**, 97–103.
- [149] Lloyd, A. L. and May, R. M. (1996) Spatial heterogeneity in epidemic models. *J. Theo. Biol.*, **179**, 1–11.
- [150] Keeling, M. (2000) Metapopulation moments: coupling, stochasticity and persistence. *J. Ani. Ecol.*, **69**, 725–736.
- [151] Keeling, M. and Rohani, P. (2002) Estimating spatial coupling in epidemiological systems: a mechanistic approach. *Ecol. Lett.*, **5**, 20–29.
- [152] Hagenaars, T., Donnelly, C., and Ferguson, N. (2004) Spatial heterogeneity and the persistence of infectious diseases. *J. Theo. Biol.*, **229**, 349–359.
- [153] Dangerfield, C. E., Ross, J. V., and Keeling, M. J. (2009) Integrating stochasticity and network structure into an epidemic model. *J. R. Soc. Interface*, **6**, 761–774.
- [154] Turing, A. M. (1952) The chemical basis of morphogenesis. *Phil. Trans. R. Soc. Lond. B*, **237**, 7.
- [155] Liu, Q. and Jin, Z. (2007) Formation of spatial patterns in an epidemic model with constant removal rate of the infectives. *J. Stat. Mech.*, p. P05002.
- [156] Galla, T. (2009) Intrinsic fluctuations in stochastic delay systems: theoretical description and application to a simple model of gene regulation. *Phys. Rev. E*, **80**, 021909.
- [157] Hanski, I. (1998) Metapopulation dynamics. *Nature*, **396**, 41–49.
- [158] Conlan, A. J. K. and Grenfell, B. T. (2007) Seasonality and the persistence and invasion of measles. *Proc. R. Soc. B*, **274**, 1133–1141.
- [159] Stone, L., Olinky, R., and Huppert, A. (2007) Seasonal dynamics of recurrent epidemics. *Nature*, **446**, 533–536.
- [160] van Herwaarden, O. A. (1997) Stochastic epidemics: the probability of extinction of an infectious disease at the end of a major outbreak. *J. Math. Biol.*, **35**, 793–813.
- [161] Kubo, R., Matsuo, K., and Kitahara, K. (1973) Fluctuation and relaxation of macrovariables. *J. Stat. Phys.*, **9**, 51–96.
- [162] Meerson, B. and Sasorov, P. V. (2009) WKB theory of epidemic fade-out in stochastic populations. *Phys. Rev. E*, **80**, 041130.
- [163] Mobilia, M. and Assaf, M. (2010) Fixation in evolutionary games under non-vanishing selection. *EPL*, **91**, 10002.